Active Dynamic Analysis and Vibration Control of Gossamer Structures Using Smart Materials

Eric J. Ruggiero

Thesis submitted to the Faculty of the
Virginia Polytechnic Institute and State University
in partial fulfillment of the degree requirements for the degree of

Master of Science
in
Mechanical Engineering

Daniel J. Inman, chair
Harry Robertshaw
Donald Leo
Walter F. O'Brien

May 7, 2002
Blacksburg, Virginia

Keywords: Inflatable structures, piezoelectric, modal, PPF control,
MIMO, gossamer spacecraft

Active Dynamic Analysis and Vibration Control of Gossamer Structures Using Smart Materials

Eric J. Ruggiero

(Abstract)

Increasing costs for space shuttle missions translate to smaller, lighter, and more flexible satellites that maintain or improve current dynamic requirements. This is especially true for optical systems and surfaces. Lightweight, inflatable structures, otherwise known as gossamer structures, are smaller, lighter, and more flexible than current satellite technology. Unfortunately, little research has been performed investigating cost effective and feasible methods of dynamic analysis and control of these structures due to their inherent, non-linear dynamic properties. Gossamer spacecraft have the potential of introducing lenses and membrane arrays in orbit on the order of 25 m in diameter. With such huge structures in space, imaging resolution and communication transmissibility will correspondingly increase in orders of magnitude.

A daunting problem facing gossamer spacecraft is their highly flexible nature. Previous attempts at ground testing have produced only localized deformation of the structure's skin rather than excitation of the global (entire structure's) modes. Unfortunately, the global modes are necessary for model parameter verification. The motivation of this research is to find an effective and repeatable methodology for obtaining the dynamic response characteristics of a flexible, inflatable structure. By obtaining the dynamic response characteristics, a suitable control technique may be developed to effectively control the structure's vibration. Smart materials can be used for both active dynamic analysis as well as active control. In particular, piezoelectric materials, which demonstrate electro-mechanical coupling, are able to sense vibration and consequently can be integrated into a control scheme to reduce such vibration. Using smart materials to develop a vibration analysis and control algorithm for a gossamer space structure will fulfill the current requirements of space satellite systems. Smart materials will help spawn the next generation of space satellite technology.

Grant Information

This work was sponsored by the Air Force Office of Scientific Research under grant number F49620-99-1-0231, by the NASA Langley Research Center under grant number LaRC 01-1103, and by the Honeywell Corporation. The author gratefully acknowledges the support.

for my wife, Jennifer…

Acknowledgements

I am quite thankful to a lot of people in seeing the successful completion of this work. First, I would like to thank God for the endless blessings and gifts He has bestowed upon me. Without His love, comfort, and guidance, not to mention answered prayers, I would never have made it to this point in my life.

I am in deep gratitude for the guidance and support of my academic advisor, Dr. Daniel J. Inman. Dr. Inman took me under his wing last fall and provided me with a thesis topic and the funds to see its fruition. His thoughtful and insightful feedback throughout the semesters continued to challenge my work and bring it to higher levels. I also extend a heartfelt thanks to Dr. Gyuhae Park. Dr. Park worked hand-in-hand with me in the laboratory and helped me maintain some form of sanity throughout endless experimental problems. Without his help, I'd still be trying to figure out the dynamic analysis portion of this research.

I was blessed with support of my thesis throughout both semesters by many others. Dr. Jan Wright, from the University of Manchester in the U.K., provided a huge boost to my thesis by working with me on the development of MIMO testing techniques and processing software in the dynamic analysis of gossamer structures. Drs. Donald Leo and Harry Robertshaw helped shed some light on my thesis work when I needed it most, especially from the controls engineering side.

Friendships formed at Virginia Tech have also helped keep me sane during some of the most trying times of my academic work. I extend my thanks to Mark, Chuck, Ean, Noah, Luciano, Kevin, Rodrigo, Curt, Akhilesh, Nikola, and everyone else who has ever been there for me.

Acknowledgements (cont.)

I also need to thank two of the most important people in the world, my parents. Without their love and financial support throughout my undergraduate career, I would not have had the opportunity to continue my education. I learned motivation, dedication, and the pursuit of excellence from their guidance and example. Thank you, Mom and Dad, and my entire family.

Last but certainly not least, I am most indebted to my wife, Jennifer. Jennifer has fully supported my education and pursuit of higher learning while delaying some of her own life goals and dreams. She has been there for me on my best days as well as my worst days, and has always offered wisdom to keep me focused on what is important in life—family and prayer. Without Jennifer, I could not have finished this thesis in two semesters. Her love and passion are the drive behind my success. Thank you, Jennifer, from the bottom of my heart.

TABLE OF CONTENTS

LIST OF FIGURES

Figure **Page**

Figure **Page**

LIST OF TABLES

CHAPTER 1: Introduction

1.1 Background

Lightweight, inflatable space structures are the future of space satellite technology. Possessing ideal space launching characteristics, such as minimal storage volume and minimal mass, these lightweight, inflatable structures will propel the space industry into the next generation of space satellite technology. However, there are certain, key issues that must be investigated before such structures can replace current satellite technology. In particular, the vibration characteristics of thin, flexible, and inflatable structures must be well understood. Space satellites must be expertly controlled from a vibration standpoint because signal transmission to and from the earth mandates tight tolerances. Vibration control is critical to mission success as well as satellite longevity.

Lightweight, inflatable structures possess unique characteristics that make them difficult candidates for vibration analysis and control. Because these structures are inflated, issues such as inflation pressure, pressure distribution, and skin wrinkling hurdle into the forefront of the vibration analyst's mind. In terms of space applications, inflated structures would undergo severe environmental changes as the satellite passed from orbital day to orbital eclipse. Such environmental changes subject the inflated satellite to pressure fluctuations and consequent shockwaves that vibrate the structure. Further, such satellites are susceptible to vibration while in orbit because of local disturbances or rigid body motion during satellite repositioning. Therefore, the vibration analysis and control for an inflated structure must be robust in order to handle multitudes of vibration sources, and must also conform to the lightweight, flexible nature of the structure. For the first time in current literature, the use of smart materials is proposed as the solution to the vibration analysis and control of a flexible toroidal structure.

Smart materials, or more specifically, piezoelectric materials, are a viable, immediate solution to the robust vibration control problem because of their unobtrusive

nature and ability to be fully integrated into any control scheme. Lead zirconate titanates (PZTs) and polyvinylidene fluorides (PVDFs), are two particular types of smart materials. In the piezoelectric family of materials, if the material is strained it produces an electric charge and, conversely, if an electric field is applied, the material strains. This property, known as the piezoelectric effect, has been developed over the past few decades for use in vibration control schemes of reliable aluminum truss-and-beam technology, as well as a myriad of other design schemes. In the past decade, significant improvements have been made in the versatility of these piezoelectric materials. Where standard PZT ceramics are hard and brittle, piezoelectric polymers (such as PVDF) and macro-fiber composite (MFC) actuators are pliable, flexible, and readily available. PVDF sensors and MFC actuators are able to conform to doubly curved surfaces, which brings inflatable structure technology back into the picture. If these PVDF and MFC patches can be fully integrated into the skin or onto the surface of an inflatable satellite, then we can measure the frequency response and implement a control scheme to control the vibration of the structure.

1.2 Motivation

Increasing costs for space shuttle missions translate to smaller, lighter, and more flexible satellites that maintain or improve current dynamic requirements. This is especially true for optical systems and surfaces. Lightweight, inflatable structures, due to their unique physical characteristics, are smaller, lighter, and more flexible than current satellite technology. Unfortunately, little research has been performed investigating cost effective and feasible methods of dynamic analysis and control of these structures due to their inherent non-linear dynamic properties. Current attempts at ground tests have been difficult because of the unique nature of the inflated structure and the consequent difficulties in sensing and actuation. The extremely flexible nature of the structure produces only localized deformation of the skin rather than excitation of the global modes. Unfortunately, the global modes are necessary for model parameter verification. The motivation of this research is to find an effective and repeatable methodology for obtaining the dynamic response characteristics of a flexible, inflatable structure. By

obtaining the dynamic response characteristics of the structure, a suitable control technique may be developed to effectively control the structure's vibration. Developing a vibration analysis and control algorithm for an inflatable space structure will fulfill the current requirements of space satellite systems, and will help spawn the next generation of space satellite technology.

1.3 Research Objectives and Contributions

There are three main objectives of this research: 1) obtaining an accurate dynamic analysis of a flexible, inflated toroidal structure; 2) establish an effective control scheme to suppress the vibration of a flexible, inflated toroidal structure; and 3) comparing and contrasting active and passive vibration control techniques of a flexible, inflated toroidal structure.

The first objective is developing a methodology using smart materials to obtain an accurate dynamic analysis of an inflatable satellite system. An accurate dynamic analysis of a test structure requires a sensor and an actuator to generate a frequency response function. Polyvinylidene fluoride (PVDF), one type of piezoelectric material, is an ideal sensor candidate for the dynamic analysis of flexible, inflatable structures. PVDF sensors conform to any surface, including the doubly curved surface of a toroidal structure, and can be fully integrated into the skin of a torus or any inflatable structure. Similarly, macro-fiber composite (MFC) actuators, produced by NASA Langley Research Center, are ideal candidates for providing input energy to inflatable structures. The thin, flexible MFC patch is also able to conform to most surfaces, including the doubly curved surface of an inflatable torus. By implementing an MFC patch to excite a torus, the rigid body modes of the structure, as well as the point deformation difficulties associated with more traditional modal testing techniques, can be avoided. Using both PVDF and MFC patches, an accurate frequency response function can be generated. Throughout experimentation, the results of the PVDF / MFC combination were compared to the results of the more conventional accelerometer / electromagnetic shaker combination. As an extension of this research, the ability to use multiple sensors and multiple actuators to

perform a multi input, multi output (MIMO) experimental modal analysis of the torus is also explored.

Secondly, the aim of this research is to actively control the vibration of a flexible, inflated toroidal structure using smart materials. Again, the MFC actuator is an ideal candidate for the active suppression of an inflated structure's vibration. In accordance with current literature, a positive position feedback (PPF) control methodology is used to effectively control the first resonant frequency of the torus. The active vibration suppression procedure is first validated on the first mode of vibration of a simply supported steel plate. Following the success of the plate experiment, the same experimental configurations are used on the inflated torus. Finally, the research evaluates the effectiveness of a viscoelastic tape as a passive control technique and compares the results to that of the active PPF controller.

1.4 Thesis Outline

The research comprising this thesis will be presented in the same order as the research objectives previously discussed. The second chapter is a literature review encompassing most of the history of gossamer technology. The third chapter presents the experimental setup and results of using PVDF film as sensors and MFC actuators as system excitation sources to obtain the frequency response function of a flexible, inflated torus. The results are compared to conventional accelerometer / electromagnetic shaker FRF generation techniques. The fourth chapter of this thesis work will delve into multi input, multi output experimental modal analysis techniques for a gossamer structure like the inflated torus. The fifth chapter discusses the experimental setup of a simply supported plate actively controlled by an MFC sensor / PZT patch actuator combination and a positive position feedback control algorithm. Using these results as a transition, chapter six explains the experimental setup of the same control techniques as used on the simply supported plate, but applied to the inflated torus. Similarly, a passive damping vibration control experiment will also be performed on the torus using a viscoelastic tape (3M damping foil #2552), and the results of both the active and passive techniques are

compared and contrasted. The final chapter, chapter seven, summarizes the important conclusions of the research and makes recommendations for future work.

CHAPTER 2: Literature Review

2.1 Introduction

On August 12, 1960, NASA successfully launched the first communications satellite into space. Echo I, a 100-foot diameter hollow ball of aluminum, was the pioneer of inflatable space satellite technology. However, because of uncertainties in meteoroid flux and difficulties in manufacturing and controllability, inflatable satellite technology nearly vanished soon after the satellite launches of the 1960s. Instead, NASA concentrated on using aluminum truss and beam elements in its satellite design. Although it has been over forty years since Echo I's successful deployment into Earth's atmosphere, significant advances in materials, or in particular, piezoelectric materials, have reopened the possibility to using inflatable satellite technology (Chmielewski et al., 2000).

Since the 1960s, gossamer spacecraft technology has, inherent to its name, floated through the scientific community like wisps of cobweb caught in the wind. Tenuous and nearly invisible, gossamer technology has always looked good on paper but, practically speaking, been difficult to implement. Recent efforts by NASA, the Air Force, and industry (in particular, L'Garde, Inc.) have spun their own nets in the wind to catch wisps of gossamer technology. Their combined efforts are collectively trying to make the dreams of yesterday become the realities of today. Having found a niche, research efforts in many disciplines are now focusing their resources on exploiting the feasibility and manifestation of gossamer spacecraft and structures.

2.2 The Importance of Gossamer Spacecraft Technology

In engineering terms, gossamer spacecraft are any such space-inflated craft exhibiting two distinct traits: ultra-low-mass and minimal stowage volume. A space

inflatable structure is, according to Artur Chmielewski, "a specific application of a membrane structure or any ultra-low-mass hybrid structure with an extensive use of membranes. [They are]… structures (load-carrying artifacts or devices) comprised of highly flexible (compliant) plate or shell-like elements " (2000). The benefits of using such structures boil down to the age-old idiom that, in terms of space mission capabilities, size does matter.

Current restrictions in space satellite technology are governed by the size of the orbiter. The larger the structure, the larger the lens, aperture, or array contained within it. By increasing the diameter of these particular components, the satellite's imaging resolution, frequency bandwidth, and sensing capabilities will correspondingly increase. Unfortunately, such satellite dimensions are infeasible with traditional composite beam and truss technology. Such structures are limited in size and mass because of the size of the Space Shuttle cargo bay as well as the high cost associated with each kilogram of mass launched into orbit. Gossamer craft are the next logical step in the progression of satellite design and construction. Their ultra-low mass and membrane construction, as described by Chmielewski (2000), make them the ideal candidates for future satellite missions. Not only will gossamer craft be able to meet the scientific community's goals of super-large craft in outer space, they will also answer the taxpayers' concerns over increasing mission costs.

When looking at the building blocks of gossamer satellites, there are three main components: inflatable struts, an inflatable torus, and some sort of lens, aperture, or array housed inside the boundary of the torus. Although all three components interact dynamically as well as statically, the key, central component is the torus. The torus serves as the boundary condition for any housed membrane or lens, and it ties together the supporting struts of the satellite or craft. Therefore, the torus will serve as the cornerstone of the papers reviewed in this chapter.

In general, the purpose of this chapter is to explore the history of gossamer spacecraft literature from an experimental standpoint. As in all engineering systems,

there is an underlying truth that the engineer must uncover, learn from, and develop. For gossamer spacecraft, the uncovering of this underlying truth begins with a strong understanding of the mathematical relationships governing the dynamic behavior of an inflated torus. This chapter will concentrate on the experimental results published thus far in the literature, ranging from initial tire experiments to state-of-the-art modal analyses of a scaled-model gossamer spacecraft component.

2.3 Historical Perspective

In "History of Relevant Inflatable High-Precision Space Structures Technology Developments," author R. F. Freeland (2000) beautifully outlines the history of deployable space structures. The origins of inflatable structure technology date back to the late 1950's to mid-1960's, during which time Goodyear Corporation developed ideas of inflatable structures for its "search radar antenna, radar calibration sphere, and lenticular inflatable parabolic reflector" (Freeland, 2000). Each of these three projects contributed significantly to the overall gossamer structure effort. The inflatable search radar antenna used rigidizable truss members and a metallic mesh to form the surface of the aperture. From the project, developed concepts included: the fabrication, assembly, and alignment of inflatable elements; techniques for attaching inflatable support members to precision mesh surfaces; and deployment techniques for a complex, inflatable structure. The radar calibration sphere, 6-meters in diameter, was constructed from multiple hexagonal-shaped membrane panels. It contributed to gossamer spacecraft by demonstrating: thin-film processes; high-precision panel assembly; inflation of a large, thin-film structure; and metalization of thin-film (for high RF reflectivity). Finally, Goodyear Corporation's lenticular inflatable parabolic reflector consisted of a reflector supported by a torus. From the experimental work, innovations in inflatable structure production and attainable precision on a much larger scale were realized.

Concurrently with Goodyear Corporation's work, NASA Langley Research Center and NASA Goddard Space Center were developing the first passive space-based

communication reflector, Echo I. On August 12, 1960, a Delta rocket deployed the Echo I communications sphere at an altitude of 1610 km (or 1000 miles).

Freeland also states that after Echo I's successful deployment, emphasis was placed on very large baseline interferometry (VLBI) axisymmetric reflector antennas, offset reflectors, and sunshade supports for large sensors and telescopes. During the development of these technologies in the early 1970's through the late 1980's, a small private firm known as L'Garde, Inc. entered the gossamer technology picture and contributed significantly to these three main efforts. L'Garde Inc.'s technological achievements throughout the 70's and 80's led to the NASA sponsored IN-STEP Inflatable Antenna Experiment that flew on May 29, 1996. A picture of the IN-STEP Inflatable Antenna Experiment (IAE) is shown below in Figure 2.1.

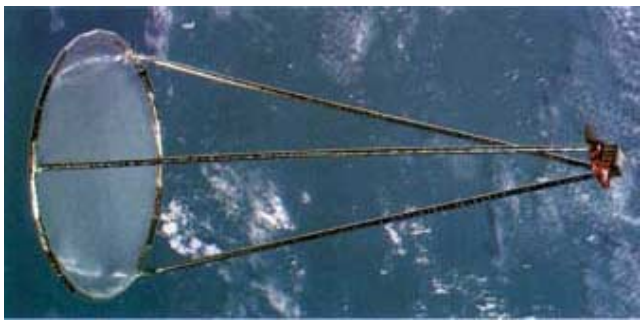

Figure 2.1. NASA's Inflatable Antenna Experiment (IAE) fully deployed in orbit.

According to Freeland, the IAE was a huge success in that it: demonstrated the fabrication of a large, space-worthy inflatable structure for about 1 million dollars; demonstrated "extremely efficient mechanical packaging by stowing a 14 x 28 m inflatable structure in a container the size of an office desk;" produced a reflective surface accurate to a few millimeters (rms); and demonstrated "the robustness of deployment for this new type of structure" (2000).

Freeland also mentions the contributions of other companies within industry to the gossamer technology initiative, as quoted below:

1) SRS Technologies (ultra thin film rib).
2) Winzen Engineering, Inc. (large-scale inflatable manufacturing).
3) Sigma Labs, Inc. (ultrahigh barrier films).
4) ITN Energy Systems, Inc. (reversible rigidizable structures).
5) Vertigo, Inc. (inflatable toroidal structures).
6) Millimeter Wave Technology, Inc. (spherical fresnel polymer reflectors).
7) United Applied Technologies, Inc. (precision film structures).
8) Adherent Technologies, Inc. (advanced materials).
9) Energen, Inc. (rigidized membrane reflectors).
10) [ILC Dover (large solar arrays and efficient packaging techniques)].

A timeline emphasizing the major contributions to gossamer technology is shown in Figure 2.2.

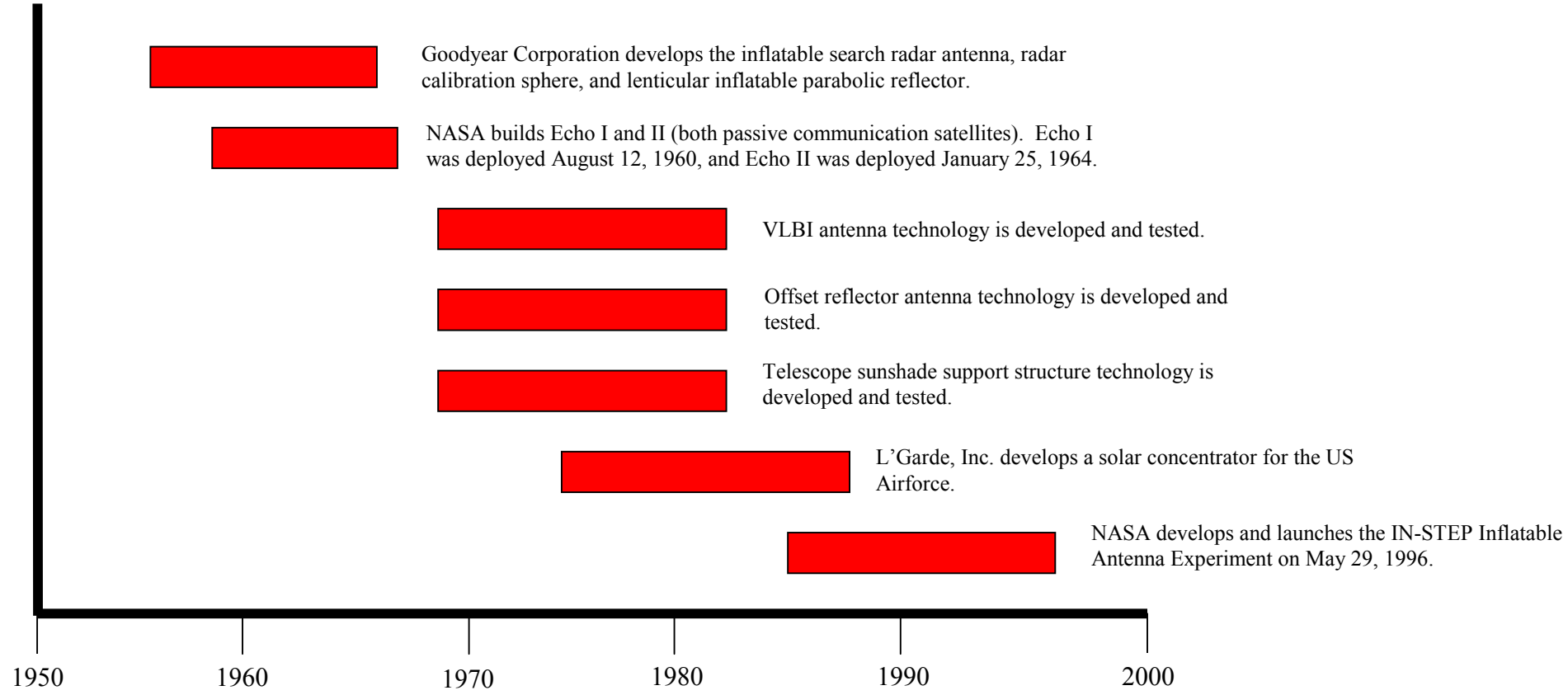

Figure 2.2. A timeline showing the years of industrial research contributing to the growth of gossamer technology.

2.4 A History of Experimental Modal Analysis Work on Gossamer Craft

The following section is dedicated to the work of many experimentalists in the field of gossamer technology. It is the compilation of these researchers' results and thoughts that has laid the track for future gossamer spacecraft projects. This section will review the historical development of experimental techniques and modal analyses of inflatable toroidal structures.

2.4.1 Experimental Modal Analysis of Tires

Although tires are a slightly older concept compared to gossamer spacecraft technology, they must be briefly addressed since they provide the foundation for this investigation. The research efforts of only a few will be presented to give but a short synopsis of some of the developments in this field. The equations governing the dynamics of an inflated tire differ from that of a gossamer toroidal structure. However, understanding the development of modal analysis methodologies for tires will prove fruitful in developing the same applications for inflated tori.

In 1973, Clark et al. performed research investigating the dynamic properties of aircraft tires. Using what they referred to as "string" theory, they predicted the behavior of aircraft tires that shimmy during taxiing. To validate the theoretical results, the group built a series of scale models representing different aircraft tires. Although the magnitude of their predictions were not accurate, the relative trends and phase agreement in their developed transfer functions were surprisingly good.

Noor and Tanner (1985) published a paper surveying the current advances in finite element modeling and computational algorithms for tire dynamic analysis. Their survey provides an excellent review of different methods of finite element analysis, highlighting important issues like material properties, loading scenarios, and tire construction techniques. At this point in history, however, the authors realized that

current experimental validation techniques were inadequate, especially in determining the dynamic response of the inflated torus.

Fast forward yet another decade, and enter the research efforts of Guan et al. (2000). In 2000, the authors presented a new method of experimental modal analysis for inflated tires. Although experimental modal analysis had been performed on tires in the early sixties through the late eighties, a clear methodology had not been established. The authors investigated the best methods of tire suspension, excitation type, and device for excitation. In terms of suspension, the authors found that by hanging the tire from a long, elastic line, they were able to reduce the rigid body modes to 1-2 Hz, well out of the frequency range of interest of their experiments. Arguably the authors' most important contribution to this area of research was their investigation of excitation sources. Guan et al. acquired their frequency response functions using a sine sweep, but the "…time length of the excitation signal was carefully selected so that the excitation ceased and that the corresponding response signal in a data frame was damped out. In this manner, not only could the leakage problem be solved, but also the reduction of resolution and the overestimation of damping due to the windowing technique was avoided" (2000). Their specified excitation source is seen throughout some of the most cutting edge modal analysis research efforts in gossamer technology. Finally, the authors also noted that point excitation sources were the best input-energy mechanisms for the tire modal analysis as opposed to a platform-based method. Their research efforts provided key modal parameters, such as damping, resonant frequencies, and effects of increased inflation pressure on these properties.

Concurrently with Guan et al., Yam et al. (2000) also performed modal analyses on tires. In particular, though, the authors' research efforts were focused on radial excitation methods as well as tangential excitation methods in order to develop accurate, three-dimensional mode shapes of the tire. The efforts of Yam et al. and Guan et al. helped establish consistent and accurate experimental modal analysis methodologies for inflated tires.

2.4.2 Experimental Modal Analysis of Gossamer Spacecraft and an Inflated Torus

While efforts were being made to identify system parameters of automotive and aircraft tires, similar efforts began to take shape for gossamer spacecraft. However, where the difficulty in modeling an automotive or aircraft tire is how to simulate real working conditions throughout the experimentation, pioneers in system modeling for gossamer craft faced many additional uncertainties. For example, the harsh environment of space, meteoroid flux, and vacuum conditions are difficult phenomena to model on earth. Further, the inflatable structures inherently contain properties that make modal analyses difficult. Their highly flexible nature, dependency on internal pressure, non-linear skin wrinkling, and susceptibility to local deformation have challenged the gossamer technology field since the launching of Echo I. The following is a review of the work performed by many modal experimentalists on multiple gossamer spacecraft designs.

In 1998, Tinker performed research at the NASA/Marshall Space Flight Center on the Shooting Star Experiment (SSE). The SSE was conceived to technologically demonstrate the possibility of solar thermal propulsion. In brief, solar thermal propulsion is obtained by concentrating solar energy (sunlight) into a thermal storage engine. Once heated to a specified level, a propellant is injected into the storage engine and then expands through a rear nozzle to produce thrust. Since only a few newtons of force are produced, the craft must be lightweight. Hence, the body of the SSE consists of a Kapton® torus and three Kapton® struts. All three pieces are inflated once the experiment has been placed in orbit. The torus holds the solar concentrator, a parabolic membrane. Tinker performed a series of analyses on the SSE in both ambient and vacuum conditions, and analyzed both the inflated struts of the assembly and the concentrator as two separate modal tests. The modal tests were performed using an electromagnetic shaker; however, Tinker was unable to directly excite the structure and therefore applied the input energy to the support plate of the entire assembly. In summary, the inflated struts were observed to behave like beams in a free-free boundary condition, and their

natural frequencies changed as a function of both "the film thickness and pressure inside the structure" (1998). Modal tests were performed on the entire assembly at pressures of 0.25, 0.5, and 1.0 psig. It is also noted that 0.5 psig is the desired on-orbit operating pressure. Further, Tinker also found during the vacuum experiments that the inflated assembly "maintained 0.5 psi relative to the external pressure. This was a significant test with very encouraging results in regard to on-orbit conditions and operability of the structure" (1998).

In 2000, Slade et al. performed further modal tests on Pathfinder 3, the inflated upper portion of the SSE, in both ambient and vacuum conditions. In particular, they concentrated on the solar concentrator (or inflated torus with Fresnel lens) measuring 1.8 meters in diameter. In both ambient and vacuum conditions, the modal analyses of the assembly were conducted using an electromagnetic shaker and a stinger for point excitation, and the response was measured using a laser vibrometer. Since the test structure was made of an optically transparent material, the researchers used sandblasted aluminum tape to enable the laser vibrometer to measure an accurate response. The research team prepared a simple finite element model of the strut – torus system as well to serve as a means of comparison. Although the model contained some error, there was general agreement between the finite element model and the modal analysis. They confirmed that the suspension system holding the structure during the modal tests influenced their results, so they tried to account for it in their finite element model by adding springs to their boundary conditions. By performing a modal analysis on the structure in both vacuum and ambient conditions, the team concluded that the damped natural frequencies of the structure shifted depending on the presence or absence of air, and the damping of the system increased (as might be expected) in the presence of air. Slade et al. recommend that future space structure modal tests should be performed in a vacuum for more accurate simulations.

Griffith and Main (2000) built a 6-foot in diameter torus out of Kapton® film. The Kapton® torus was assembled from three pairs of thermally formed panels and joined using an epoxy. Along the centerline of the torus shell is a continuous flap approximately

2.5 inches wide that the authors used as the joining region between panels. Griffith and Main performed a modal analysis on the small-scale gossamer craft by using a modified impact hammer as the method of excitation and an accelerometer to measure the frequency response function. They performed the modal tests at two different inflation pressures, namely 0.8 and 1.0 psig. Air was supplied to the structure using a small aquarium pump. The authors observed the first three in-plane and first three out-of-plane mode shapes. Unfortunately, the modified impact hammer was unable to distribute energy into the system evenly in the global sense, and therefore the frequency response curves generated by the tests had relatively poor coherence. However, the authors were able to note that the damped natural frequencies of the system increased with increased pressure, and that the test article demonstrated more non-linear behavior (such as breathing modes and shell wrinkling) at lower pressures.

Leigh et al. (2001) built an increasingly complex finite element model of the Pathfinder 3 vehicle continuing the work of Slade et al. The research team first concentrated on the strut elements of the structure. They took into account the inflation of each strut by pre-stressing the elements of the model, and were able to obtain similar results compared to experimental data. Next, the team built the torus out of shell elements. Compared to Griffith and Main's (2000) work at the University of Kentucky, the team's in-plane modes were nearly identical with the experimental data, but their out-of-plane resonant frequencies were considerably higher. To try and account for the discrepancy, the team assembled a more complex finite element model that included the joining flap along the centerline of the torus. The team qualified their results as "encouraging," although both in-plane and out-of-plane measurements were high. The team also ran into some difficulty because the "numerous local modes of the joint flanges [obscured] the torus modes of interest" (2001).

2.4.3 Use of Smart Materials in the Modal Analysis of Gossamer Spacecraft

The modal analysis techniques used by Slade et al. (2001) and Griffith and Main (2000) emphasized some of the downfalls associated with more traditional modal methodologies in terms of gossamer structures. Slade et al. (2001) were unable to obtain consistent results with a laser vibrometer due to a number of factors, including their method of excitation and choice of structural suspension during testing. Similarly, Griffith and Main (2000) were unable to obtain frequency response functions of an inflated torus with good coherence even with their modified impact hammer. As previously outlined, there are several reasons why obtaining the frequency response function of an inflated structure is quite difficult. Several other methods of modal testing are available, and one method that shows increasing promise is the use of piezoelectric patches and other smart materials.

Piezoelectric materials are a family of materials that demonstrate electro-mechanical coupling. That is, when the material is mechanically strained, the material produces a corresponding electric charge, and similarly, when an electric field is applied across the material, it mechanically strains. Mathematically, this relationship is governed by two constitutive equations, namely

$$\begin{Bmatrix} S \\ D \end{Bmatrix} = \begin{bmatrix} s & d \\ d & \varepsilon \end{bmatrix} \begin{Bmatrix} T \\ E \end{Bmatrix},$$

where S is strain in m/m, D is electric displacement in C/m^2, s is the mechanical compliance in m^2/N, d is the piezoelectric strain coefficient in C/m, ε is the dielectric permittivity in F/m, T is stress in N/m^2, and E is electric field in V/m. Piezoelectric materials have been known since 1880; however, it wasn't until the latter half of the twentieth century that they were used more heavily in industry. Since World War II, advances in material science and creation of new, synthetic materials have continued to exploit the electromechanical coupling exhibited by these materials.

In 1998, Tzou provided the vibration community with an excellent review of multiple smart materials and their corresponding applications. Tzou's review includes piezoelectric materials, shape memory alloys, magnetostrictive materials, and magnetorhealogical fluids, to name but a few. Also in 1998, Wang wrote an article outlining the use of piezoelectric patches as both actuators and sensors in the generation of a system frequency response function. Wang used PZT (lead zirconate titanate) patches as actuators and PVDF (polyvinylidene fluoride) patches as sensors to mathematically derive the frequency response function generated through their use. He provides excellent comparison charts between other methods of sensing and actuation.

The idea of using piezoelectric patches to obtain frequency response functions and extracting modal parameters is a rather mature idea. In 1991, Rubenstein et al. implemented multiple control laws via piezoceramic transducer sensors and actuators to reject steady-state disturbances to a simply supported plate. In 1994, Sun et al. published their work regarding structural modal analysis using collocated piezoelectric actuators and sensors. Even in 1994 the authors realized that the "…attachment of conventional transducers onto a testing structure may result in considerable errors in the extracted system parameters, especially with lightweight and flexible structures" (Sun et al., 1994). The authors performed a modal analysis using collocated sensors and actuators on a cantilevered beam. They supported the integration of PZT patches for modal analysis because they found that the patches had negligible effect on the dynamics of a thin, flexible beam undergoing vibration. Sun et al. (1995) published another work investigating a new method that measures the coupled impedance of two PZT sensors to extract the frequency response function of a thin, lightweight system in 1995.

In 2000, Sirohi and Chopra (2000a) investigated the behavior of piezoelectric sheet actuators. In particular, the authors investigated the free strain response of the actuators under DC excitation, as well as the magnitude and phase of the free strain response under different excitation voltages and frequencies. Later that year, the authors published another paper investigating the underlying advantages and disadvantages associated with using piezoelectric strain sensors. Their research found that the

"performance of piezoelectric sensors surpasses that of conventional type strain gages, with much less signal conditioning required, especially in applications involving low strain levels and high noise levels" (2000b).

In 2000, Wang and Chen performed a modal analysis of a simply supported plate using only PZT patches as actuators and PVDF patches as sensors. Wang and Chen's work included a theoretical development of the interaction between the smart actuators and sensors with the steel plate, generation of a column in the frequency response function matrix, generation of the plate's mode shapes, and extraction of the plate's modal parameters. They acknowledged that smart materials have a "major advantage… over the conventional structural testing [in that the] piezoceramic transducers can be integrated into the structure," and that the idea of using smart materials for system identification "…is also important to other applications such as structural vibration and acoustic control" (2000).

Agnes and Rogers (2000) tried to obtain a frequency response function of an inflated structure. The inflated structure, a children's swimming pool (5 foot major diameter and 1 foot cross-sectional diameter) with the floor panel removed, was excited using an electromagnetic shaker and, separately, with a PVDF patch. In both cases, the vibratory response of the structure was measured using a laser vibrometer around the perimeter of the face of the torus. The torus was hung vertically within a square frame and attached to the frame by four equivalent springs. Both the shaker and the PVDF patch excited the torus from 0-50 Hz. The authors used the multivariate mode indicator function (MMIF) to identify the resonant frequencies of the torus. Further analysis was deemed impossible, due to "the presence of significant non-linear effects, noise attributable to unmeasured disturbances, and the low level of signal in both tests" (2000).

Concurrently with Agnes and Rogers, Briand et al. (2000) performed research on an inflated tire inner tube using an electromagnetic shaker as the input and a PVDF sensor as the output to generate a frequency response function. The authors were able to excite the structure from 0-100 Hz, and obtained good coherence in their results. The

results of the modal analysis were then compared to a finite element model of the inner tube, and the results were favorable. Throughout the article, the authors also discuss the possibility of using SMA fabrics and films as actuators.

Park et al. (2001) performed a modal analysis of an inflated tire inner tube in 2001. The research team used an electromagnetic shaker as a point input to the torus, and compared the frequency response functions generated using an accelerometer and PVDF patches as sensors. The torus was suspended vertically using a long, elastic wire. The authors used the unified matrix polynomial approach (UMPA) pseudo least squares method to extract the modal parameters of the torus. The work also included an investigation of bimorph actuators and macro fiber composite (MFC) actuators. The MFC actuator is an experimental actuator from NASA Langley Research Center (Wilkie et al., 2000). The advantages of using the bimorph or MFC for actuation in the modal analysis included negligible mass loading effects and significantly "…less interference with the suspension modes of the free-free torus than excitations from the shaker" (2001). Finally, the authors attempted to control the vibration of the 4th out-of-plane mode using a positive position feedback controller. Both the bimorph actuator and MFC actuator were able to reduce the vibration of the rubber torus by approximately 50%.

Although piezoelectric materials are only one of many possible solutions in obtaining accurate modal analyses of inflatable structures, the piezoelectric family offers other potential successes further down the line. New, highly flexible PZT patches, such as the MFC actuator or PVDF sensor, can be fully integrated into the skin of an inflated structure and have negligible effect on the dynamic parameters of the system. PZT patches can act as sensors and actuators, a condition known as "self-sensing" (Dosch et al., 1992). And in terms of vibration control, piezoelectric materials offer the potential for controlled vibration suppression.

2.5 The Future of Gossamer Spacecraft Technology

Vibration control of gossamer spacecraft and membranes on the order of microns is critical to future mission success. The achievement of such tight vibration tolerances is the motivation behind the dynamic parameter identification and the active vibration control experiments of the Kapton® torus in this thesis. Piezoelectric materials are one possible answer to the proposed problem.

Another potential benefit of pursuing the marriage of piezoelectric technology and gossamer spacecraft is the possibility of on-orbit shape control. In 1994, Salama et al. proposed the use of piezo-induced deformations to achieve a higher degree of on-orbit surface accuracy with inflatable antennas. Given recent advances in the fabrication of PVDF and MFC materials, shape control of gossamer spacecraft is now not only feasible but also cost effective.

NASA is considering gossamer technology in its future Space Shuttle missions. Table 2.1 outlines NASA's Space Shuttle missions integrated with gossamer technology, starting with the launching of the Inflatable Antenna Experiment in 1996.

Table 2.1. Synopsis of recent and future gossamer spacecraft missions as outlined by NASA (Dornheim).

1996	Inflatable Antenna Experiment, on Spartan deployed by shuttle.
1999-2000	Inflatable solar array test, small 300-watt class, on Spartan deployed by shuttle.
2000	Next-Generation Space Telescope sunshield test. On Shuttle Mission 107 in June 2000.
2000	Inflatable Solar Array Experiment, large 1 2-kw. class, prototype for Deep Space 4/Champollion. Shuttle flight.
2000-1	Synthetic aperture radar antenna experiment, shuttle flight.
2002	Solar Orbit Transfer Vehicle experiment. Inflatable solar reflector is baseline.
2002-3	Deep Space 5. Mission to be defined in May, one contender is an inflatable solar sail.
2003	Deep Space 4/Champollion. Comet lander mission to have inflatable solar arrays to power ion engine. NOAA Geostorm. Uses solar sail to remain at sub orbital speed between Earth and Sun, may build on Deep Space 5.
2008	Advanced Radio Interferometry between Space and Earth (Arise). Has 25-meter inflatable antenna.

The next chapter will explain the use of smart materials in the dynamic analysis of an inflated torus.

CHAPTER 3: Dynamic Analysis of an Inflatable Torus Using Smart Materials

3.1 Background

As outlined in the motivation of this work, one of the critical factors that the future of gossamer technology hinges upon is the dynamic analysis of such structures. By identifying the modal parameters of inflatable systems, efforts in active vibration control and even on-orbit shape control suddenly become feasible. Extending the work of Park et al. (2001), the next step in the process is to apply the same modal analysis techniques as used on the inflated tire to a scaled-model gossamer spacecraft component—an inflated Kapton® torus.

Section 3.2 outlines the experimental procedure undertaken in the dynamic analysis of the inflated torus using an electromagnetic shaker as the input excitation. Section 3.3 presents the same experiment but uses a macro-fiber composite (MFC®) actuator as the excitation source instead of the electromagnetic shaker. In both sections 3.2 and 3.3, the resonant frequencies and first few in-plane and out-of-plane mode shapes of the inflated torus are presented. Similarly, in both experiments, polyvinylidene fluoride (PVDF) sensors are used to sense the response of the torus, and the PVDF results are compared to the results obtained using a more traditional accelerometer. Although the methodology of sections 3.2 and 3.3 are valid, there are certain downfalls associated with only using single input single output modal analysis techniques on the torus because of the torus' near axi-symmetric shape. These downfalls are highlighted in section 3.4. The chapter concludes in section 3.5 with a summary of the experimental results.

3.2 Experimental Modal Analysis of an Inflated Torus Using Traditional Excitation Methods

The inflated structure was first tested using more traditional modal analysis techniques, including an electromagnetic shaker as the excitation source and PVDF sensors and an accelerometer (as the baseline sensor measurement) to determine the frequency response function of the inflated torus. Wang and Chen (2000) discuss in detail the relationship between acceleration and strain measurements in performing modal analysis. In this study, the in-plane and out-of-plane modes of the test structure were investigated.

3.2.1 Test Structure: A Kapton Torus

The test structure was an inflated torus with a 1.8 m ring diameter and a 0.15 m tube diameter, as shown in Figure 3.1. The torus was made of flat sheets of polyamide film Kapton (46μm thick) and fabricated at the Emerging Technology Laboratory at the University of Kentucky. Three 120^{o} segments were joined together to form the complete torus. The method of fabrication resulted in variations along the thickness of the joined flap region. In addition, the joint epoxy added significant mass and stiffness to the bonded surface region. The width of the bonded flap material measured 5.1 cm. Table 3.1 lists the physical properties of the structure. The internal pressure of the torus was maintained at 0.5 psi throughout the experimentation using a small aquarium pump. The air pump continuously supplied air into the torus, even during testing, to maintain the desired internal pressure. Due to the small size of the pump and the negligible surface area of the insertion point of the tube, the pump noise and airflow had no noticeable effect on the measured frequency response functions (FRFs). However, it should be noted that research by Leigh et al. (2001) on inflatable concentrators demonstrated that a larger volume of continuous airflow, or, in space applications, the pressure shock within the inflatable structure as it travels from orbital day into orbital eclipse, would cause excitation within a lightweight, flexible structure.

Figure 3.1. The Kapton® torus under experimental investigation.

Table 3.1. Summary of the physical properties of the Kapton® torus.

Property	**Value**
Ring Diameter	1.8 m
Tube Diameter	0.15 m
Internal Pressure	0.5 psi
Elastic Modulus	2.55 GPa
Mass Density	1418 kg/m^3
Poisson's Ratio	0.34
Thickness	46 μm

To minimize the effects of boundary conditions, and to more closely simulate a free-free structure, the torus was suspended from the ceiling using a rubber wire (as shown in Figure 3.1). With the suspended wire, the rigid body mode occurs at 1.2 Hz. Therefore, the influence of this rigid body mode is negligible on the frequency range of interest, namely 10 to 200 Hz.

3.2.2 Excitation

The excitation method was carefully selected to minimize the interference between the electromagnetic shaker and the torus. The stinger of the electromagnetic shaker was glued onto the torus, as shown in Figure 3.2. Under this setup, the excitation

was considered to be a unidirectional point input, and could be configured for either in-plane or out-of-plane excitation.

Figure 3.2. Electromagnetic shaker attachment to the skin of the torus.

3.2.3 Sensors

To measure the dynamic response, an accelerometer (PCB Model 352C22) and a PVDF sensor were attached to the torus. Simultaneous measurements were taken from both devices and then compared. As shown in Figure 3.3, a specially designed PVDF sensor (Measurement Specialties SDT1-028K) was used to reduce electromagnetic interference (EMI) effects. The PVDF sensor is equipped with a protective coating and a shielded cable that protects it against a surrounding 60 Hz electromagnetic field. These sensors are bonded to the surface of the structure with double-sided carpet tape.

Figure 3.3. PVDF sensor attached to the skin of the inflated torus.

3.2.4 Experimental Procedure

The torus was excited in the out-of-plane direction and in the radial (in-plane) direction to measure the out-of-plane and in-plane modes. For acquisition of the torus's modal parameters in either direction, the sensors were arranged at sixteen evenly spaced locations (as shown by the white tape marks in Figure 3.1).

Force, acceleration, and strain (from PVDF sensors) data were collected through a DSPT SigLab multi-channel dynamic signal analyzer. A chirp signal excited the structure from 5 to 100 Hz. To ensure enough input energy at each frequency from excitation, the chirp input frequency for each test was divided into three sub-ranges (5-35, 35-65, and 65-100 Hz). Furthermore, the time period of excitation was held for as long as possible (130,000 samples at each sub-range) so that the excitation ceased and that the corresponding response signal in a data frame was damped out (Guan et al., 2000). Control of the excitation signal length was realized using a sampling number function in the SigLab signal analyzer. The careful selection of excitation signal (specific length and bandwidth) was found to be critical for a flexible inflatable torus when trying to obtain reliable vibratory responses with reasonable accuracy. Ten runs were averaged to estimate the frequency response functions.

3.2.5 Results and Analysis

After completing the data measurements, a modal analysis was performed using the Unified Matrix Polynomial Approach (UMPA) pseudo least square method (Allemang et al., 1994). This method determines an orthogonal polynomial to curve-fit the measured data, and provides eigenvalues and eigenvectors of the system. A typical curve-fitted diagram is shown in Figure 3.4 for out-of-plane frequency response functions (FRF) measured at 16 different locations. This figure shows multiple FRF measurements taken using a single accelerometer at 16 evenly spaced intervals around the perimeter of the torus (in the frequency range of 10 – 40 Hz). The extracted information from the

UMPA pseudo least square method was input to a MATLab program to plot the resulting mode shapes at resonant frequencies.

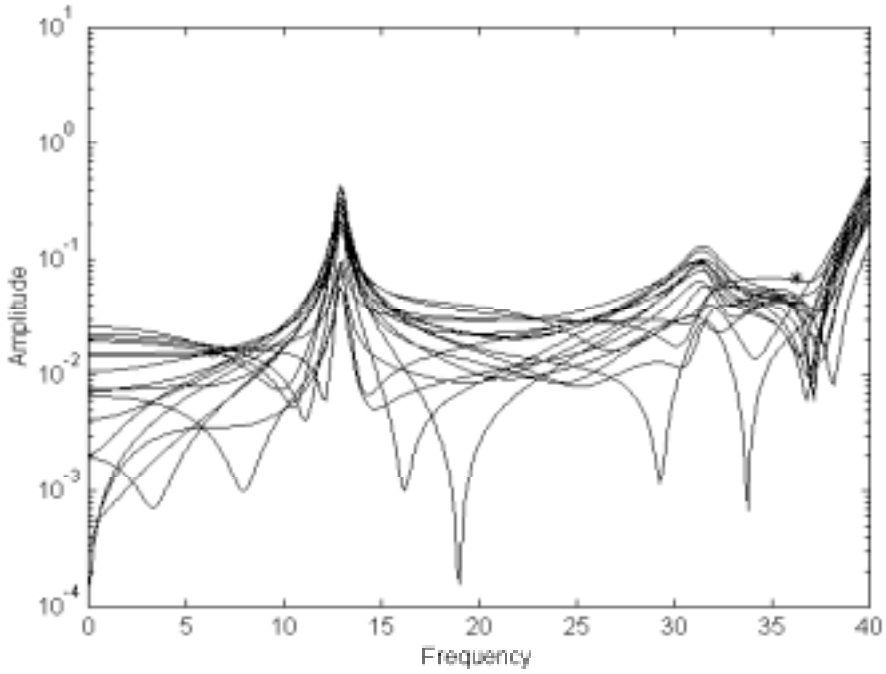

Figure 3.4. A sample curve-fitted FRF from the collected modal data using the UMPA pseudo least squares method.

From the modal analysis, three main types of mode shapes were identified. The structure not only demonstrated ring (in-plane and out-of-plane) mode shapes, but also demonstrated shell mode shapes at some resonant frequencies. Lewis's finite element study (Lewis, 2000) demonstrates the significant impact various aspect ratios play on the mode shapes of a toroidal structure. In his study, the vibratory response of a torus is dominated by shell modes if the aspect ratio is greater than 0.3, but, for a torus of small aspect ratio (less than 0.1), the shell mode activities are less significant. Similarly, the detailed FEA model developed by Leigh et al. (2001) also predicted similar shell behavior from a torus.

Figure 3.5 shows transfer functions of the out-of-plane motion measured with the accelerometer and the PVDF sensors. The coherence plot, which indicates the correlation between a single input and a single output measurement, is also shown to indicate that the

test results are reasonable. Both FRF curves contain distinct resonant frequencies near 13 and 32 Hz at the first two out-of plane resonant frequencies. Another resonant peak is identifiable near 65 Hz, but hard to distinguish from a shell mode near the same frequency. The offset seen between the PVDF sensor FRF curve and the accelerometer FRF curve in Figure 3.5 is caused by the amplification of the PVDF signal by the SigLab data acquisition system. Since the FRF curve is a ratio of the output signal to input signal, the amplification of the PVDF signal shifts the FRF curve vertically. Further, at another sensor location, the two signals may be very different in nature, but they will share the same resonant frequency peaks.

Figure 3.6 shows a sample transfer function measured in the in-plane direction. The first two resonant peaks are identified near 16 and 42 Hz as the in-plane modes. However, as the frequency increases, it is harder to identify resonant frequencies because of the presence of numerous shell modes. The apparent spike in the PVDF FRF curves in both Figures 3.5 and 3.6 is the result of an electromagnetic interference effect from surrounding electronic equipment at 60 Hz. The relatively small size of the sensor made it susceptible to the EMI effect, even with its shielded coating.

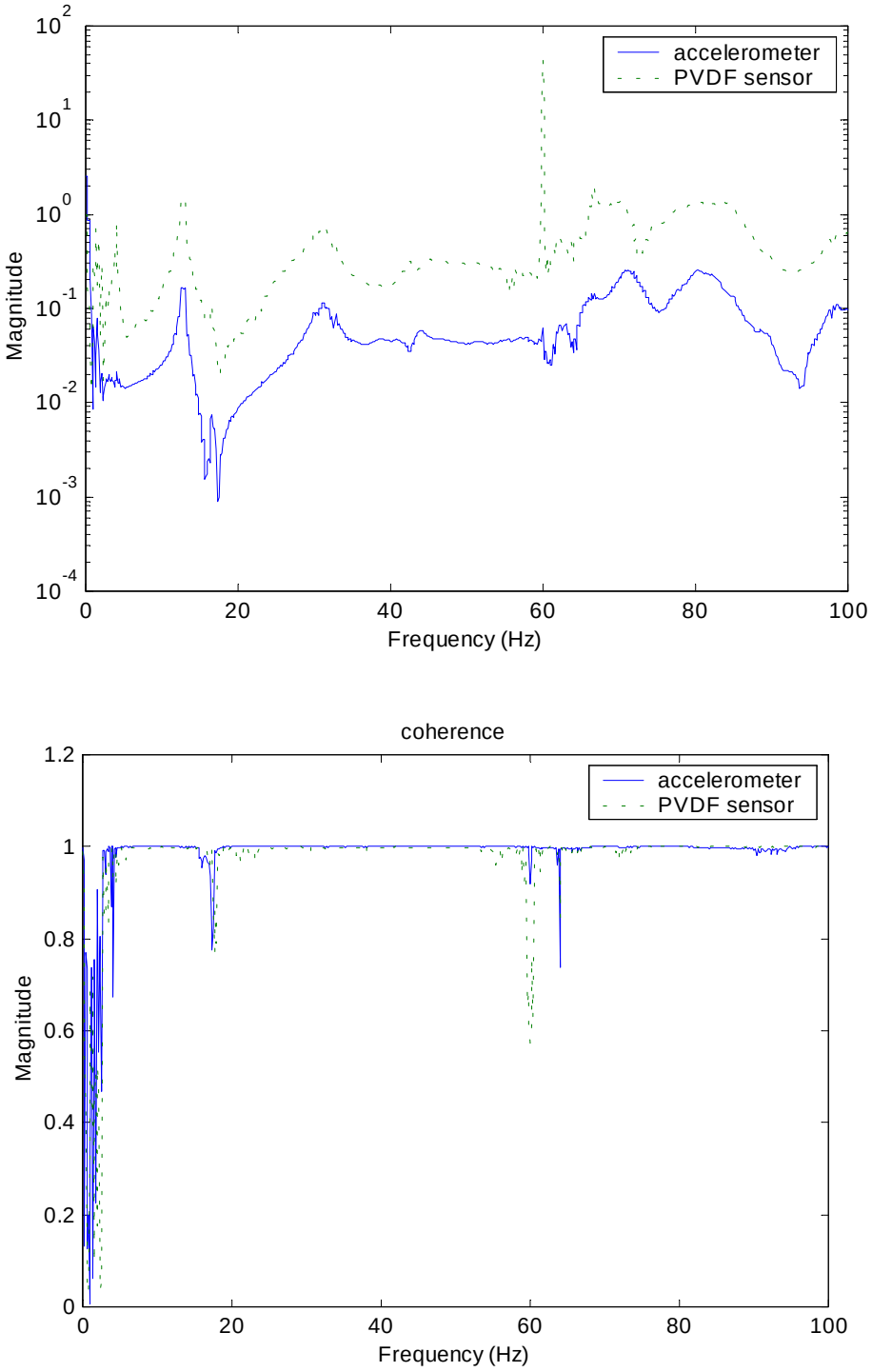

Figure 3.5. Out-of-plane FRF curve (top) and measured coherence (bottom) under electromagnetic shaker excitation and measured with a PVDF sensor and an accelerometer (to provide a baseline measurement comparison).

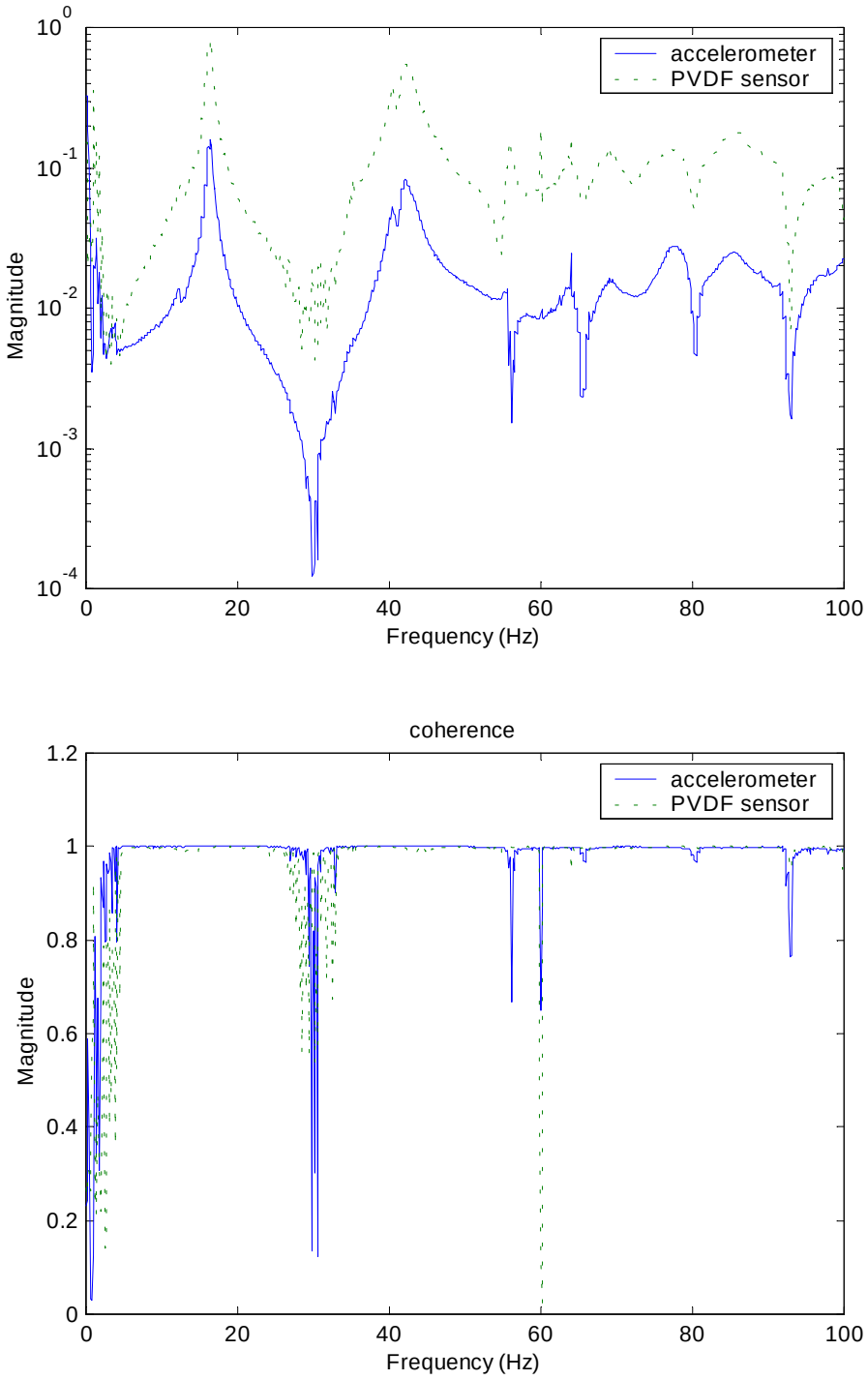

Figure 3.6. In-plane FRF curve (top) and measured coherence (bottom) under electromagnetic shaker excitation and measured with a PVDF sensor and an accelerometer (to provide a baseline measurement comparison).

Mode shapes contain important information for identifying the nature of resonant frequencies (i.e. in-plane, out-of-plane, or shell modes). FRFs alone are inadequate for determining the nature of a resonant frequency, especially near shell mode activity. Therefore, from the collected curve-fitted data, the mode shapes associated with each resonant frequency were plotted in MATLab. As found with finite element techniques, a structure's mode shapes are expected to have a sequential number of nodal lines (Allemang et al., 1994). Therefore, from the collected in-plane and out-of-plane data and under this assumption, we were able to identify the ring mode shapes and differentiate them from the shell modes. Figures 3.7 and 3.8 show the first three out-of-plane resonant frequency mode shapes, and the first two in-plane resonant frequency mode shapes, using an accelerometer and a PVDF sensor, respectively. These mode shapes are generated using the FRF analysis results extracted from the UMPA pseudo least square method. The discrepancy between the apparent smoothness of mode shapes in Figures 3.7 and 3.8 is attributed to imperfect bonding between the PVDF sensor and the double-sided tape used to attach the sensor to the skin of the torus. PVDF sensor results are expected to be more accurate if the sensors are permanently fixed to the skin of a torus with a better adhesive, such as super glue. Table 3.2 summarizes the modal results.

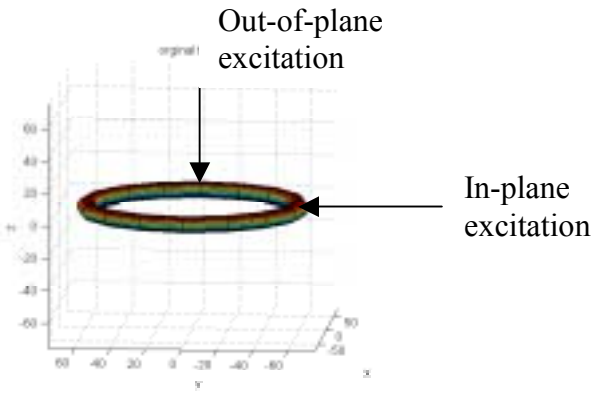

Out-of-Plane

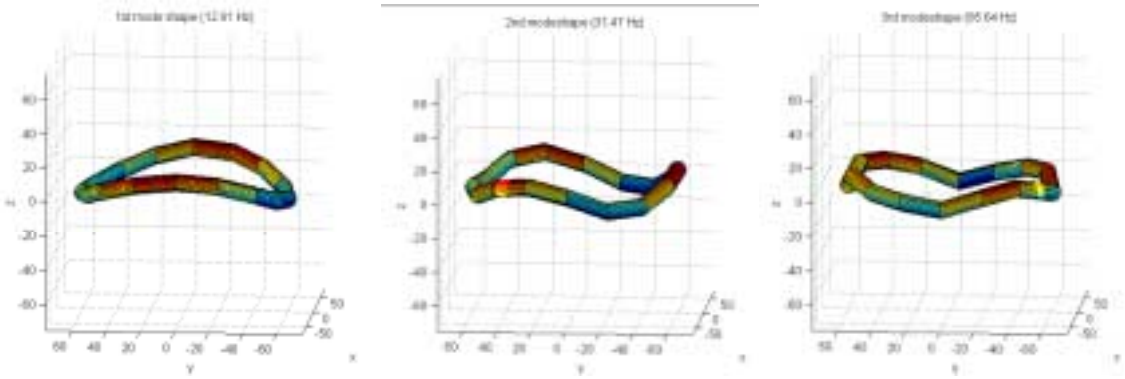

In-Plane

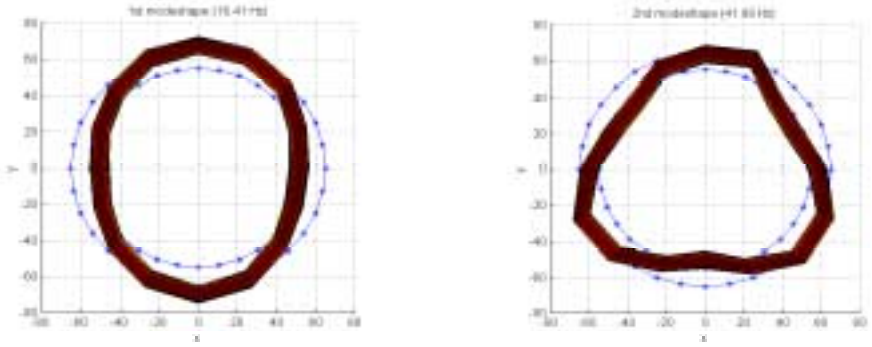

Figure 3.7. Out-of-plane and in-plane mode shapes identified using an accelerometer as a sensor.

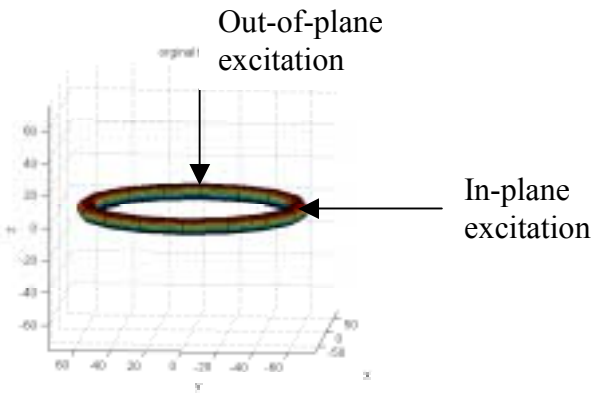

Out-of-Plane

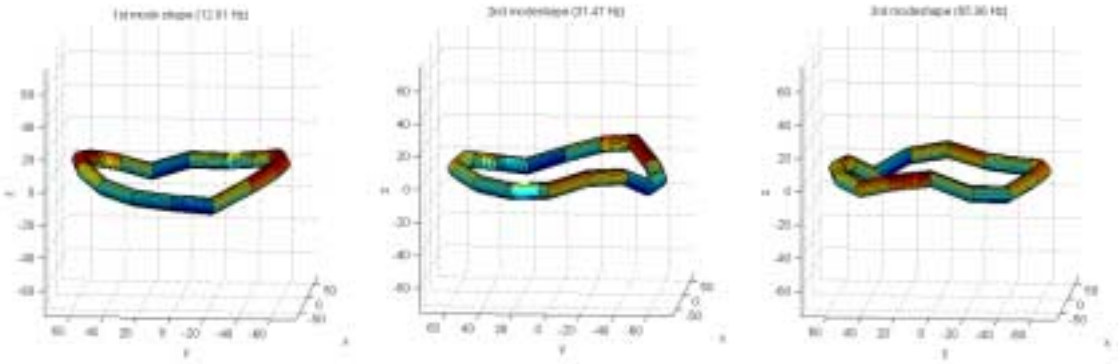

In-Plane

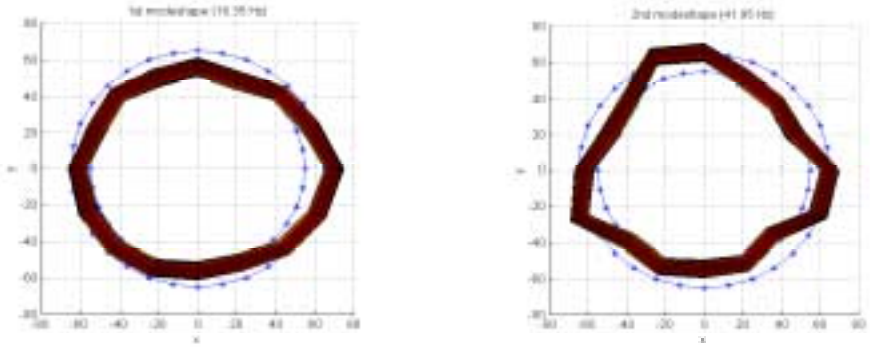

Figure 3.8. Out-of-plane and in-plane mode shapes identified using a PVDF sensor.

Table 3.2. Summary of the out-of-plane and in-plane natural frequencies of the inflated torus as identified from the modal analysis.

In-Plane (Hz)			Out-of-Plane (Hz)		
Mode	Accelerometer	**PVDF sensor**	Mode	Accelerometer	PVDF sensor
1	16.41	16.35	1	12.91	12.91
2	41.99	41.95	2	31.47	31.47
			3	65.64	65.96

The data measured with the PVDF sensors are consistent with those acquired with an accelerometer. These results are consistent with the analytical work performed by Wang and Chen (2000). The identified resonant frequencies using the PVDF sensors are almost identical to those measured with the accelerometer (all are within 0.1%). The experimental results validate the usefulness of PVDF sensors for measuring the dynamics of inflatable space structures. PVDF sensors offer several advantages in the dynamic analysis of inflatable structures. These sensors are flexible enough to conform to the doubly curved surface of the toroidal shell. Thus, they can be fully integrated unobtrusively into the skin of an inflatable structure. In addition, it has been found that PVDF sensors have a minimal effect on the vibratory response of tori even with small aspect ratios. In general, the addition of PVDF sensors decreases the natural frequencies of the torus slightly, as expected from the additional mass, but has little effect on the mode shapes (Williams et al., 2001). PVDF sensors provide an accurate and a logical method for finding the modal frequencies of gossamer spacecraft.

3.3 Macro-fiber Composite Actuation of an Inflated Structure

After identifying the sensing capability of the PVDF films, the next experiment used smart actuators as an excitation source for modal testing actuation. The goal of this portion of the research is to overcome the difficulties associated with using a traditional

shaker input-accelerometer output test. Furthermore, the actuator, if incorporated in an active control scheme, has the potential to actively suppress the vibration of an inflatable structure.

The following experimental procedure is an extension of Park et al.'s (2001) previous work on applying smart actuators, such as an MFC®, to an inflatable structure, but is closer in scale, aspect ratio, and in material of an actual space structure. The MFC® offers high performance and flexibility suitable for applications with inflatable structures. A summary of representative properties and applications of the MFC® device can be found in the Appendix.

3.3.1 Experimental Configuration of the MFC® Actuator

Experiments were performed using the MFC® actuator as the excitation device of an inflated torus. The same configuration was used as described in the shaker-input experiment in section 3.2.4. The actuator was bonded to the surface of the torus with double-sided tape, as shown in Figure 3.9. The SigLab analyzer produced an 8 V chirp signal varying from 10-200 Hz. The input signal was then amplified by a factor of 100 through a TREK High Voltage Power Supply (model 50/750), and thus applied 800 volts to the actuator. Both an accelerometer and a PVDF sensor were used to measure the dynamic response.

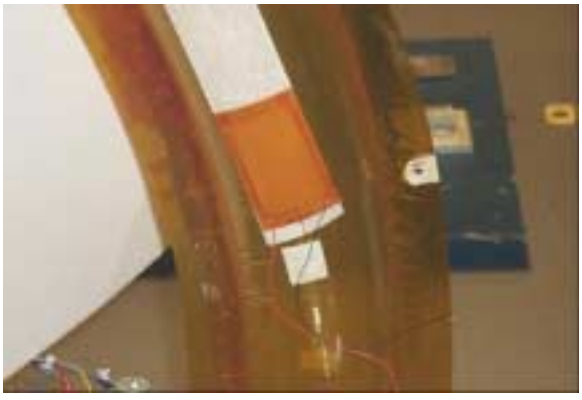

Figure 3.9. MFC® actuator attached to the skin of the torus with double-sided carpet tape.

3.3.2 Results and Analysis

A group of typical frequency response and coherence curves resulting from MFC® actuation are illustrated in Figures 3.10 and 3.11. As shown, the MFC® actuation is effective up to 200 Hz, where the shaker was only able to excite up to 100 Hz. In addition, the sensors clearly pick up the signal 180 degrees apart from the actuator (on both sides), which indicates that the actuator is able to excite the entire torus. However, there are some limitations associated with the SISO methodology presented, and such limitations will be discussed in section 3.4.

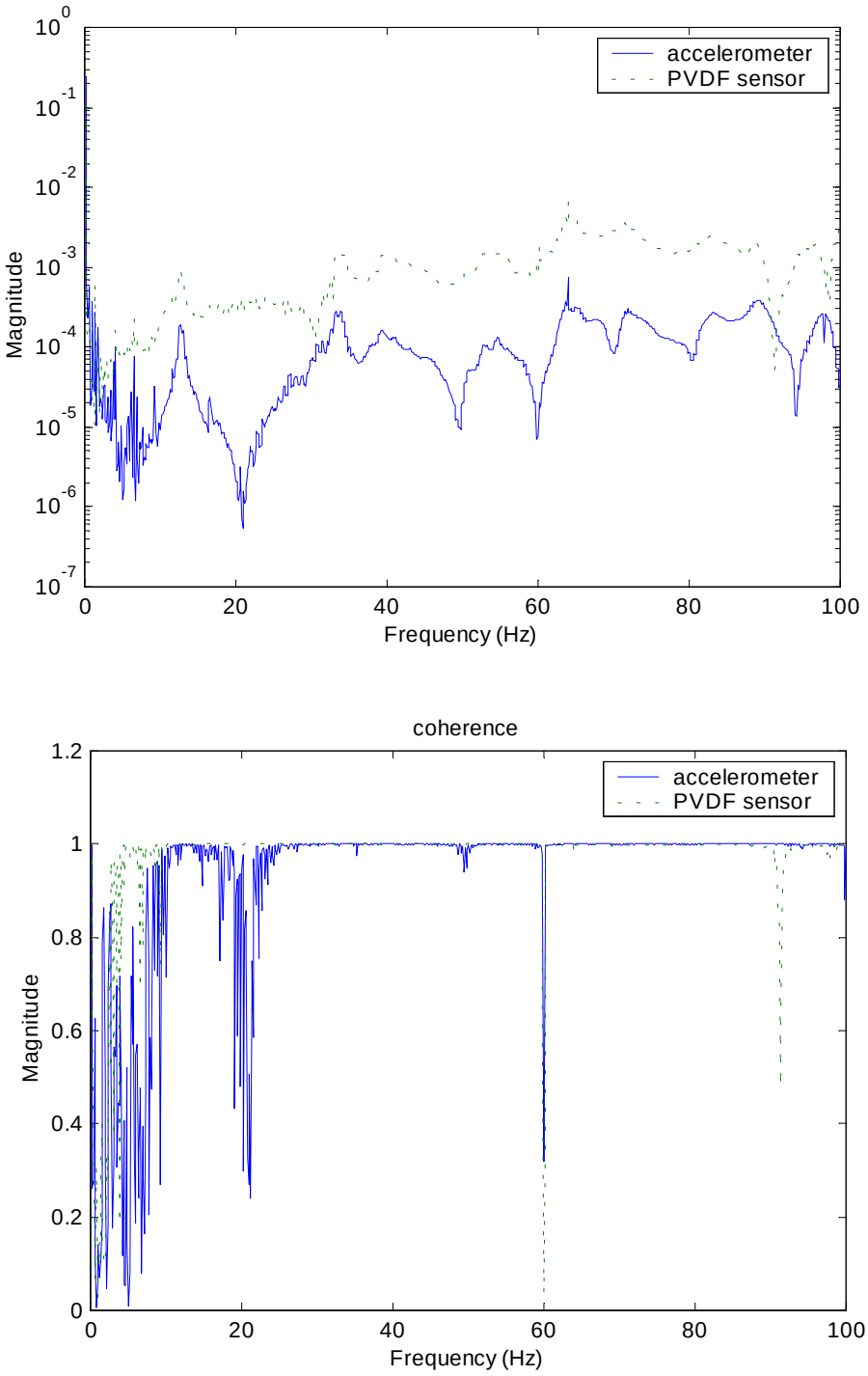

Figure 3.10. Sample FRF curve (top) and corresponding coherence measurement (bottom) using an MFC® actuator as the method of excitation (10 – 100 Hz range).

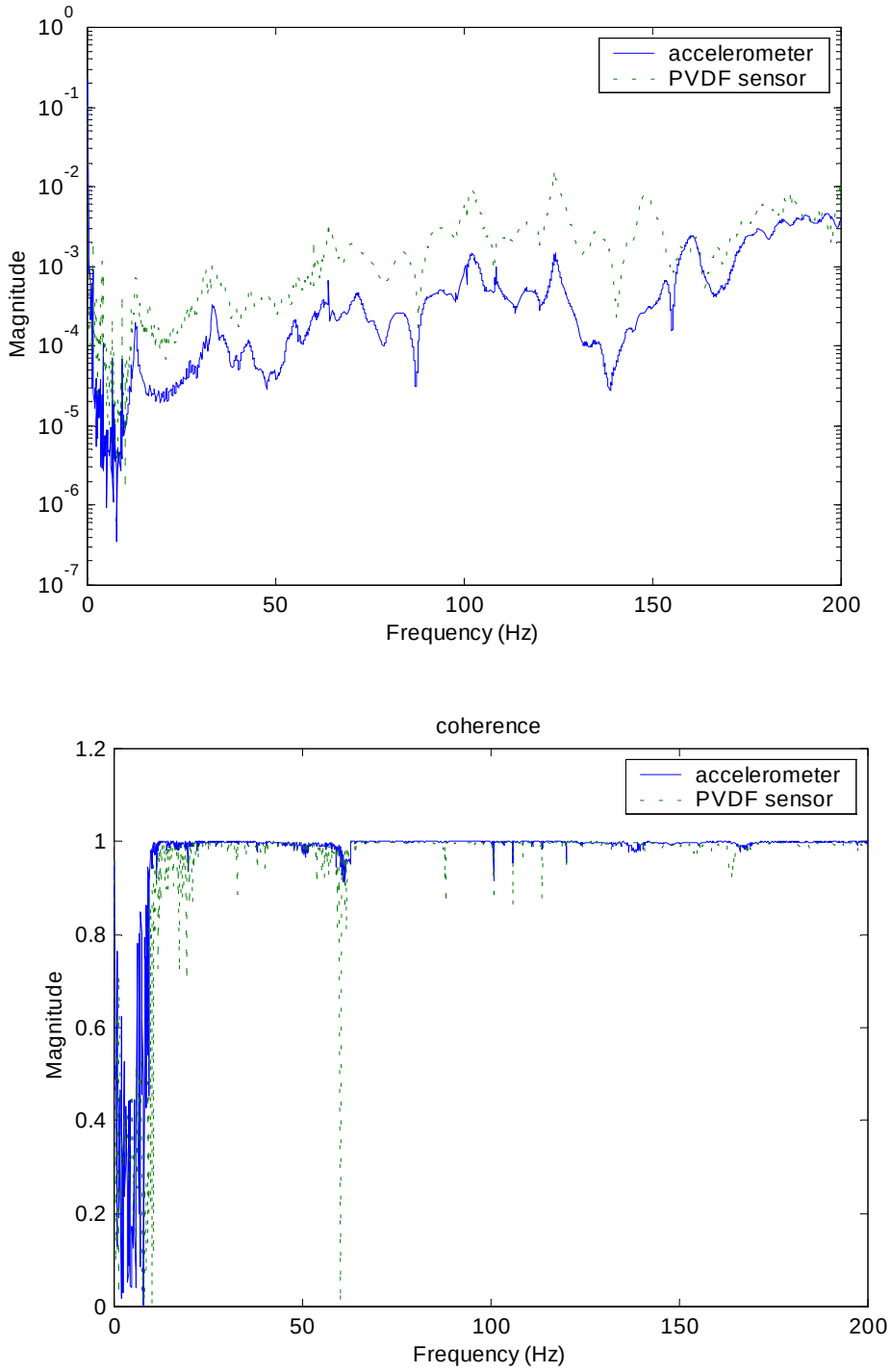

Figure 3.11. Sample FRF curve (top) and corresponding coherence measurement (bottom) using an MFC® actuator as the method of excitation (10 – 200 Hz range).

The identified resonant frequencies and mode shapes (out-of-plane only, measured with an accelerometer) are illustrated in Figure 3.12. The identified resonant frequencies are almost identical between MFC® and shaker excitation. When compared to Figure 3.7, the out-of-plane mode shapes do not appear to be as smooth looking. The reason for this discrepancy is related to the methods of excitation. In Figure 3.7, a shaker aligned in the out-of-plane direction specifically excited the out-of-plane modes. In Figure 3.12, the MFC® actuator, due to its physical geometry, could not specifically excite the out-of-plane modes. Since the MFC® actuator excites both planes of motion, the resulting mode shapes show significant contributions from both planes of excitation. The MFC® actuator is light enough so that the mass loading of the actuator is negligible, of great advantage compared to conventional sources of excitation. The identified resonant frequencies of both in-plane and out-of-plane modes are summarized in Table 3.3. Since the in-plane measurement points are located along the joined region of the torus (where the structure is noticeably stiffer), it was difficult to obtain the in-plane motions. In contrast, the out-of-plane motions were much easier to measure.

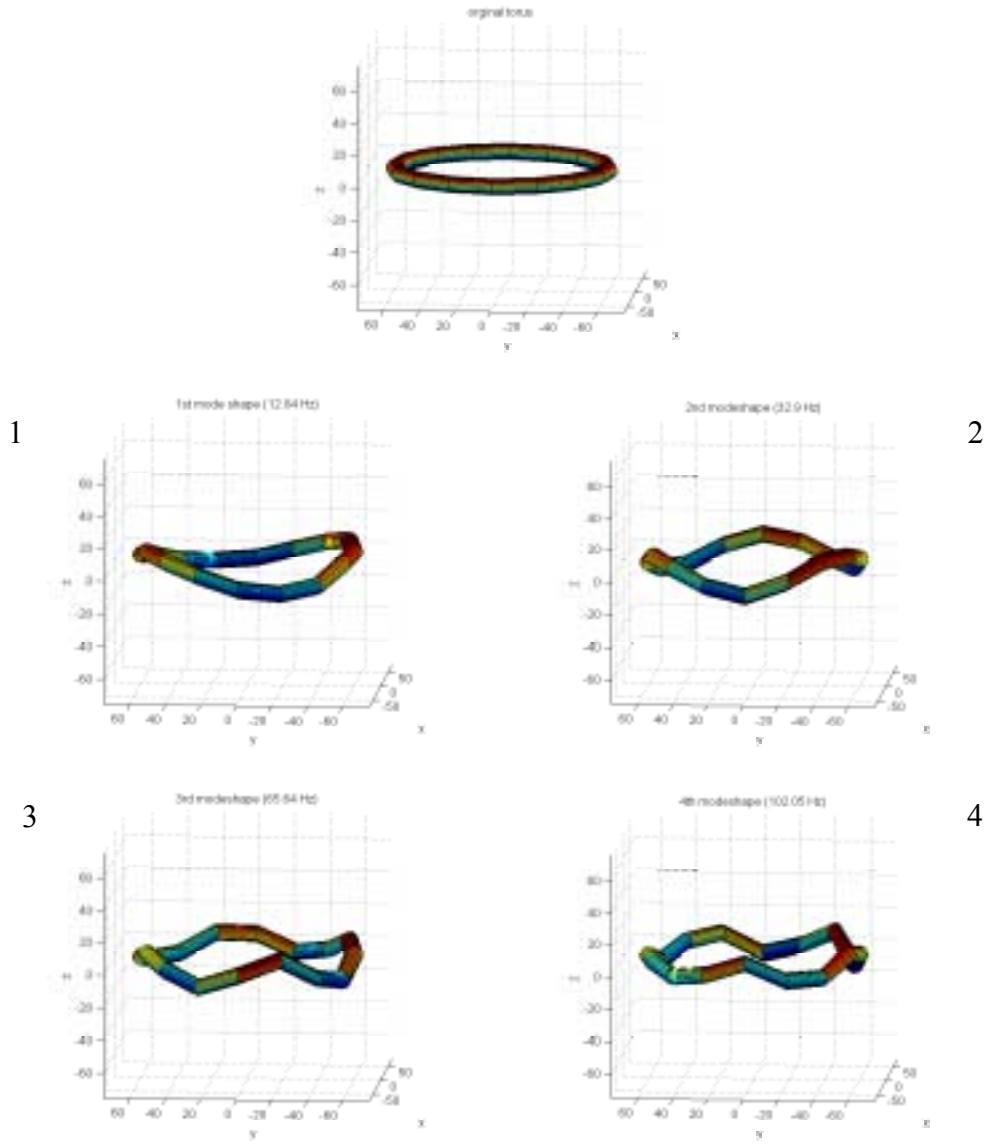

Figure 3.12. Identified out-of-plane mode shapes using an accelerometer as a sensor and an MFC® actuator as the input energy device. The mode shapes are numbered to show increasing nodal lines at higher frequencies.

Table 3.3. Identified in-plane and out-of-plane resonant frequencies of the inflated torus using an MFC® actuator as the input energy device.

In-Plane (Hz)			Out-of-Plane (Hz)		
Mode	Accelerometer	PVDF sensor	Mode	Accelerometer	PVDF sensor
1	16.37	16.31	1	12.84	12.81
2	40.24	40.74	2	32.9	31.7
3	68.1	67.78	3	65.64	65.4
			4	102.05	100.92

It was obvious during the tests that the MFC® excitation produced less interference with suspension modes of the free-free torus than excitations from the shaker. Without connections to the ground (except for an electrical cable), these actuators and the PVDF sensor can be considered an integral part of an inflated structure. The MFC®-PVDF combination could also be used as control devices of an inflatable structure for both vibration suppression and static shape control.

3.4 The Limitations of SISO Experimentation

Single input single output (SISO) experimental modal analysis techniques are cost effective and relatively straightforward methods of structural dynamic analysis. However, SISO dynamic analysis techniques are limited in terms of their ability to properly identify the true dynamic behavior of structures. Because the gossamer torus is nearly symmetric (the true symmetry is broken by the added epoxy mass along the lining of the torus as well as the pendulum boundary condition), we would expect to see two mode shapes at particular resonant frequencies that are identical in nature but orthogonal to one another. This phenomenon, called mode pairing, is typical of near axi-symmetric structures like the torus (Lewis, 2000). Figure 3.13 demonstrates the mode pair phenomenon at the first out-of-plane resonant frequency (12.8 Hz) of the torus.

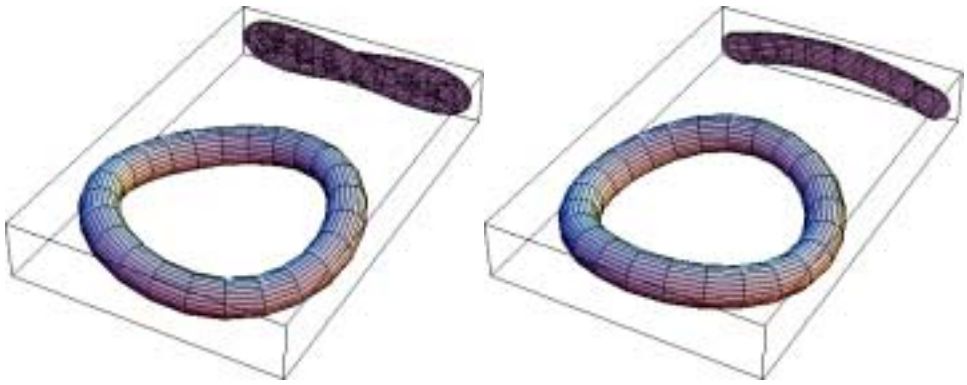

Figure 3.13. Orthogonal mode pair of an axi-symmetric torus found at the first out-of-plane resonant frequency. The cross-section of each mode pair is also shown.

Unfortunately, the separation between the mode pairs may be at such a small scale that the signal noise of the sensor or the resolution of the data acquisition system may not be able to distinguish the two resonant responses. Or, in a more likely fashion, the dual peaks may be smeared together as one, and consequently be misinterpreted as a single mode. One method of trying to correct this problem is to increase the number of inputs and outputs of our experimental modal analysis. The benefits of a multiple input multiple output modal methodology will be discussed in the next chapter.

3.5 Chapter Summary

In this experiment, the extremely flexible nature of the inflatable torus made collecting modal parameter information quite difficult. In particular, local excitation with a shaker and a MFC® as a point input only exaggerated the local properties of the structure. To eliminate the localized effect, the structure was excited over a small bandwidth (30 Hz) and the sampling rate of the SigLab Analyzer was consequently increased. By focusing on the small bandwidth, the entire structure was provided with sufficient input energy, and the global modes were thereby excited. Also, by increasing the sampling rate, the signal analyzer was able to extract most of the modal

characteristics of the torus. SISO experiments are easy to perform, do not require expensive hardware, and can be used to get a strong understanding of the dynamic behavior of a structure.

Although the previous two experiments demonstrated the feasibility of using smart materials to obtain reliable FRF measurements, the ability of the SISO technique to accurately extract the modal pairs of the torus is highly doubted. Further, the question remains as to whether the MFC® actuators have enough actuation authority to excite the global modes of a true gossamer space structure, which could be up to 25 m in diameter. Chapter 4 explores the use of multiple actuators and sensors in the dynamic characterization of a gossamer structure.

CHAPTER 4: Multi-Input Multi-Output Experimental Modal Analysis of an Inflated Torus

4.1 Background

In space, the inflatable torus used for a telescope or radiometer design could have a diameter as large as 30 m. Although one MFC® actuator could globally excite the test set-up during the previous experiments, which has a 1.8 m diameter, it is still questionable that a single MFC® patch could produce adequate actuation for modal parameter identification in structures closer in scale to an actual gossamer satellite. In order to overcome this limitation, experiments were performed in which a multiple number of MFC® actuators were used to provide input excitations. This chapter outlines the theoretical background as well as the actual testing of the prototype gossamer structure using multi-input multi-output (MIMO) techniques.

4.2 MIMO Theoretical Development

The formulation of the MIMO testing technique equations is based upon the single-input single output (SISO) techniques outlined in Chapter 3. In the SISO experimentation, a single MFC® patch was used to excite the torus and a single sensor was used to sense the torus's vibratory response. The relationship between the input signal and the output signal formed the frequency response function of the torus. In a MIMO testing configuration, two MFC® actuators are used to simultaneously excite the torus while two MFC® sensors are used to measure the response. A schematic of the two types of system excitation, namely SISO and MIMO, are shown in Figures 4.1 and 4.2, respectively.

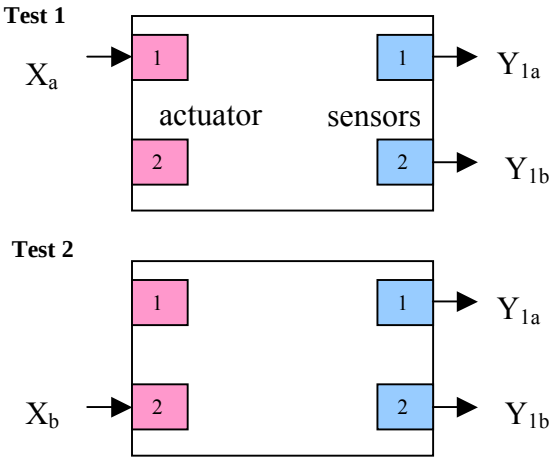

Figure 4.1. SISO tests to estimate FRFs.

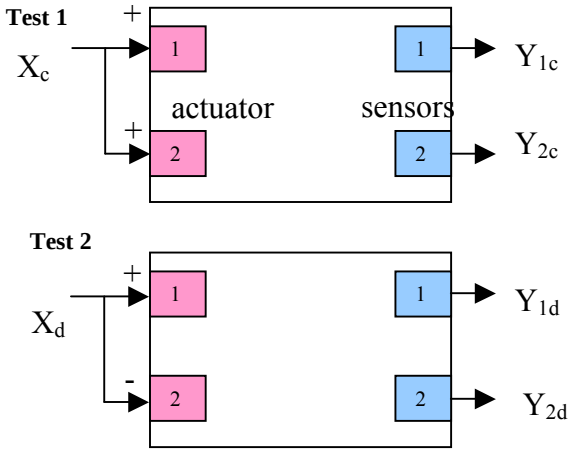

Figure 4.2. MIMO tests to estimate FRFs.

With two actuators and two sensors in place, we can estimate frequency response functions with a few experiments. Two experiments (as shown in Figure 4.2) will give the following FRF matrix:

$$H_1 = \begin{bmatrix} H_{11} & H_{12} \\ H_{21} & H_{22} \end{bmatrix}, \tag{4.1}$$

where $H_{11} = \frac{Y_{1a}}{X_a}, H_{21} = \frac{Y_{2a}}{X_a}, H_{12} = \frac{Y_{1a}}{X_b}, \quad H_{22} = \frac{Y_{2a}}{X_b}$. In the formulation, Y refers to the sensor output at a given MFC® sensor, and X refers to the input signal to a given MFC® actuator.

Each column of the FRF matrix can be constructed during the experiment in a SISO experiment. This is common practice in modal testing for almost all structures. However, for flexible, large-scale inflatable structures, only exciting a single point may cause poor distribution of input energy throughout the structure and result in somewhat distorted frequency responses.

For the multi-input testing, a single in-phase signal is applied to both actuators for the first experiment (test 1 in Figure 4.2) and, for the second experiment (test 2 in Figure 4.2), a single out-of-phase signal is supplied to both actuators, as illustrated by the "+" and "–" signs.

By using a multi-input test, we can estimate the same FRF matrix after a post-processing procedure. This method provides better energy distribution and even better actuation forces. The method is based on the "multi-phase stepped sine" test, but may also be used with a chirp signal. In either case, it is imperative that the transient response at the tail end of the frequency sweep is allowed to completely die out (Guan et al., 2000); otherwise, uncorrelated data will be introduced into the averaged FRF. In order to estimate the FRF matrix, the following procedure is required.

For test 1,

$$\begin{Bmatrix} Y_{1c} \\ Y_{2c} \end{Bmatrix} = H \begin{Bmatrix} X_c \\ X_c \end{Bmatrix} = H \begin{Bmatrix} 1 \\ 1 \end{Bmatrix} X_c$$

and for test 2,

$$\begin{Bmatrix} Y_{1d} \\ Y_{2d} \end{Bmatrix} = H \begin{Bmatrix} X_d \\ -X_d \end{Bmatrix} = H \begin{Bmatrix} 1 \\ -1 \end{Bmatrix} X_d$$

By dividing Equations (4.2) and (4.3) by X_c and X_d, respectively, we get

$$\begin{Bmatrix} Y_{1c} \big/ X_c \\ Y_{2c} \big/ X_c \end{Bmatrix} = \begin{Bmatrix} H_{1c} \\ X_{2c} \end{Bmatrix} = H \begin{Bmatrix} 1 \\ 1 \end{Bmatrix},$$

$$\begin{Bmatrix} Y_{1d}/X_d \\ Y_{2d}/X_d \end{Bmatrix} = \begin{Bmatrix} H_{1d} \\ X_{2d} \end{Bmatrix} = H \begin{Bmatrix} 1 \\ -1 \end{Bmatrix}.$$

And by adding the two columns leads to

$$\begin{bmatrix} H_{1c} & H_{1d} \\ H_{2c} & H_{2d} \end{bmatrix} = H \begin{bmatrix} 1 & 1 \\ 1 & -1 \end{bmatrix}.$$

Now, the FRF matrix, H, can be constructed by post-multiplying by the inverse of the matrix in Equation (4.6). Theoretically, the FRF matrix H_1 (in Equation (4.1)) and H (in Equation (4.6)) must be the same, unless the structure shows significant non-linearity. Only two pairs of sensors/actuators are described in this section, but one may use any number of actuators if necessary.

4.3 The MIMO Experiment

Experiments were performed following the procedure outlined in section 4.2. Four MFC® patches were attached to the torus at 90 degree intervals as shown in Figure 4.3. First, the torus was checked for non-linearity in the first few modes of interest. Then the FRFs, both SISO and MIMO, were measured and compared. The torus was maintained at 0.75 psi during this phase of the experimentation.

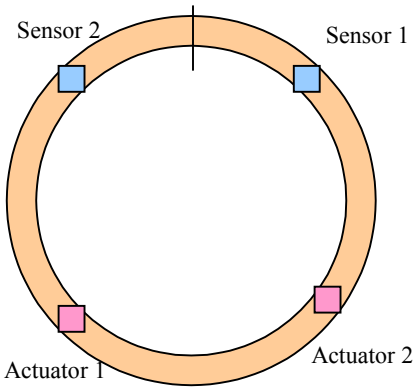

Figure 4.3. Experimental setup with multiple sensors and actuators.

4.3.1 Linearity Check

In order to establish the linearity of the test structure, the frequency response function was generated using two distinct input voltages, 250V and 500V. An MFC® actuator was used to excite the torus, and an MFC® sensor was used to sense the vibratory response. This is the first time in the known literature that the MFC® device has been used as a sensor. By overlaying the two FRFs, any deviation between the two curves will identify some sort of nonlinear behavior. Such an assumption is based on the fact that for a linear system, increasing the input by a factor should increase the output by the same factor. The results of the linearity check are shown below in Figure 4.4.

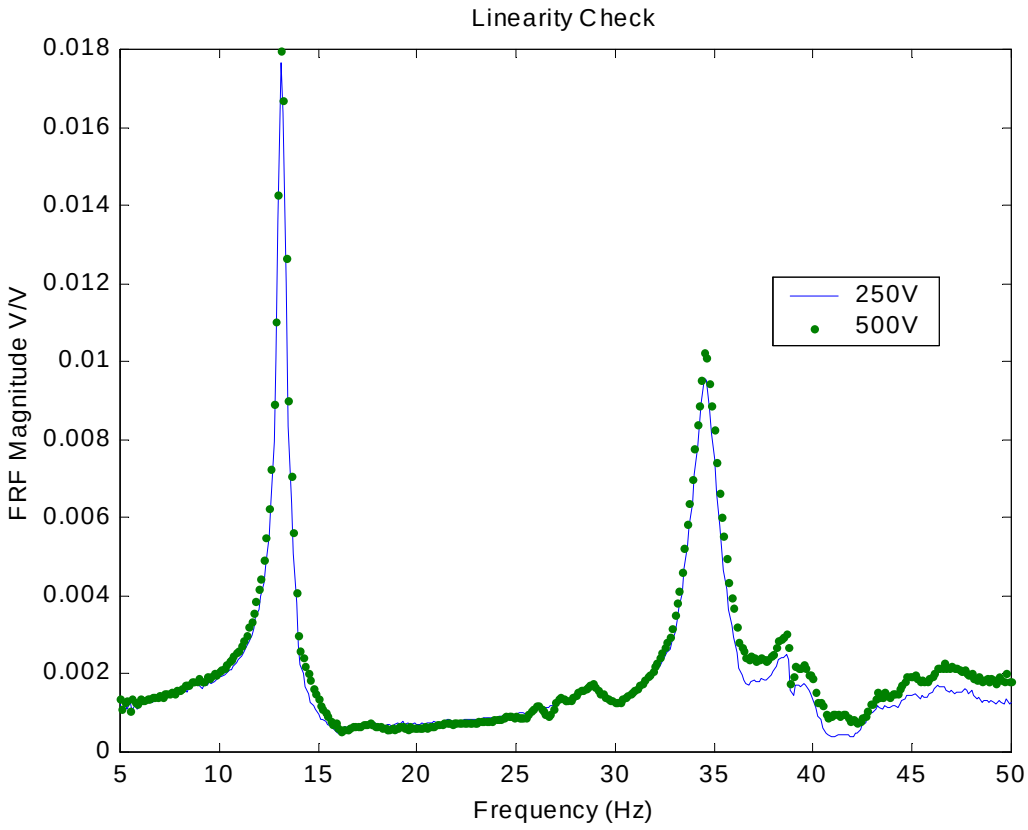

Figure 4.4. Linearity check FRF results from the torus.

As shown in Figure 4.4, the torus primarily demonstrates linear system behavior from 5 - 50 Hz. Therefore, the theoretical development for a MIMO testing technique as presented in section 4.2 should be applicable to the torus.

4.3.2 MIMO Experimental Results

The experiment was performed using similar data acquisition techniques outlined in Chapter 3. A chirp signal was applied to the torus sweeping from 5 to 50 Hz. The signal was applied for 4 seconds, and then turned off for 4 seconds. The 'burst' chirp signal effectively allowed the transient response of the torus to die out before the next FRF curve was estimated (Guan et al., 2000). A series of ten averages were used in the FRF estimation. As shown in Figure 4.5, the MIMO testing identifies better FRFs with higher coherence functions even for this structure. By providing a better distribution of input energy, this method can avoid exaggerated local excitations.

Experimental results are shown in Figures 4.6 and 4.7 in the frequency range of 5 to 50Hz. In both figures, note that the nomenclature refers to the input first, and then the output. So for example, H11 refers to actuating at MFC® 1 (in Figure 4.3) and sensing with MFC® 1 (in Figure 4.3).

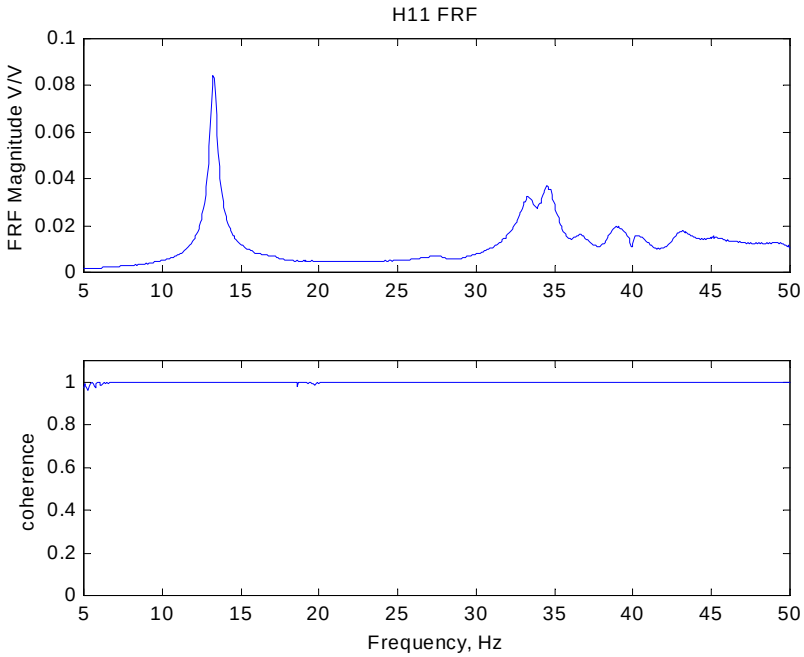

Figure 4.5. Sample MIMO FRF curve (top) and measured coherence function (bottom).

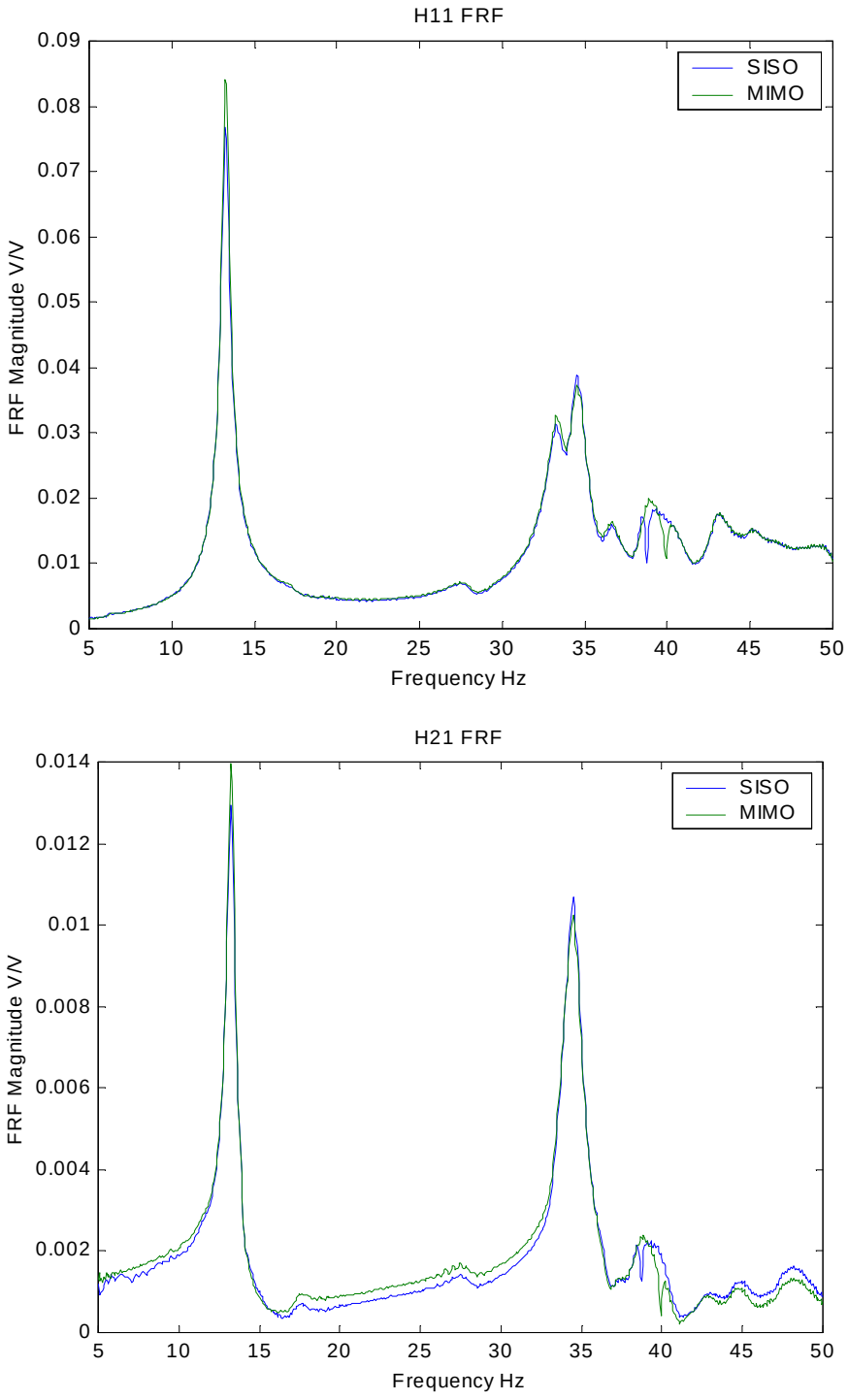

Figure 4.6. H_{11} (top) and H_{21} (bottom) FRF comparison between SISO and MIMO testing methods.

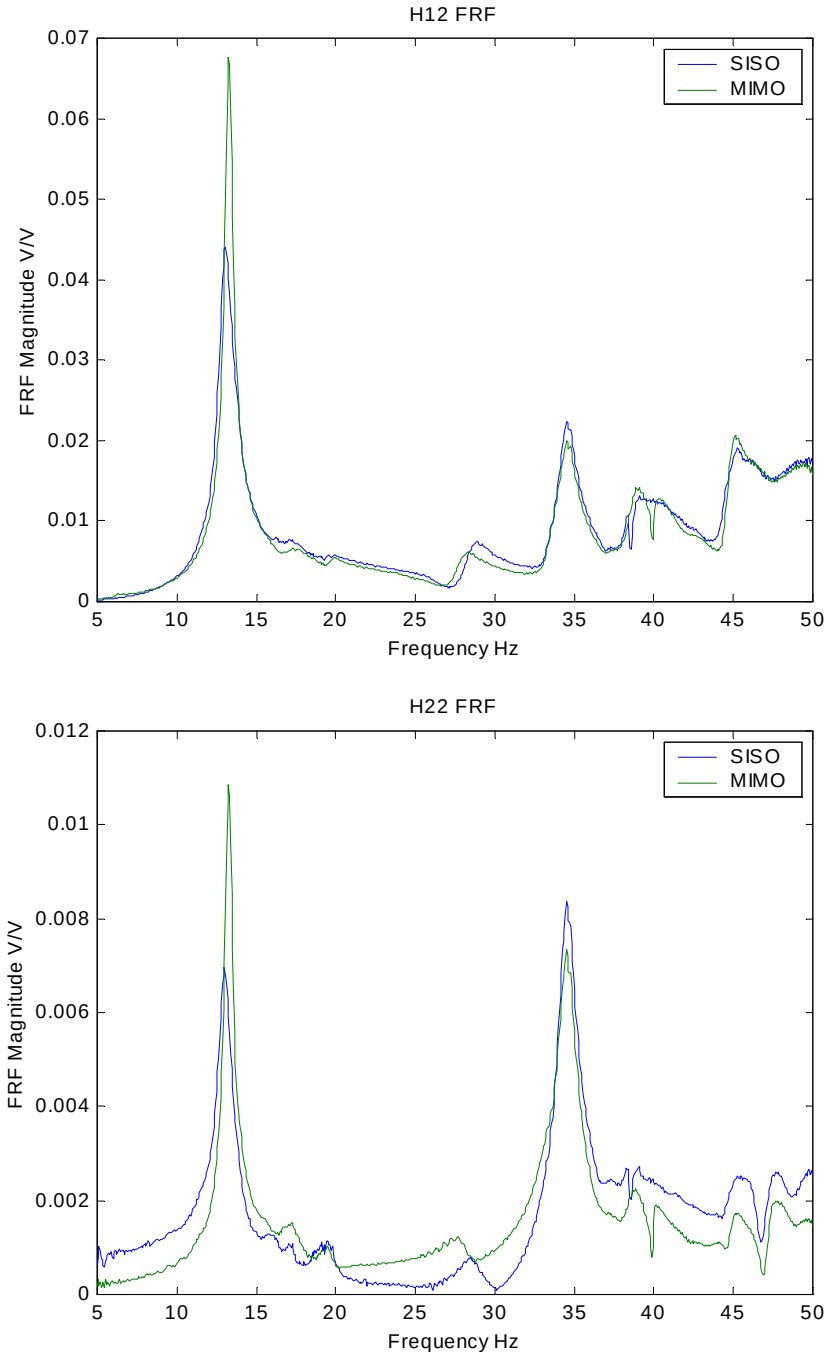

Figure 4.7. H_{12} (top) and H_{22} (bottom) FRF comparison between SISO and MIMO testing methods.

4.3.3 Post-Processing the Results

After collecting the FRF data as reported in section 4.3.2, the MIMO frequency response function matrix, *H*, from Equation 4.6, was constructed in MATLab. The FRF matrix, *H*, was then the input for a polyreference function (least squares) code developed in part by Dr. Jan Wright at the University of Manchester (UK). In brief, the polyreference function estimates the total number of modes within a specified bandwidth and calculates the eigenvalues and corresponding damping coefficients while trying to curve fit a given FRF. A stability criterion is established within the program to continuously check to see if the damping coefficients have stabilized to some value. A sample stability diagram depicting the polyreference function's output is shown in Figure 4.8. A summary of extracted modal data for the first five modes is shown in Table 4.1.

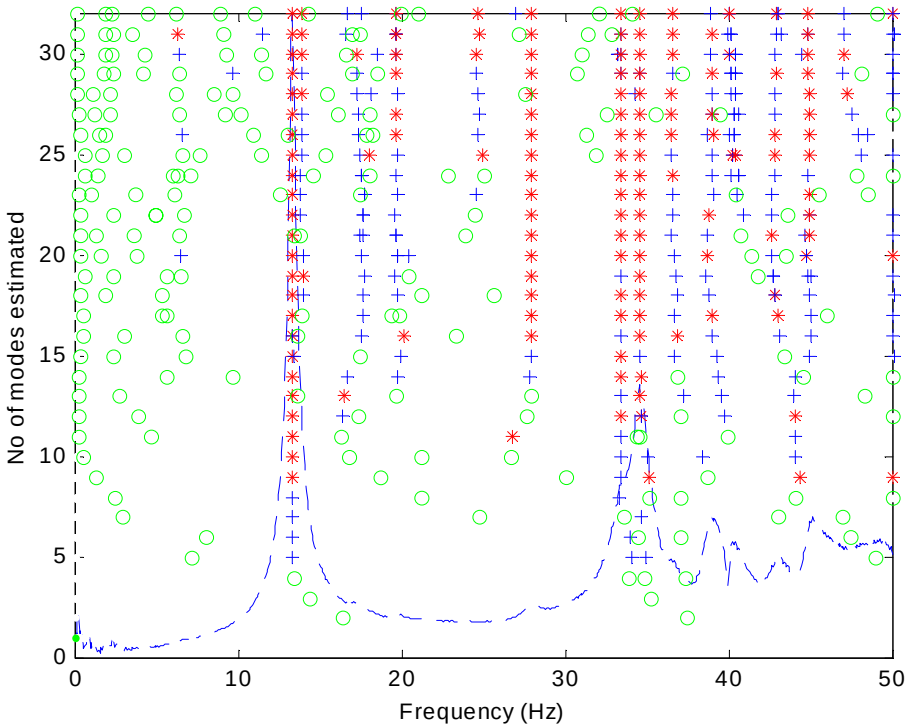

Figure 4.8. Output plot of the polyreference function program. The vertical alignment of symbols are at identified eigenvalues of the FRF. Red stars indicate when the damping coefficient and eigenvalue have settled to within 1/100 of the previous calculated value.

Table 4.1. Comparison between SISO and MIMO identified eigenvalues of the torus (at 0.75 psi).

Mode #	Frequency Identified (Hz)	
	SISO	**MIMO**
1	13.7	13.26
Mode Pair	N/A	13.85
4	33.5	33.41
Mode Pair	N/A	34.53
5	43.1	42.81
Mode Pair	N/A	44.89

The identified FRFs are almost identical from both single-input and multi-input experiments. This is mainly due to the fact that single MFC® can provide enough excitation for the torus, which would not be possible for a large-scale inflatable torus. Further, as shown in Table 4.1, the MIMO testing technique is able to decipher the modal asymmetry, which occurs when a mass imbalance on a symmetric structure splits a resonant peak in two. The split mode at a given frequency is known as a mode pair, and they can be seen in the stability diagram of Figure 4.8.

4.4 Chapter Summary

MIMO dynamic testing techniques are demonstrated for a prototype gossamer torus. A theoretical model is developed for a two actuator, two sensor system. Experimental results are presented to validate the theoretical development. The methodology presented in this research gives better results than the more traditional SISO technique. In particular, the MIMO dynamic analysis technique is able to identify pairs of modes that occur at nearly identical frequencies. SISO experiments are not reliable when it comes to the accurate identification of mode pairs because they are unable to positively decipher mode pairs from signal noise in measured FRFs. For example, the

mode pair at 13.26 and 13.85 Hz was originally interpreted as a single mode at 13.7 Hz (Table 4.1). Depending on the application, the smearing of mode pairs into single modes may adversely affect a control algorithm, depending on the algorithm's sensitivity to the identified resonant frequencies of the system. Further, when considering the magnificent scale of future gossamer satellites, multiple piezoelectric patches like the MFC® actuator will be necessary for proper control and sensing authority in the global sense of the structure.

CHAPTER 5: Positive Position Feedback Control of a Plate Using an MFC® Sensor

5.1 Introduction

This chapter focuses on the dynamic analysis and active vibration suppression of a simply supported plate using positive position feedback (PPF) controller and MFC® actuators and sensors. The goals of performing these experiments are to 1) validate the methodology developed in Chapter 3, and 2) understand the capabilities of MFC® actuators/sensors. A successful demonstration of vibration analysis and control of a plate using these devices can help identify the capabilities and limitations of the MFC® devices. Once the method is understood and validated for a simple structure, applications for a more complicated structure, like the inflated torus, will be relatively easier.

An outline of the chapter is as follows. Section 5.2 gives background information on PPF controller. Section 5.3 discusses the analytical solutions for the natural frequencies of a simply supported plate and describes the experimental setup for the modal analysis of the same. Section 5.4 describes the experimental setup for implementing the PPF controller on the plate and details the experimental results. Finally, Section 5.5 summarizes the results.

5.2 Background on Positive Position Feedback Control Theory and Implementation

The idea of a PPF controller was first introduced by Goh and Caughey (1985). A PPF controller, sometimes referred to as a PPF filter, can be understood through a set of equations describing the interaction between the behavior of the structure as well as the compensator. Using a PPF controller, vibration of the different modes of a structure can be targeted individually. The equation governing the vibration of a structure at the n^{th} mode can be described by the following equation:

$$\ddot{\xi}_n + 2\zeta_n \omega_n \dot{\xi}_n + \omega_n{}^2 \xi_n = f_n \tag{5.1}$$

where ξ_n is the modal coordinate, ω_n is the natural frequency, ζ_n is the modal damping, and f_n is the modal force. The modal force generated by the controller is given by

$$f_n = g_n \omega_n{}^2 \eta_n \tag{5.2}$$

where g_n is a positive scalar gain and η is generated by the controller, which is described by the following second-order differential equation:

$$\ddot{\eta} + 2\zeta_f \omega_f \dot{\eta} + \omega_f^2 \eta = \omega_f^2 \xi \tag{5.3}$$

In Equation (5.3), ω_f and ζ_f are called the frequency and damping ratio of the PPF controller. Usually, the controller assumes a higher damping ratio than the damping ratio of the structure. It can be seen from Equations (5.1) and (5.3) that the controller uses modal coordinates to obtain η, which is subsequently fed back to the structure. A block diagram of the PPF controller is shown in Figure 5.1.

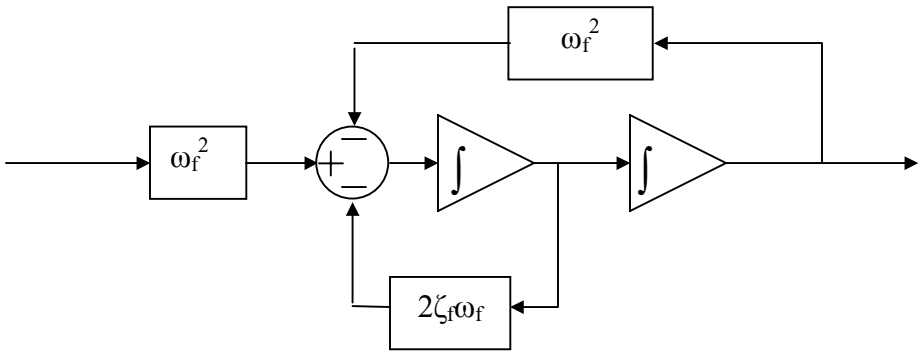

Figure 5.1. A block diagram of a PPF controller.

Fanson and Caughey used pairs of PVDF sensors and actuators to control the vibration of an aluminum beam using a Positive Position Feedback algorithm (Fanson

and Caughey, 1987). The authors used ceramic sensors and actuators on a cantilevered aluminum beam. They also developed a root locus plot to show how the poles of their system were manipulated with the introduction of a PPF controller. The results of the authors' experiments proved the robustness of the PPF controller. Using just two collocated sensor / actuator pairs, the authors were able to control the first six modes of vibration of the structure.

Poh and Baz (1990) developed an extended PPF controller model and called it a Modal Positive Position Feedback controller. The main difference between the two control algorithms is that the MPPF controller uses first order filters to achieve similar controller characteristics as the second-order PPF design. The authors validated their approach by controlling the second mode of vibration of a flexible truss structure using a single piezoceramic actuator.

When it comes to gossamer structures, PPF control stands out as a strong candidate for vibration control. PPF control design features two main benefits when compared to more traditional feedback control algorithms. First, the PPF controller is relatively simple to design and implement into a dynamic system. Second, PPF controllers are rather robust in the presence of parameter uncertainties and improperly modeled (or unknown) system dynamics. Fanson and Caughey (1987) recognized in their work that the phenomenon of spillover (the presence of uncontrolled modes within the bandwidth of the closed loop system) could be avoided by using PPF control because the filter rolls off at high frequency and doesn't put energy into any of the residual modes. In addition, is not destabilized by finite actuator dynamics. When looking at structures as complex as a gossamer torus or strut, parameter uncertainties and unmodeled system dynamics are the norm. Therefore, PPF control is one possible choice for the control of these structures and demonstrating its effectiveness will open the possibility of more advanced control algorithms. Further, the results will help establish a practical basis for implementing more advanced algorithms with the torus or similar structures.

5.3 Dynamic Analysis of a Simply Supported Plate

This section describes the experimental setup and results of using piezoelectric actuators to sense the vibration of a simply supported plate. First, the closed-form solution to the simply supported plate vibration problem is presented. Then, the experimental setup for obtaining the vibratory response of the plate is explained. Finally, the experimental results are compared to the analytical predictions to validate the dynamic analysis technique.

5.3.1 Analytical Solution to the Simply Supported Plate Vibration Problem

A diagram of the simply supported plate under investigation is given in Figure 5.2. A summary of the physical properties of the steel plate is given in Table 5.1.

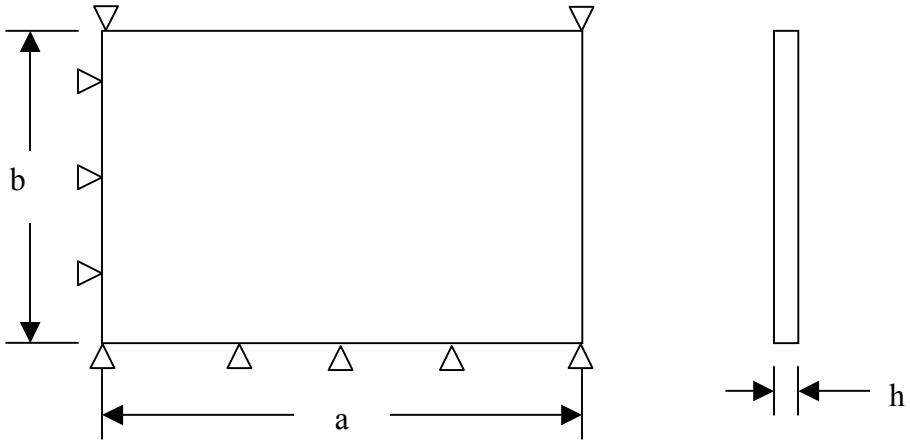

Figure 5.2. Orthographic views of the simply supported steel plate.

Table 5.1. Summary of the physical properties of the cold-rolled steel plate of Figure 5.1.

Property	***Notation***	***Dimension***
Length	a	0.6 m
Width	b	0.5 m
Height	h	0.003 m
Elastic Modulus	E	190 GPa
Poisson's Ratio	v	0.4
Density	p	7920 kg/m^3

The natural frequencies of the system are given by (Meirovitch, 1992)

$$\omega_{mn} = \pi^2 \left[\left(\frac{m}{a} \right)^2 + \left(\frac{n}{b} \right)^2 \right] \sqrt{\frac{D_E}{\rho h}}, \tag{5.3}$$

where

$$D_E = \frac{Eh^3}{12(1-v^2)}. \tag{5.4}$$

A summary of the first three natural frequencies, as predicted by Equation (5.3), is given in Table 5.2.

Table 5.2. The first three natural frequencies of the plate.

Natural Frequency #	**Frequency (Hz)**
1	49.3
2	109.9
3	136.5

5.3.2 Experimental Modal Analysis of the Simply Supported Plate

The next step in the experimental procedure was to perform an experimental modal analysis of the actual test plate. A picture of the test plate is shown in Figure 5.3.

Figure 5.3. The simply supported test plate under investigation.

The test plate was originally fabricated at the Mechanical Engineering shop at Virginia Polytechnic Institute and State University, and was subjected to vibration control tests by Rubenstein et al. (1991). The test plate is held on its edges by a thin steel shim stock, and, correspondingly, the shim stock is bolted to the casing. Such a setup ensures a simply supported boundary condition.

Multiple PZT patches were available for use on the test plate, and designated as Sensors 1-5 throughout the experimentation (as shown in Figure 5.4).

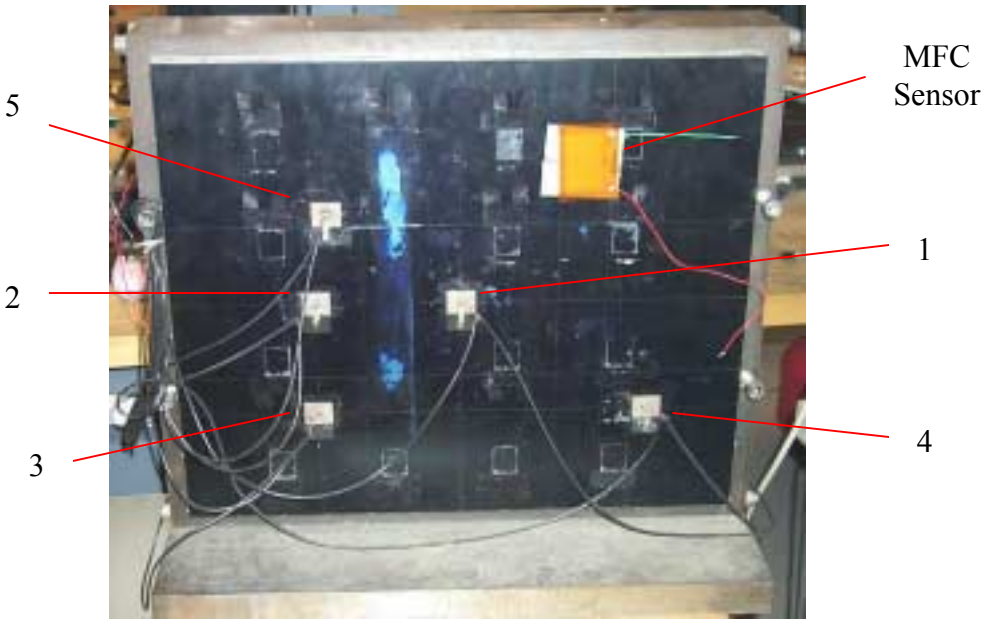

Figure 5.4. The PZT patch location designations assigned to the experiment.

A PZT patch (location 2 in Figure 5.4) and an MFC® device were used as an actuator and sensor, respectively, during the dynamic analysis. A schematic diagram of the experimental setup is shown in Figure 5.5.

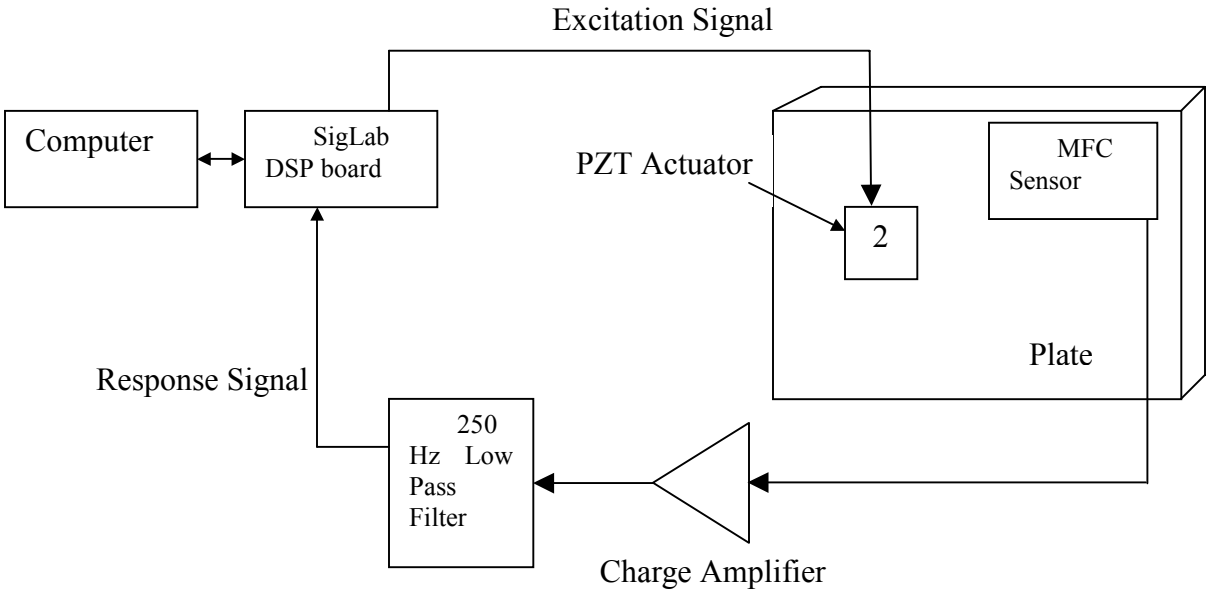

Figure 5.5. Diagram of the experimental setup for the test plate under dynamic analysis.

A simple charge amplifier was designed and built around the measured capacitance of the MFC® sensor (1.19 nF). A diagram of the charge amplifier circuit is shown in Figure 5.6. A picture of the circuit is shown in Figure 5.7.

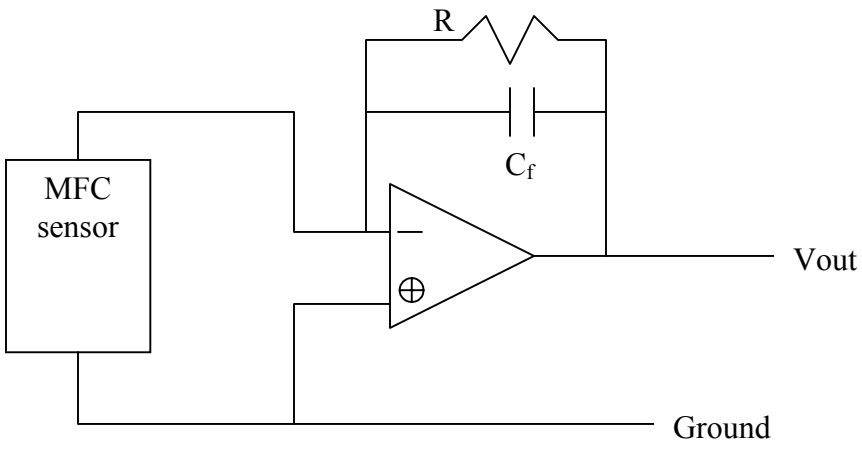

Figure 5.6. Charge amplifier circuit used to amplify the output signal of the MFC® sensor.

Figure 5.7. Photograph of the actual charge amplifier used in the experiment.

Referring to Figure 5.6, the feedback capacitance, C_f, was 24 nF, the feedback resistance, R, was 6.32 MΩ, and the operational amplifier was model LM348/LM248. The output of the charge amplifier was filtered through a 250 Hz Ithaco low pass filter (model 4302) to eliminate any high-frequency content in the sensed vibratory signal. Further, because of

the high voltage applied to the PZT patch (~100 V), the steel plate had to be properly grounded or else the electromagnetic effect would deteriorate the signal from the MFC® patch.

Under the experimental setup as shown in Figure 5.5, the dynamic response of the plate was obtained using a 5 V chirp signal (from 30 to 200 Hz) in SigLab. Both an accelerometer and an MFC® sensor were used to record the vibratory response of the plate. A comparison between the two readings is shown in Figure 5.8. Notice the similarity between the two curves, especially at the resonant frequencies. The same trends between the MFC® signal and the accelerometer signal established in Chapter 3 for the dynamic analysis of the torus again hold true for the dynamic analysis of the plate.

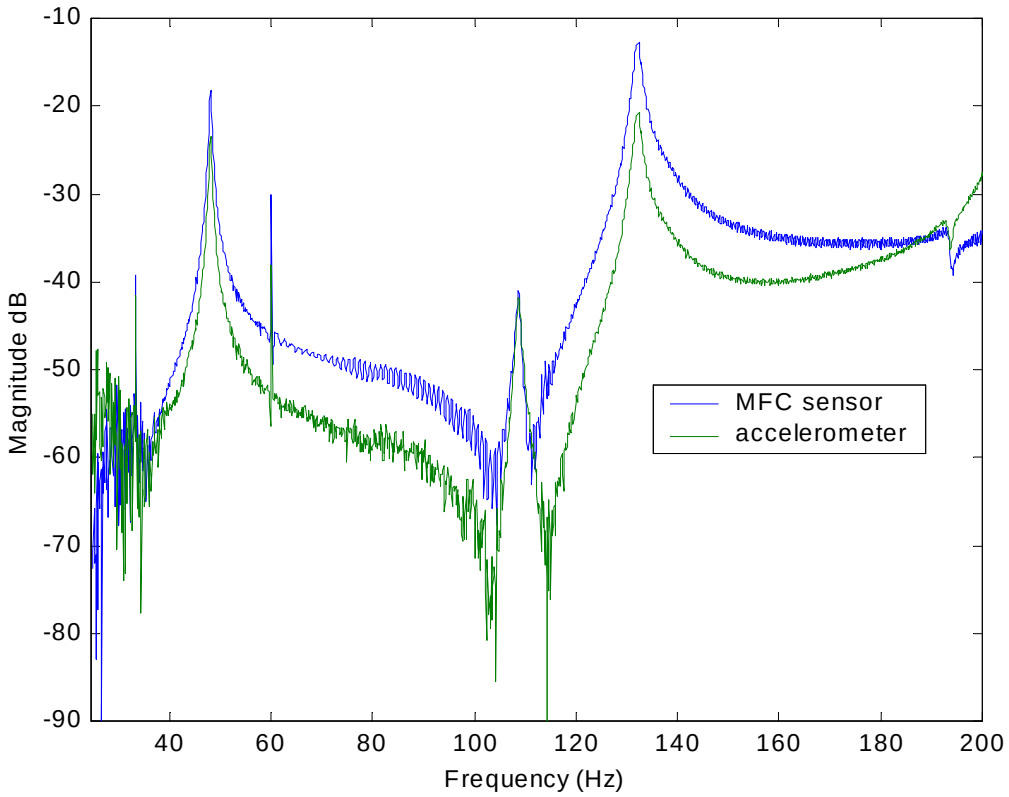

Figure 5.8. Frequency response function of the test plate (excited from 30 – 200Hz), as sensed by an MFC® patch (blue) and accelerometer (green).

A comparison between the experimentally determined resonant frequencies and the analytically determined resonant frequencies of the simply supported plate is given in Table 5.3.

Table 5.3. Comparison between the analytically and experimentally determined resonant frequencies of the simply supported plate.

Mode #	Identified Resonant Frequency (Hz)		Analytical - Experimental % Deviation
	Analytical	Experimental	
1	49.3	49.0	0.61
2	109.9	108.0	1.73
3	136.5	132.8	2.71

As shown in Table 5.3, there is less than 3% deviation between the experimental and analytical resonant frequencies. The superior sensing capabilities of the MFC® device were further evidenced by the dynamic analysis experiment. After determining the natural frequencies of the test plate using PZT patches and the MFC® sensor, the next step is to control its first mode of vibration using a PPF controller.

5.4 Vibration Control of a Simply Supported Plate Using a PPF Controller

Cole (1992) designed a single input, multiple output LQG control technique to actively reduce the vibration of a simply supported plate. Cole used one of five PZT actuators (1.2" x 1.0") and sixteen PZT sensors (1.0" x 1.1") in the experiment. The actuators were placed at the antinodes of the plate's first five modes. The sensors were organized in a grid fashion on the face of the plate. The SIMO LQG controller attacked the modes of the plate that fell below 200 Hz due to limitations in the data acquisition system used. In Cole's experiment, a 1 V signal was applied to a single PZT actuator to act as the system disturbance, and a single actuator was used to implement the control law. However, the control algorithm could only reduce the vibration of the test plate by

50% (with an applied control voltage of 2.5 V) when attacking the algorithm's most effective resonant frequency.

Although less complicated in design than a MIMO LQG controller, a PPF controller will be designed and implemented on the test plate to attack the first mode of vibration. In the design of a PPF controller, only three compensator parameters need to be determined—the compensator gain, g, filter frequency, ω_f, and the filter damping ratio, ζ_f. McEver (1999) proposed an optimal placement method for these parameters as a function of the system pole/zero spacing. He found that the amount of damping that could be added to the closed-loop system by the PPF filter could reach approximately 80% critical damping for high gains. Following McEver's procedure, a filter frequency of $\omega_f \approx \sqrt{2}\omega$ was chosen as a starting point throughout the experimentation.

The first mode of the simply supported plate is at 49.0 Hz. Since the piston mode generates the greatest amount of displacement at the center of the plate, the MFC® sensor was collocated with the PZT actuator near the center. The MFC® sensor was fastened to the plate using an epoxy to help limit the loss of energy between the vibration of the plate and the charge generated by the MFC® device. The output of the MFC® patch was fed into the charge amplifier, and the amplified signal was fed into the digital PPF controller through a dSPACE board. The output of the PPF controller was fed into a power amplifier (50x), and the final control signal was fed back to Patch 1 from Figure 5.4. Similar to the dynamic analysis experiment in section 5.3, a 5 V chirp signal was used to excite the structure from 30 – 200 Hz. A diagram of the experimental setup is shown in Figure 5.9.

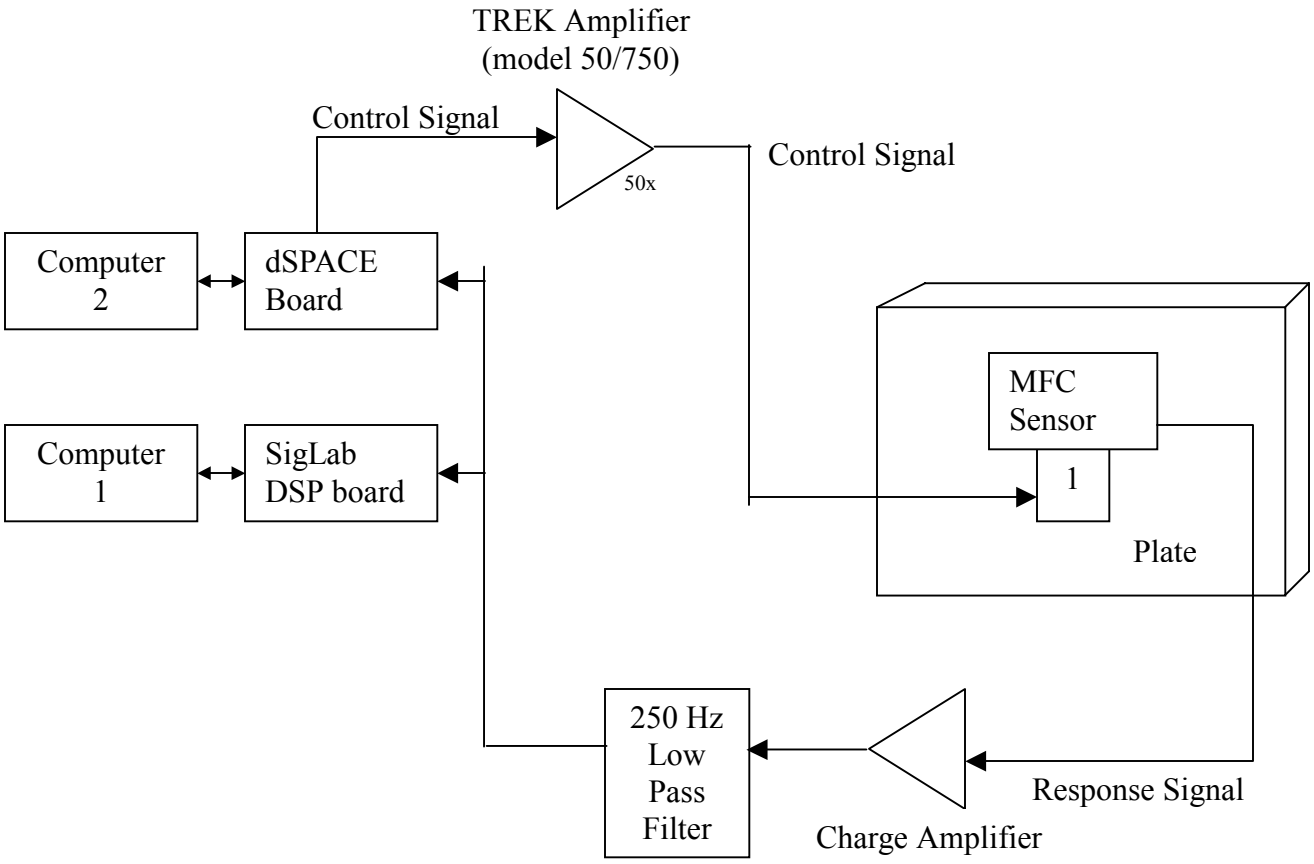

Figure 5.9. Diagram of the PPF control experimental setup.

The next step was the actual design of the PPF filter. The filter parameters were chosen based on the experimental work performed by McEver (1999). After some design iteration, the PPF filter frequency was set at 50.4 Hz, approximately 1.05 times the resonant frequency of the plate. The damping ratio was set at 0.15 to try and increase the damping of the system. Finally, the filter gain was set in real time to 7.12.

The controller was designed in the continuous domain and then mapped into the z-domain using the trapezoidal rule. The design was approached from the continuous domain primarily because it was easier to understand the placement of the poles throughout the iteration process. By setting the filter parameters in a MATLab code, the filter was then compiled and used as the input to a SIMULINK block diagram. SIMULINK is a visual-based interface between MATLab and Control Desk (the software

that runs the dSPACE board). Figure 5.10 shows the SIMULINK file that was used to implement the digital PPF filter.

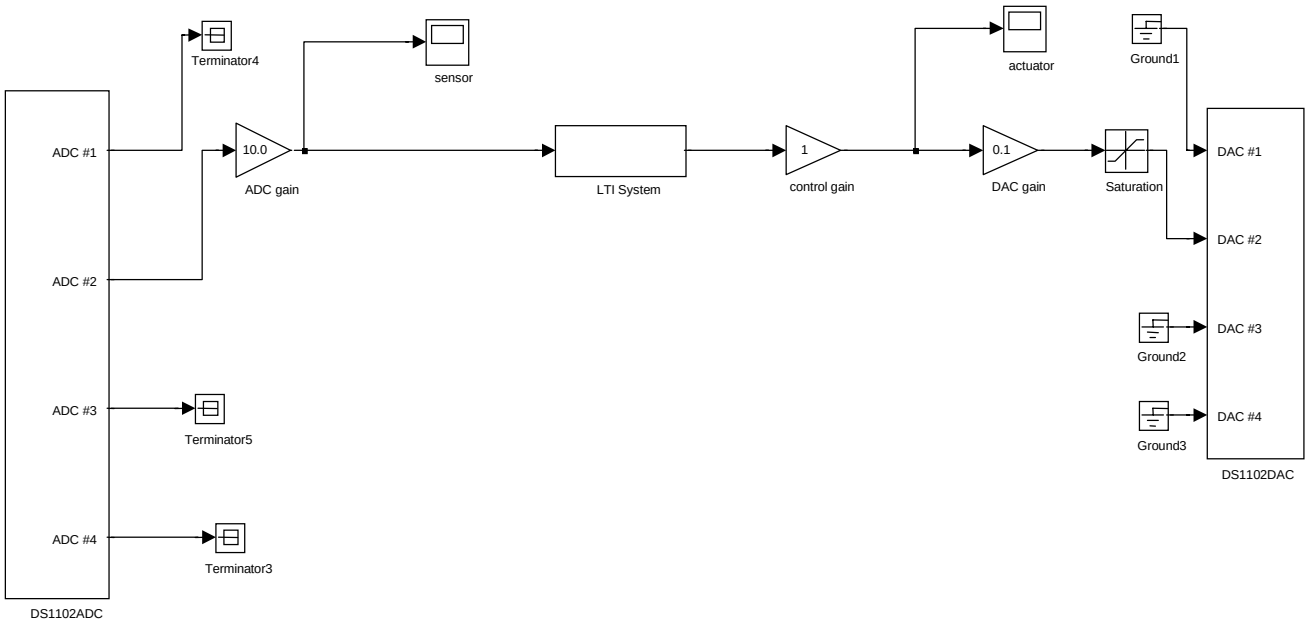

Figure 5.10. SIMULINK block diagram used to implement the PPF controller.

The results of the PPF filter are graphically shown below in Figure 5.11. Note that the magnitude of the first resonant peak has been reduced by 80%. The real time response of the system, as sensed by the MFC® sensor, and the control voltage applied to the PZT actuator are shown in Figure 5.12.

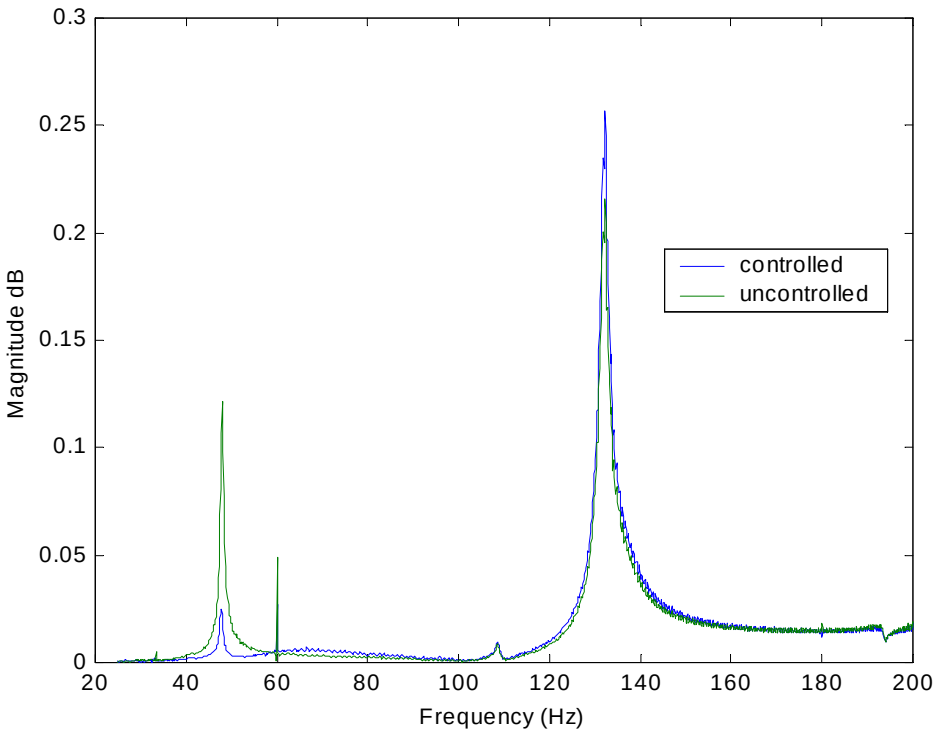

Figure 5.11. The first mode of the plate is reduced by 80% using a PPF controller.

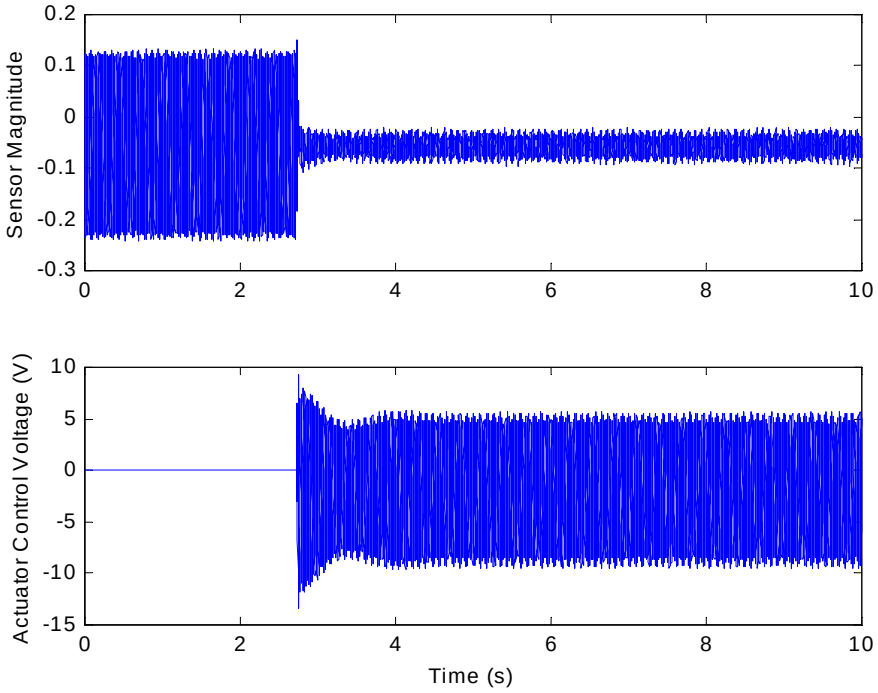

Figure 5.12. The real time response of the plate before and after the PPF controller was initiated (top). The controller was turned on at approximately 3 seconds. The required control effort is also shown (bottom).

The PPF controller was able to reduce the overall magnitude of the first mode by 80%. Compared to Cole's work (1992), the PPF controller was much more effective at reducing the vibration of a single mode (80% reduction as opposed to 50% reduction). The reason for the increased vibration suppression is that Cole's work relied heavily on the transfer function models he developed theoretically, whereas the PPF control experiment only required knowledge of the modal properties of the plate (i.e. resonant frequency and approximate damping ratio). Considering the ease of implementation and effective results using the PPF controller with the test plate, the same control technique will be applied to the inflated torus.

5.5 Chapter Summary

A dynamic analysis of a simply supported plate is presented using similar experimental modal analysis techniques as those developed in Chapter 3. In the latter half of the chapter, a digital PPF controller was designed and implemented to the control the first mode of vibration of a simply supported plate. The goal of the research presented in this chapter was two-fold: 1) to validate the dynamic analysis methodology developed in Chapter 3, and 2) to demonstrate the effectiveness of using the MFC® device as a sensor. The PPF controller designed around the MFC® sensor was able to reduce the magnitude of the vibration levels of the first mode of the plate by nearly 80% with a maximum control effort of 10V. The next chapter will evaluate the feasibility of using the PPF active control techniques developed in this chapter to attack the first mode of vibration of the gossamer torus.

CHAPTER 6: Comparison Between Active and Passive Control Techniques for an Inflatable Torus

6.1 Background

In terms of vibration control of a gossamer torus, two approaches can be undertaken—namely 1) an active control algorithm, or 2) a passive control device. However, in determining the effectiveness of each method, an analysis must be performed that compares not only the vibratory reduction, but also the trade-offs associated with that reduction. In particular, the additional mass or altered boundary conditions imposed on the structure must be taken into account when evaluating the effectiveness of a specified method.

An outline of the chapter is as follows. Section 6.2 outlines the experimental setup of implementing a PPF controller to control the vibration of the first mode of the torus. Section 6.3 outlines the experimental setup and results of using a viscoelastic tape to reduce the vibration of the torus. Section 6.4 compares the results of both the active and passive methods attempted in this experimentation. Finally, section 6.5 summarizes the significant findings of the chapter.

6.2 Active Control of the Gossamer Torus Using a PPF Controller

The experimental setup consisted of the Kapton torus and three MFC® patches. As opposed to the plate experiment in Chapter 5, the vibration disturbance, vibration sensor, and PPF controller were all implemented with MFC® patches. A full MFC® actuator patch supplied the vibration disturbance, and the PPF controller MFC® actuator and vibration MFC® sensor were equal halves of a full patch. Such an experimental setup more closely simulates actual working conditions for a space satellite relying solely on smart material technology. A photograph of the experimental setup is shown in Figure 6.1. A schematic of the experimental setup is shown in Figure 6.2.

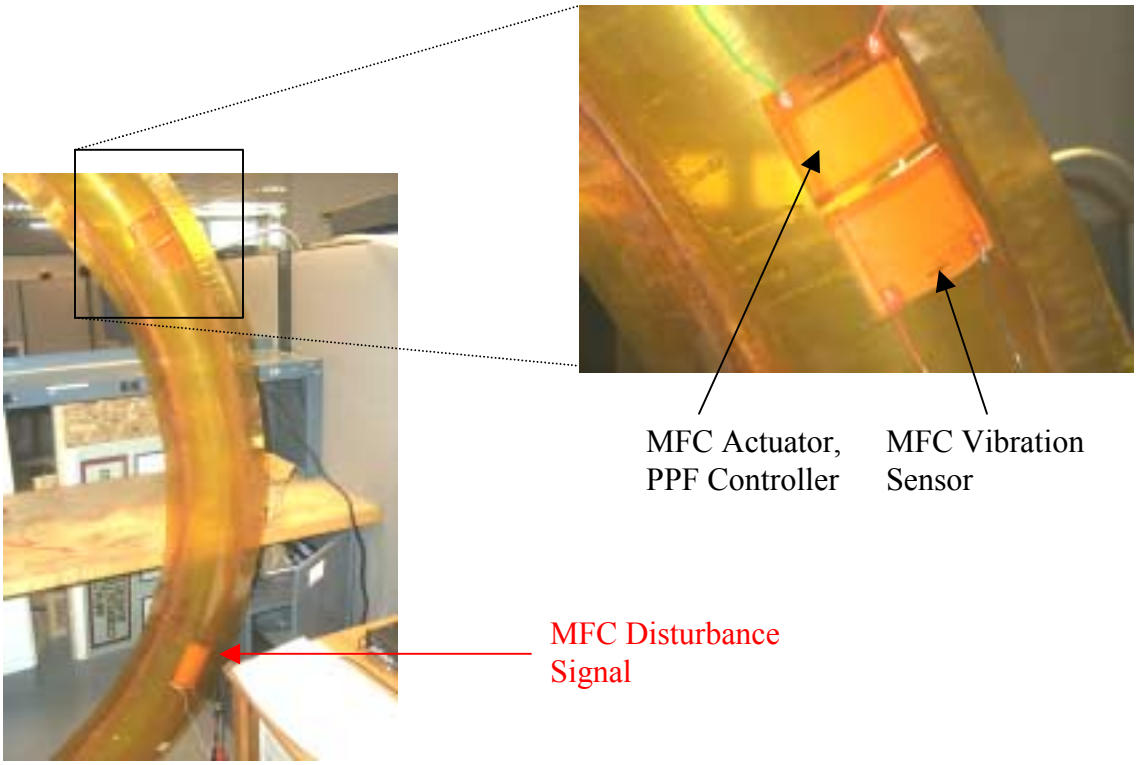

Figure 6.1. The active PPF controller experimental setup.

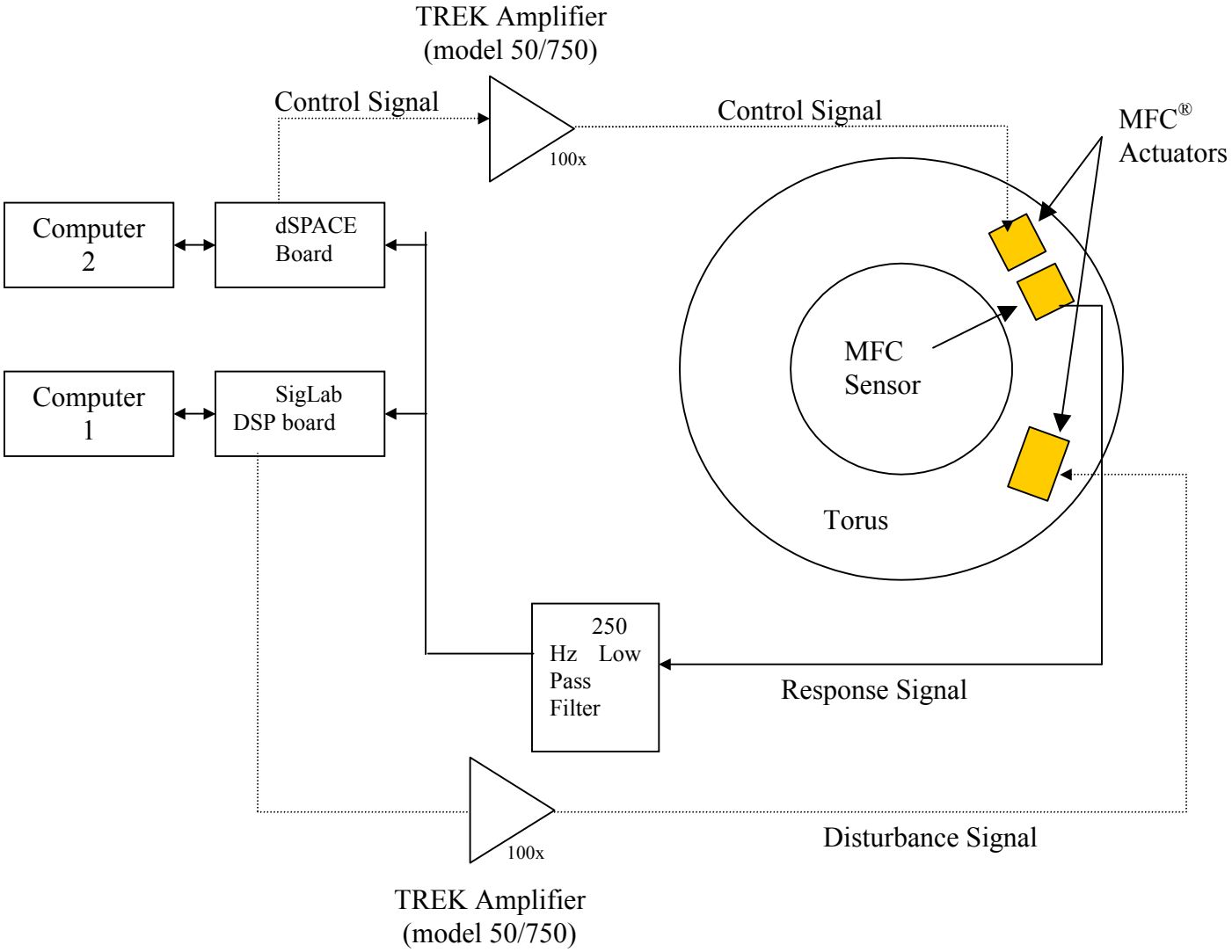

Figure 6.2. Schematic diagram of the experimental setup to actively control the gossamer torus.

The PPF controller was built and implemented digitally using the same iterative process outlined in section 5.3. The first mode of vibration of the torus (at 0.5 psi) occurs at 12.8 Hz. Therefore, the PPF filter was tuned to 13.44 Hz, approximately 1.05 times the natural frequency of the system. It was experimentally determined that a damping ratio of 0.10 and a filter gain of 2.95 most significantly reduced the vibration of the first mode of vibration of the torus. Figure 6.3 shows a 70% reduction in magnitude of the

first mode of vibration, and Figure 6.4 shows the contrast in the vibratory response of the torus and the control effort as a function of time as the PPF controller is activated. The maximum control effort used by the MFC® actuator is 215 V.

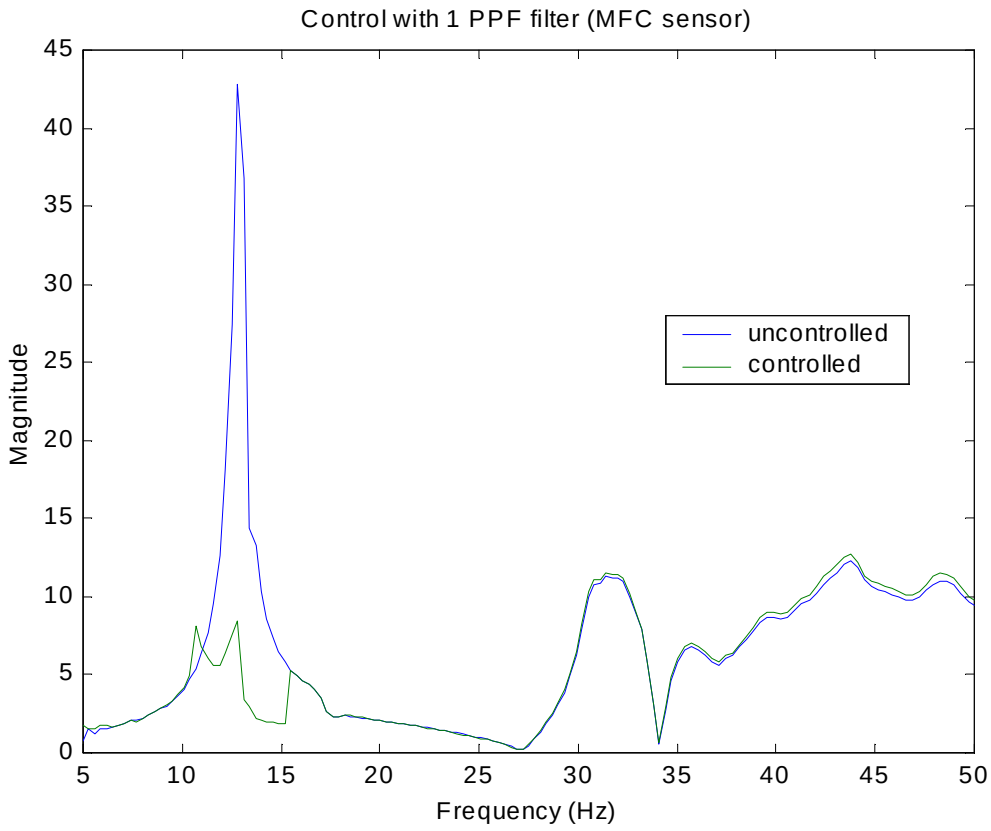

Figure 6.3. The PPF controller reduces the magnitude of the first mode of vibration by 70%.

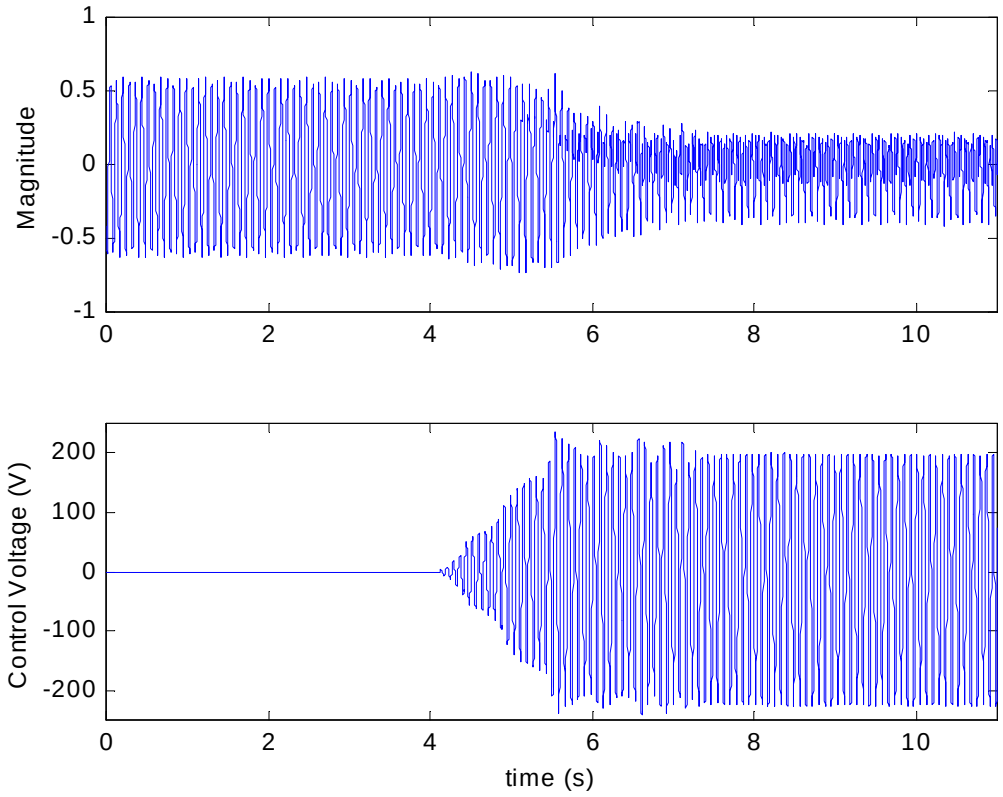

Figure 6.4. The vibratory response of the torus is shown before and after the PPF controller is activated at 4 seconds (top). The magnitude of the response is reduced by 70%. The actuator control voltage (215 V max.) is also shown (bottom).

6.3 Passive Control of the Gossamer Torus Using Viscoelastic Tape

Another possibility for vibration control is the use of viscoelastic tape (3M damping foil #2552). However, in order to directly compare the effects of the viscoelastic tape on the torus to that of the active control technique, the viscoelastic tape was cut to the exact area of the MFC® actuator patch (2.25" x 1.69"). The patch was placed in the same position as the active controller patch in the previous experiment. Comparatively, the viscoelastic tape had a mass of 3.3229 g and the MFC® actuator had a mass of 2.5647g. A photograph of the experimental setup is shown in Figure 6.5.

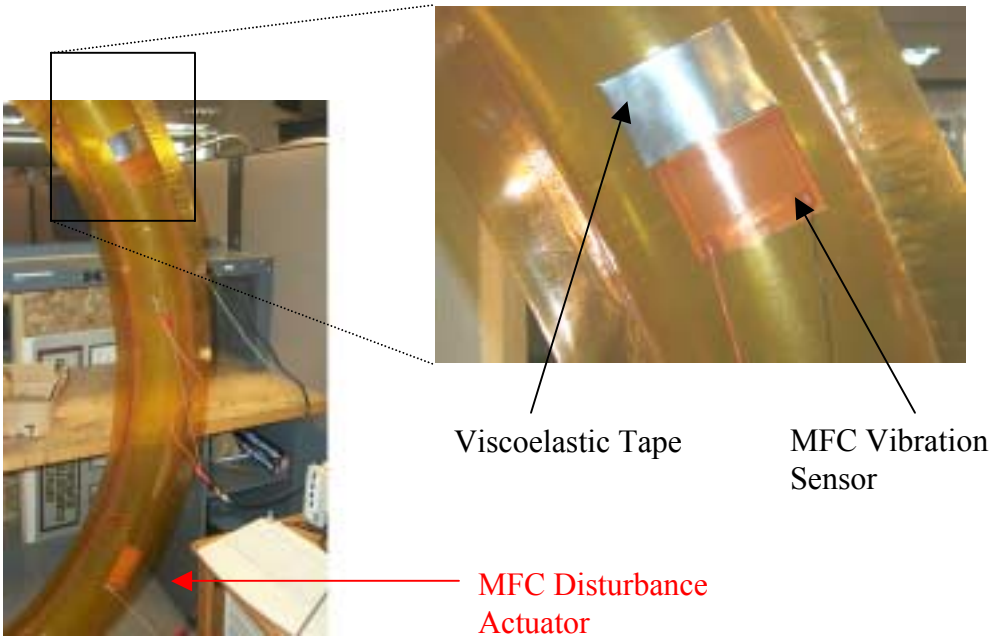

Figure 6.5. Passive vibration control experimental setup, highlighting the MFC® vibration sensor and viscoelastic patch (at right).

After setting up the experiment, the dynamic response of the torus was measured using the process outlined in Chapter 3. The results of the experiment are shown in Figure 6.6, where the vibratory of the response with and without the viscoelastic tape is compared.

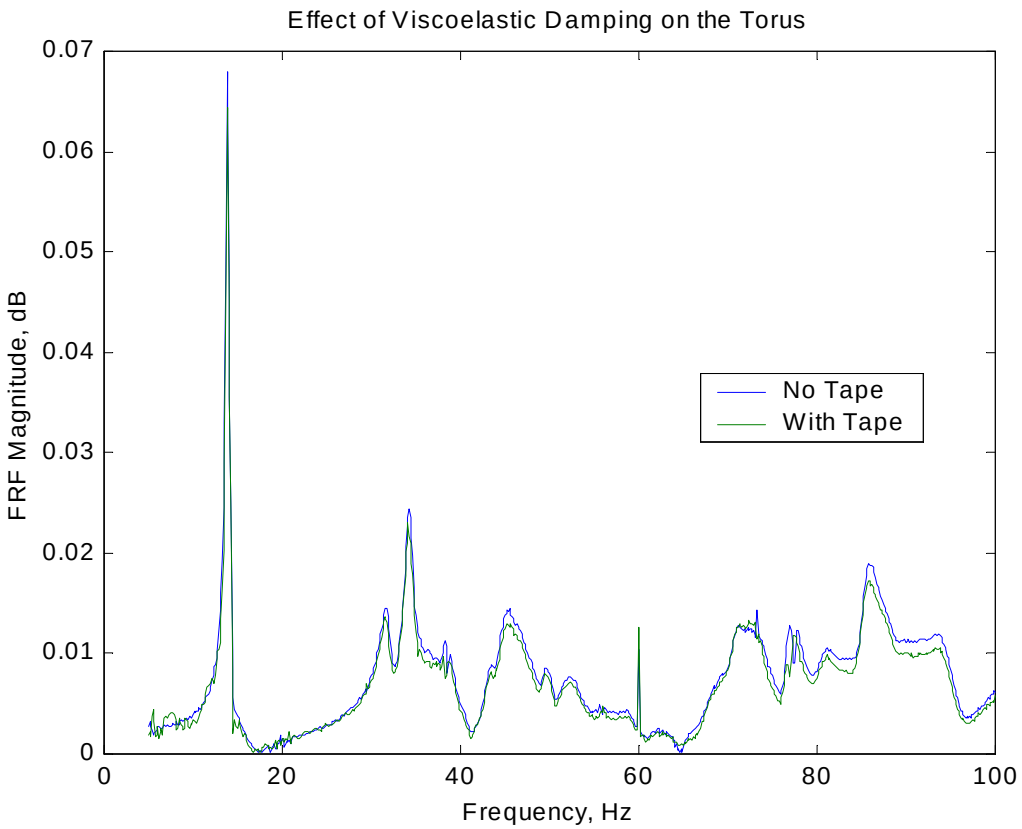

Figure 6.6. The effect of applying viscoelastic tape on the skin of the torus has negligible effect on the torus.

6.4. Comparison Between Active and Passive Methods of Vibration Control for the Torus

In comparing the results of Figures 6.3 and 6.6, it is quite clear that the active control methodology is much more effective than the passive methodology. Further, the MFC® actuator had a mass of only 2.5647 g compared the viscoelastic tape that had a mass of 3.3229 g. However, it should be noticed that the crude experimentation was designed to see if viscoelastic could affect the lower frequency ranges, and that the material used was not necessarily optimized for the torus. Further, although the MFC® patch weighs less than the VEM patch, it should also be noted here that the active

controller requires additional hardware (such as a computer system and power amplifier). Where the PPF filter was able to reduce the magnitude of the first mode by 70%, the viscoelastic tape was only able to reduce the magnitude of the first mode by less than 1%. In addition, the PPF filter was only able to attack the first mode of vibration where the viscoelastic tape was able to demonstrate some vibration reduction at higher modes (at 47 Hz, 83 Hz, and 89 Hz in Figure 6.6, for example). However, multiple PPF filters can be tuned so that a single MFC® patch could have control authority over a much larger bandwidth than the single PPF filter case. For instance, Hegewald (2000) designed multiple PPF filters to control the vibration of a test plate over a large bandwidth.

6.5 Chapter Summary

A Positive Position Feedback filter was designed and implemented to control the first mode of vibration of the gossamer torus. The controller was implemented on the skin of the inflated torus using three MFC® patches—one to act as the disturbance input, one to sense the vibration of the structure, and the final patch to counteract the vibration of the torus. With a peak control voltage of 215 V, the MFC® patch was able to reduce the first mode of vibration of the torus by 70%. In the second half of the experiment, the active controller was removed and replaced with a piece of viscoelastic tape (3M damping foil #2552). Recording the system's FRF yet again using this passive technique had negligible effect on the torus' dynamic response. Although the VEM experiment was performed under non-optimal conditions and with limited investigation, the negligible reduction at lower resonant frequencies is in agreement with general trends in VEM damping. Comparatively, the MFC® actuator had less mass (neglecting additional computational or power hardware) than the viscoelastic tape (2.5647 g as opposed to 3.3229 g), further asserting its compatibility with lightweight, inflatable space structures. Therefore, considering the negligible mass loading effect and boundary conditions imposed by the active MFC® controller, the MFC® controller is the best candidate for future control algorithm implementation.

Chapter 7: Conclusions and Future Work

The topic of this work was the active dynamic analysis and control of a gossamer torus. Gossamer structures, like the torus, are the building blocks of future space satellites. Current imaging and communication limitations are governed by the overall size of the satellite lens or aperture in orbit. By demonstrating means of dynamic analysis and control of these lightweight structures, this research provides a feasible means for deploying gossamer satellites into space.

The first aspect of this research was the dynamic analysis of a 6-foot diameter Kapton torus. The torus was suspended from a single bungee cord to minimize any effect on the structure's behavior and most closely simulate a free-free boundary condition. A major contribution of this research was the use of smart materials, or more specifically, piezoelectric materials, as sensing and actuating devices for experimental modal analysis of gossamer structures. Smart materials are not the final answer to the identification of the modal parameters of inflatable, gossamer systems. They do, however, possess lightweight, non-influential characteristics that make them a better choice for system dynamic characterization.

The structure was excited in two ways in the first set of dynamic analysis experiments. The first method used an electromagnetic shaker to excite the torus in two orthogonal directions to obtain the in-plane and out-of-plane mode shapes of the torus. A PVDF sensor was used to obtain the frequency response function of the torus from 0 to 100 Hz. An accelerometer was also used throughout the experiment to further validate the results obtained from the PVDF sensor. The first three out-of-plane and first two in-plane resonant frequencies and corresponding mode shapes were plotted using both the PVDF sensor acquired data and the accelerometer acquired data. The resonant frequencies differed by less than 0.4% between each measurement device.

The second method of excitation of the torus was a Macro-fiber Composite (MFC®) actuator from NASA Langley Research Center. The MFC® actuator provides

several advantages compared to traditional piezo-composite materials, including high strain energy, conformability, and durability. It uses both active and composite technologies, in addition to inter-digitated electrodes, and offers high performance and flexibility suitable fur use in inflatable structures. Because of these highly-compatible gossamer structure characteristics, the MFC® device was used to excite the torus from 0-200 Hz. Again, a frequency response function was generated using both a PVDF sensor and an accelerometer, and excellent agreement was found as compared to the original, more conventional electromagnetic shaker excitation technique.

For the first time in the known literature, the dynamic testing of a gossamer-type structure was successfully performed using smart materials. Previous attempts at identifying the frequency response function of an inflatable torus or similar structure had proven ineffective or produced results with a tremendous amount of uncorrelated content. Further, the testing methodology outlined is simple to implement and, more importantly, relatively inexpensive to use. Despite the success of the analysis, there were two major short falls attributed with the single input single output methodology presented. First, the technique is unable to distinguish between orthogonal mode pairs located at nearly identical natural frequencies. Axi-symmetric structures like the torus demonstrate orthogonal mode pairs that would be identical, ideally, if the torus were perfect, but once the symmetry is lost, the modes tend to split slightly from each other. SISO techniques tend to smear the two peaks into one since they are so close to each other in frequency. A second issue associated with the SISO technique is that it is highly doubtful that a single MFC® patch will be able to excite a true gossamer spacecraft, like a 25 m in diameter torus. Although the SISO method was effective in the global sense for the smaller torus, global excitation becomes an issue for true gossamer satellites.

Because of the two critical issues uncovered from the SISO modal analysis techniques, a multiple input multiple output technique (MIMO) was investigated on the torus. However, instead of using PVDF sensors or accelerometers, the test consisted of multiple MFC® actuators and sensors. For the first time in the known literature, the MFC® device was used as a sensor. After validating an assumption that the inflated torus

behaved linearly over the frequency range of interest, a MIMO post-processing algorithm was developed. Two sensors and two actuators were used to perform just two experiments, and from the two experiments, the collected sensory data was processed to find a matrix transfer function between the input and output of the system. The data was further processed to identify the resonant frequencies of the torus. The MIMO technique was able to distinguish the mode pairs and provide a better method of global excitation of the structure. Therefore, it is highly recommended that future work on modal analysis of gossamer structures use the MIMO analysis technique identified in this research.

Having established a reliable, effective methodology for the dynamic analysis of a gossamer structure, the next phase of the experiment was to demonstrate the feasibility of using active control techniques to control the vibration of the gossamer torus. In the first half of the control experiment, a Positive Position Feedback controller was designed and implemented on a simply supported plate. PPF control is a strong candidate for preliminary control of a gossamer structure because it is relatively simple to design and practically implement, and it is rather robust in the presence of system uncertainty. The first experiment was performed on the simply supported plate to ensure that the MFC® could be used as a sensor in the PPF control feedback loop, as well as to understand the practical nature of implementing a PPF controller in general. Using a PPF filter to attack the first mode of vibration of the simply supported plate, the magnitude of the first mode was reduced by 70%. The PPF control design only required a peak control voltage of 10 V applied to a PZT patch collocated with the MFC® sensor to control the plate's vibration.

In the second phase of the active control experiment, a similar PPF controller was designed to suppress the first mode of vibration of the torus. The PPF controller was implemented using MFC® actuators as both the controller and sensor, and the torus was disturbed using another MFC® actuator. Following the same procedure established to control the plate, the first mode of vibration of the torus was reduced in magnitude by 70%.

As a follow-up experiment, the final phase of experimental control techniques explored the possibility of using a passive viscoelastic damping material to control the vibration of the torus. A piece of 3M damping tape (#2552) was cut to cover the same effective area as the MFC® actuator. Comparatively, the viscoelastic material had a greater mass than the MFC® actuator (3.3229 g as opposed to 2.5647 g). By taking a modal analysis of the torus with and without the tape adhered to the torus' skin, it was found that the viscoelastic tape had negligible effect on reducing the vibration of the torus. The VEM damping experiment, although crude, was able to demonstrate the inability of the passive technique to affect the lower modes of the torus. In the same vein, the mass comparison of the MFC® and VEM techniques is not compatible if the hardware associated with the active controller is taken into account.

PPF control is by no means the ultimate answer to the vibration control of gossamer structures. The purpose of the active control experiments was to validate a cost-effective, easily implemented controller and verify that vibration suppression could be performed on the torus or similar gossamer structures. Having shown the effectiveness of PPF control, and by establishing a methodology for using smart materials in the control scheme for gossamer structures, the next step will be to develop more rigorous, intensive system models and control algorithms. Multivariate or sliding mode control may be much more aggressive and effective techniques to control the dynamics of the torus. However, efforts will need to be focused on the accurate system modeling of the torus or similar gossamer structures. By developing realistic system models, more rigorous control algorithms can be developed and implemented. Similarly, computational models of the MFC® actuator / sensor would prove highly valuable in future projects integrating MFC® technology.

Gossamer technology and related structures have some exciting times ahead. Once viewed as tenuous and nearly invisible, gossamer technology is slowly coming into full view of the scientific community. With continual advances in material science, control algorithms, and energy production, gossamer technology will continue to attract

attention. And with the deployment of a 25-meter inflated antenna in outer space before 2010, it will be hard to classify gossamer technology as tenuous anymore.

APPENDIX A: MATLab Code

The following MATLab code was used to generate the eigenvectors of the torus data (UMPA pseudo least squares method), and to generate the corresponding mode shapes of the torus. (c) S. O'F. Fahey 4-1997

```
function [Coeff]=forsythe(q,x,w,type);

% forsythe.m                          (c) S. O'F. Fahey 4-1997
%                          ver 5.2.1997
%
% This matlab (tm) function determines the coefficients of Forsythe
% orthogonal polymonials, up to order q
%
% [coeff] = FORSYTHE( q,x,w,'type' );
%
% where, q = degree of highest order polynomial, 1 x 1
%       x = domain of control variable, n x 1
%       w = complex weighting vector on omega, n X p
%       'type' = orthogonal condition,
%            's' for sum [default], 'v' for vector
%       Coeff = coefficients of Forsythe polynomials, q x q [s],
%             and q X pq [v]
%
% Orthogonal conditions;
% sum_i sum_k w_ik' P(x_i)'_j P(x_i)_n w_ik =
%                                1 if j equals n, else 0 [s]
% sum_i w_ik' P(x_i)'_j P(x_i)_n w_ik =
%                     1 if j equals n, else 0 for every k [v]

% for [s],
%  [Coeff]=[c_{q*q}]
% for [v],
%  [Coeff]=[ c1_{q*q} | c2_{q*q} | ... | cp_{q*q}]

% ************************************************** check inputs
disp(' ');
if (exist('type')==1)==0 type=[]; end;
if (exist('w')==1)==0 w=ones(size(x,1),1); end;

if size(x,2)>1
  disp('??? Error using ==> forsythe.m');
  disp('    INPUT NOT COLUMN');end;
if q>size(x,1)
```

```
  disp('??? Error using ==> forsythe.m');
  disp('    INPUT NOT SUFFICIENT SIZE'); end;

% ********************************************************************
% ********************************************************************
% ************************************************************ sum loop
if isempty(type) | type=='s' | type=='S'

  % ********************************************************** set up
  p=zeros(q);
  normal=zeros(1,q);
  Ow=ones(1,size(w,2));
  for i=1:q XX(:,i)=x.^(i-1); end; %i
  xx=(x*Ow);

  % ************************************************ first polynomial
  p(1:1,1)=[1];

  % ************************************************ second polynomial
  if q>1
    XXpw=((XX*p(:,1))*Ow ).*w;

    an=sum(sum(conj( XXpw ).* ( xx.*XXpw )));
    ad=sum(sum(conj( XXpw ).* ( XXpw )));
    a(1)=an/ad;

    p(1:2,2)=[-a(1)*p(1:1,1); 1];

    normal(1)=ad;
    XXpw0=XXpw;
  end;

  % ************************************** remaining polynomials
  for k=3:q

    XXpw=((XX*p(:,k-1))*Ow ).*w;

    an=sum( sum(conj( XXpw ).*( xx.*XXpw)));
    ad=sum( sum(conj( XXpw ).*( XXpw)));
    a(k-1)=an/ad;

    bn=sum( sum(conj( XXpw0 ).*( xx.*XXpw )));
    bd=sum( sum(conj( XXpw0 ).*( XXpw0 )));
    b(k-2)=bn/bd;

    p(1:k,k)=[0;p(1:k-1,k-1)]-b(k-2)*[p(1:k,k-2)]-a(k-1)*p(1:k,k-1);
```

```
    normal(k-1)=ad;
    XXpw0=XXpw;
  end; %k

  XXpw=((XX*p(:,q))*Ow ).*w;
  normal(q)=sum( sum(conj( XXpw ).*( XXpw )));

% ********************************************************************
% ********************************************************************
% ********************************************** vector loop
elseif type=='v' | type=='V'

  % ********************************************************* set up
  p=zeros(q,q*size(w,2));
  normal=zeros(1,q*size(w,2));
  Ow=ones(1,size(w,2));
  c=q*[0:size(w,2)-1];

  for i=1:q XX(:,i)=x.^(i-1); end; %i
  xx=(x*Ow);

  % ********************************************** first polynomial
  p([1:1],1+c)=ones(1,size(w,2));

  % ********************************************** second polynomial
  if q>1
    XXpw=((XX*p(:,1+c)) ).*w;

    an=sum(conj( XXpw ).* ( xx.*XXpw ));
    ad=sum(conj( XXpw ).* ( XXpw ));
    a(1,:)=an./ad;

    p([1:2],2+c)=[-a(1,:).*p(1:1,1+c); Ow];

    normal(1+c)=ad;
    XXpw0=XXpw;
  end;

  % ****************************************** remaining polynomials
  for k=3:q

    XXpw=((XX*p(:,k-1+c)) ).*w;

    an=sum(conj( XXpw ).*( xx.*XXpw));
    ad=sum(conj( XXpw ).*( XXpw));
```

```
    a(k-1,:)=an./ad;

    bn=sum(conj( XXpw0 ).*( xx.*XXpw ));
    bd=sum(conj( XXpw0 ).*( XXpw0 ));
    b(k-2,:)=bn./bd;

    p(1:k,k+c)=[zeros(1,size(w,2));p(1:k-1,k-1+c)]...
      -(ones(k,1)*b(k-2,:)).*p(1:k,k-2+c)...
      -(ones(k,1)*a(k-1,:)).*p(1:k,k-1+c);

    normal(k-1+c)=ad;
    XXpw0=XXpw;
  end; %k

  XXpw=((XX*p(:,q+c)) ).*w;
  normal(q+c)= sum(conj( XXpw ).*( XXpw ));
else
  disp('??? Error using ==> forsythe.m');
  disp('    TYPE INCORRECT');
  p=nan;
  normal=nan;
end; %if-elseif-else 's' and 'v'

% ********************************************************** normalize
Coeff=p./(ones(size(p,1),1)*sqrt(normal));

function [freq,damp,ampl,phas,eigenvalues,eigenvectors,A,B]=opmodal(m,n,omega,h,w);

% opmodal.m                    (c) S. O'F. Fahey 4-1997
%                          ver 5.2.1997
%
% Matlab (TM) Program was written by Sean O'Flaherty Fahey.  This code uses an
% UMPA pseudo least square method to determine an orthogonal polynomial fit
% to complex data with arbitrarily spaced amplitude and frequency information.
%
% [ freq,damp,ampl,phas,eigenvalues,eigenvectors ] = opmodal( m,n,omega,h,w )
%
% where, m = degree of polynomial (num)erator
%        n = degree of polynomial (denom)inator
%        [h1 h2 ... hn] = input Xfer {columns} function to be fit
%        omega = frequency corresponding to input function
%        w = weighting vector(s)
%
%        [freq, damp] = resonant frequency and damping
%        [ampl,phase] = amplitude and phase at resonance
%        [eigenvalues,eigenvectors] = complex poles and modeshapes
```

```
% ****************************************************************
set-up
j=sqrt(-1);          % defines imaginary
L=length(omega);       % length incoming x-fer to be fit
q=max([n+1 m+1]);          % max size polynomial

%
*****************************************************************
**
% *** Consider H & OMEGA this way to numerically force c.c. results ********
%
*****************************************************************
**
if exist('w')~=1
  w=ones(size(h));
  disp('    ')
  disp('   opmodal.m -- no weight')
end;

H=[conj(h([L:-1:1],:));h];
OMEGA=[-omega(L:-1:1);omega];
w=[w([L:-1:1],:);w];
N_XFER=size(H,2);

if size(w,2)~=N_XFER
  w=w(:,1)*ones(1,N_XFER);
  disp('    ')
  disp('   opmodal.m -- even weight applied across spectra')
end;

% ************************************************************
estimation
% *** references;                                    *******
% *** [1] Richardson M., Formenti D.L. "Parameter estimation from FR *******
% *** Meas using RFP", Proc. IMAC, 1982, pp.167-182.              *******
% *** [2] Beliveau J.-G., Class notes, CE, UVM, Burlington, VT 05405 *******
% *** [3] Allemang R.J., Brown D.L., Fladung W., Modal Parameter     *******
% *** Estimation: UMPA, IMAC 1994, pp.501-514.                    *******
%
*****************************************************************
**

%
*****************************************************************
**
% *** comments about sources: the large majority of this code is based *****
```

```
% *** on [1].  [2] gives helpful suggestions and [3] gives an **************
% *** overview of the process ********************************************
%
************************************************************************
**

% ******************************************************* estimation set-
up
[Coeff1]=forsythe(m+1,j*OMEGA,w,'v');
[Coeff2]=forsythe(n+1,j*OMEGA,H.*w,'s');

for i=1:q
    Poly_term(:,i)=(j*OMEGA).^(i-1);
end; %i


% ********************************************************** mdof
spatial
X=zeros(N_XFER*(m+1),n);Z=zeros(n,n);G=zeros(N_XFER*(m+1),1);
%Y=zeros(N_XFER*(m+1),N_XFER*(m+1));F=zeros(n,1); %<<code checker>>

for k=1:N_XFER
  r=(k-1)*(m+1);
  P(:,1:m+1)=((w(:,k)*ones(1,m+1)).*Poly_term(:,1:m+1))*Coeff1(1:m+1,r+1:r+(m+1));
  T(:,1:n)=( (w(:,k).*H(:,k)) *ones(1,n) ).*( Poly_term(:,1:n+1)*Coeff2(:,1:n) );
  W(:,1)=w(:,k).*H(:,k).*( Poly_term(:,1:n+1)*Coeff2(:,n+1) );

  X(r+1:r+m+1,1:n)=[-P'*T];
  %Y((k-1)*(m+1)+1:k*(m+1),(k-1)*(m+1)+1:k*(m+1))=[P'*P]; %<<code checker,
?==I>>
  Z=Z+(T'*T);
  G(r+1:r+m+1,1)=[P'*W];
  %F=F-(T'*W); %<<code checker, ?==0>>
end;


% ***************************************************** parameter
estimator
B=[[diag(ones(min(size(X)),1))-X'*X]\[-X'*G]];  AA=G-X*B;

% ************************************************* parameter
normalization
B=Coeff2*[B;1]./Coeff2(n+1,n+1);

for k=1:N_XFER
  r=(k-1)*(m+1);
```

```
  A(:,k)=( Coeff1(1:m+1,r+1:r+m+1)*AA(r+1:r+m+1) )./Coeff2(n+1,n+1);
end;


% ************************************************** generate output data
for k=1:N_XFER
  [Res(:,k),Pole] = residue(A([m+1:-1:1]',k),B([n+1:-1:1]'));
end; %k

I=find(imag(Pole)>0);

% ********************************************************** output
results
eigenvalues=Pole(I);
damp=sqrt( 1./((imag(eigenvalues)./real(eigenvalues)).^2+1) );
freq=-real(eigenvalues)./damp;

eigenvectors=Res(I,:); %recall residues are not \phi_i\phi_j /M
ampl=abs(eigenvectors);
phas=angle(eigenvectors);
A=A;B=B;

function
[freq,damp,ampl,phas,eigenvalues,eigenvectors,HH]=vopmodal(m,n,omega,h,w);

% vopmodal.m                    (c) S. O'F. Fahey 4-1997
%                         ver 5.2.1997
%
% Matlab (TM) Program was written by Sean O'Flaherty Fahey. This code uses an
% UMPA pseudo least square method to determine an orthogonal polynomial fit to
% complex data with arbitrarily spaced amplitude and frequency information.
%
% [ freq,damp,ampl,phas,eigenvalues,eigenvectors,H ] = vopmodal( m,n,omega,h,w )
%
% where, m = degree of polynomial (num)erator
%       n = degree of polynomial (denom)inator
%       [h1 h2 ... hn] = input transfer {columns} functions to be fit
%       omega = frequency corresponding to input function
%       w = weighting vector(s)
%
%       [freq, damp] = resonant frequency and damping
%       [ampl,phase] = amplitude and phase at resonance
%       [eigenvalues,eigenvectors] = complex poles and modeshapes
%    [H] = generated transfer functions
%
% A graphical interface window will appear requiring user input.  The minimum
% and maximum frequencies to be considered should be clicked.
```

```
% ****************************************************************
set-up
q=max([n+1 m+1]);         % max size polynomial
N_XFER=size(h,2);

if exist('w')~=1
  w=ones(size(h));
  disp('    ')
  disp('   vopmodal.m -- no weight')
end;

% ********************************************************* find reduced
set
% *** This allows reducing the xfer function visually when it is  **********
% *** not desirable to fit the entire range of motion **********************
%
**********************************************************************
**
figure; plot(omega,w);ylabel('weight')
%subplot(3,1,1);plot(omega,w);ylabel('weight')
figure; plot(omega,angle(h));ylabel('phase')
%subplot(3,1,2);plot(omega,angle(h));ylabel('phase')
figure;semilogy(omega,abs(h)); xlabel('frequency');ylabel('amplitude');
%subplot(3,1,3);semilogy(omega,abs(h)); xlabel('frequency');ylabel('amplitude');
grip=ginput(2);

[junk, l1] = min( abs(omega-min(grip(:,1))) );
[junk, l2] = min( abs(omega-max(grip(:,1))) );

[freq,damp,ampl,phas,values,vectors,A,B]=opmodal(m,n,omega(l1:l2),h(l1:l2,:),w(l1:l2,:
));

% ********************************************************** for output
plot
for i=1:q; Pn(:,i)=(j*omega).^(i-1); end;

% ****************************************** regenerate transfer function
for k=1:N_XFER HH(:,k)=(Pn(:,1:m+1)*A(:,k))./(Pn(:,1:n+1)*B); end; %k

% ************************************************************* plot
result
clf;figure
semilogy(omega,abs(h),'g.',omega,abs(HH),'m-',omega([l1 l2]),abs(h([l1 l2])),'b*');
title(['Fit:  m(num)=' num2str(m) ' & n(den)=' num2str(n)]);
xlabel('Frequency');ylabel('Amplitude'); figure
```

```
plot(omega,angle(h),'g.',omega,angle(HH),'m-',omega([l1 l2]),angle(h([l1 l2])),'b*');
ylabel('Phase');

% ********************************************************** output
results
freq=freq; damp=damp; ampl=ampl'; phas=phas';
eigenvalues=values; eigenvectors=vectors;

% ********************************************************** output file

fid = fopen('damping.txt','a');
fprintf(fid,'Natural frq. : \t %f \t Zeta : \t %f \t Ampl. : \t %f \n', freq, damp,ampl);
fclose(fid);
```

The following code plots the mode shapes of the torus.

```
%clear all
close all

nc=12;            %number of circles around the torus. A torus lies in x-y plane
nsc=36;            %number of points (nodal points) around the small circles
                %(nordal circle)

Ro=60;            % radius of a torus
Ri=10;            % radius of a nordal circle

theta=[0:nsc]*2*pi/nsc;   %Angle between noral points in nordal circles
Phi=[0:nc]*2*pi/nc;       %Angle between nordal circles

%create nordal circles.  a nordal circle lies in y-z plane. starts at (y,z)=(0, Ri)
%and clockwise.
for i=1:nc+1
  for j=1:length(theta)
    eval(['circle',int2str(i),'y(',int2str(j),')=Ri*sin(theta(j));'])
    eval(['circle',int2str(i),'z(',int2str(j),')=Ri*cos(theta(j));'])
    eval(['circle',int2str(i),'x(',int2str(j),')=Ri*sin(theta(j))*0;'])
  end
end

for i=1:nc+1                % and then orient them according to Phi.
  Trans=[cos(Phi(i))   sin(Phi(i)) ;
       -sin(Phi(i))   cos(Phi(i))];
  eval(['ocircle',int2str(i),'xy=Trans*[circle',int2str(i),...
        'x; circle',int2str(i),'y];'])
end
```

```
%Put each circle into initial torus shapes coordinate.
%Starts at (x,y)=(0,Ro) and clockwise
RX=Ro*sin(Phi);
RY=Ro*cos(Phi);

for i=1:nc+1                %put each circle into the original position.
  eval(['ncircle',int2str(i),'x=transpose(ocircle',int2str(i),'xy(1,:)+RX(',int2str(i),'));'])
  eval(['ncircle',int2str(i),'y=transpose(ocircle',int2str(i),'xy(2,:)+RY(',int2str(i),'));'])
  eval(['ncircle',int2str(i),'z=transpose(circle',int2str(i),'z);'])
end

%create an initial torus shape
for i=1:nc+1
  eval(['X(:,',int2str(i),')=ncircle',int2str(i),'x;'])
  eval(['Y(:,',int2str(i),')=ncircle',int2str(i),'y;'])
  eval(['Z(:,',int2str(i),')=ncircle',int2str(i),'z;'])
end

figure
surf(X,Y,Z)
axis square; axis([-60 60 -60 60 -60 60]); view(-10,10)
xlabel('x'), ylabel('y'),zlabel('z')
title('orginal torus')
% Create mode shapes

% since the accelerometer masuremnts are obtained from the normal direction of
% the nordal circles in y-z plane, the nordal points move like,
% (yn,zn)=Ma*(sin(theta), cos(theta)), where Ma is the shape magnitude.

% Since this experiment considers z-direction only (out of plane) motion
% change the coordinate of z in nordal circels.

nmodes=3;         %number of modes we want to plot


Zi1=[-0.0345
    0.0343
    0.0693
    0.0507
   -0.0224
   -0.0828
   -0.0518
    0.0287
    0.0925
```

```
    0.0598
   -0.0393
   -0.0790
-0.0345]; %24 Hz damp = 0.08
Zi1=Zi1./max(abs(Zi1))*10;
title1=('1st mode shape (23.96 Hz)');

Zi2=[  0.2257
    0.4133
   -0.0624
   -0.3983
    0.0485
    0.5934
    0.1621
   -0.2379
    0.0778
    0.4870
    0.1094
   -0.2134
   0.2257];  %53 Hz    0.09
Zi2=Zi2./max(abs(Zi2))*15;
title2=('2nd modeshape (52.38 Hz)');


Zi3=[-1.3816 *0.8
    0.2763
    1.4244
    0.4246
   -0.1354
    0.9344
    0.8383
   -0.1860
   -0.0196
    0.4296
   -0.4350
   -1.7055
 -1.3816*0.8];  %16.94 Hz   damp=0.0827
Zi3=Zi3./max(abs(Zi3))*10;
title3=('3rd modeshape (78.87 Hz)');

Zi4=[-1.0787*0.5
    0.4266
   -0.6227
   -0.1931
    0.3553
   -0.7060
```

```
   0.7548
  -0.5747
  -0.0834
   0.8087
  -0.6785
   0.3874
-1.0787 * 0.5]; %25.31   0.0970
 Zi4=Zi4./max(abs(Zi4))*10;
 title4=('4th modeshape (25.31 Hz)');

 Zi5=[-0.9529
   0.4896
  -1.6044
   1.4800
   0.5779
  -1.1432
   1.5177
  -1.4306
   1.1719
  -1.1610
   1.1908
  -0.6865
-0.9529]; %56    0.1034
 Zi5=Zi5./max(abs(Zi5))*10;
 title5=('5th modeshape (56 Hz)');



for k=1:nmodes
     for i=1:nc+1                % put the magnitude of mode shape at each node
     for j=1:length(theta)

     eval(['ncircle',int2str(i),'z(',int2str(j),')=circle',int2str(i),'z(',int2str(j),')+Zi',int2str(k),'(',
int2str(i),');'])
     end
     eval(['Z',int2str(k),'(:,',int2str(i),')=ncircle',int2str(i),'z;'])
     end

     figure
     eval(['surf(X,Y,Z',int2str(k),')'])
     axis square; axis([-75 75 -75 75 -75 75])
  xlabel('x'), ylabel('y'),zlabel('z'), view(-10,10)
  eval(['title(title',int2str(k),');'])
end
```

The following MATLab code was used throughout the MIMO experimentation. © Jan Wright and Eric Ruggiero

```
% Calculate (2x2) FRF Matrix from Torus Tests - low frequency - LINEARITY CHECK for
% results from 2 voltage levels - using combined actuator FRF approach

clear all
close all

f1 = input('Enter lower frequency for plotting ');
f2 = input('Enter upper frequency for plotting ');

% FRF Matrix constructed from using two 'combined patch' tests [1 1] and [1 -1]
% approach similar to Multi-phase Stepped Sine but only uses single chirp output
% but switching patch leads to obtain -1 signal

% Low voltage level
**********************************************************

load 5V_C_1_31.vna SLm -mat
f=SLm.fdxvec';
E=SLm.xcmeas(1,2).xfer;
F=SLm.xcmeas(1,3).xfer;
clear SLm

load 5V_D_1_31.vna SLm -mat
f=SLm.fdxvec';
G=SLm.xcmeas(1,2).xfer;
H=SLm.xcmeas(1,3).xfer;
clear SLm

df = f(2) - f(1);
fp1 = round(f1/df) + 1;
fp2 = round(f2/df) + 1;

% Correct FRFs for combined patch tests to a classical FRF matrix related to the two separate patches

H2(1,1,:)=.5*E(:)+.5*G(:);
H2(2,1,:)=.5*F(:)+.5*H(:);
H2(1,2,:)=.5*E(:)-.5*G(:);
H2(2,2,:)=.5*F(:)-.5*H(:);

figure
```

```
plot(f(fp1:fp2),
abs(squeeze(H2(1,1,fp1:fp2))),f(fp1:fp2),abs(squeeze(H2(2,1,fp1:fp2))),...
f(fp1:fp2), abs(squeeze(H2(1,2,fp1:fp2))),f(fp1:fp2),abs(squeeze(H2(2,2,fp1:fp2))));
title('FRFs for low voltage level - combined actuator approach')
xlabel('Frequency (Hz)')
ylabel('FRF Magnitude V/V')

% Same but at high voltage level
*******************************************

load 10V_C_1_31.vna SLm -mat
f=SLm.fdxvec';
Eh=SLm.xcmeas(1,2).xfer;
Fh=SLm.xcmeas(1,3).xfer;
clear SLm

load 10V_D_1_31.vna SLm -mat
f=SLm.fdxvec';
Gh=SLm.xcmeas(1,2).xfer;
Hh=SLm.xcmeas(1,3).xfer;
clear SLm

% Correct FRFs for combined patch tests to a classical FRF matrix related to the two
separate patches

H2h(1,1,:)=.5*Eh(:)+.5*Gh(:);
H2h(2,1,:)=.5*Fh(:)+.5*Hh(:);
H2h(1,2,:)=.5*Eh(:)-.5*Gh(:);
H2h(2,2,:)=.5*Fh(:)-.5*Hh(:);

figure
plot(f(fp1:fp2),
abs(squeeze(H2h(1,1,fp1:fp2))),f(fp1:fp2),abs(squeeze(H2h(2,1,fp1:fp2))),...
f(fp1:fp2), abs(squeeze(H2h(1,2,fp1:fp2))),f(fp1:fp2),abs(squeeze(H2h(2,2,fp1:fp2))));
title('FRFs for high voltage level - combined actuator approach')
xlabel('Frequency (Hz)')
ylabel('FRF Magnitude V/V')

% Overlay two sets of FRFs

figure
subplot 221
plot(f(fp1:fp2),abs(squeeze(H2(1,1,fp1:fp2))),f(fp1:fp2),abs(squeeze(H2h(1,1,fp1:fp2))),'
.')
title('H11 FRF for low voltage level - combined actuator approach')
xlabel('Frequency (Hz)')
```

```
ylabel('FRF Magnitude V/V')
legend('5V','10V')
subplot 222
plot(f(fp1:fp2),abs(squeeze(H2(2,1,fp1:fp2))),f(fp1:fp2),abs(squeeze(H2h(2,1,fp1:fp2))),'
.')
title('H21 FRF for low voltage level - combined actuator approach')
xlabel('Frequency (Hz)')
ylabel('FRF Magnitude V/V')
legend('5V','10V')
subplot 223
plot(f(fp1:fp2),abs(squeeze(H2(1,2,fp1:fp2))),f(fp1:fp2),abs(squeeze(H2h(1,2,fp1:fp2))),'
.')
title('H12 FRF for low voltage level - combined actuator approach')
xlabel('Frequency (Hz)')
ylabel('FRF Magnitude V/V')
legend('5V','10V')
subplot 224
plot(f(fp1:fp2),abs(squeeze(H2(2,2,fp1:fp2))),f(fp1:fp2),abs(squeeze(H2h(2,2,fp1:fp2))),'
.')
title('H22 FRF for low voltage level - combined actuator approach')
xlabel('Frequency (Hz)')
ylabel('FRF Magnitude V/V')
legend('5V','10V')


% Plot Nyquist form for FRFs at HIGH Level

figure
subplot 221
polar(angle(squeeze(H2h(1,1,fp1:fp2))), abs(squeeze(H2h(1,1,fp1:fp2)))), title('H11 polar
plot')
subplot 222
polar(angle(squeeze(H2h(2,1,fp1:fp2))), abs(squeeze(H2h(1,1,fp1:fp2)))), title('H21 polar
plot')
subplot 223
polar(angle(squeeze(H2h(1,2,fp1:fp2))), abs(squeeze(H2h(1,1,fp1:fp2)))), title('H12 polar
plot')
subplot 224
polar(angle(squeeze(H2h(2,2,fp1:fp2))), abs(squeeze(H2h(1,1,fp1:fp2)))), title('H22 polar
plot')
```

****
The following is the polyreference program written in part by Dr. Jan Wright and Eric Ruggiero.
****

```
% Program torus_poly

% Permits analysis of part of frequency range

% Calculate impulse response function matrix from FRF matrix
% Use LSCE / Polyreference to identify natural frequencies and damping ratios
% - where possible notation as per Cooper's paper in MSSP 1990 4(2) pp157-172
% H is FRF matrix / frequency is array of np2+1 frequencies for which FRF is calculated
% FRF carried through from torus_frf
% freq_est and zeta_est are estimated values returned
% - modal_mass_est and psi_est are generated in jan_lsfd
% Copy values from torus_frf

H=HH;
frequency = f;

% Expected max no of modes

nmodes = input('Enter expected no of modes in analysis ');

[r,e,nfreq] = size(H);                  % number of responses, exciters, frequency
points in H

fnyq = frequency(nfreq);                % Nyquist frequency
df = frequency(nfreq)/(nfreq-1);        % frequency step in FRF
dt = 1/(2*fnyq);                            % time step in IRF when generated
np21 = nfreq;                               % data point at Nyquist frequency
np22 = np21 + 1;                            % point beyond Nyquist
np2 = nfreq - 1;                            % half number of time points
npts = 2 * np2;                             % number of time points
t = (1:npts)*dt;                            % vector of time values

% Calculate sum blocks for H for use in stabilisation diagram

if e == 1
  H_sum = squeeze(sum(abs(H)));
  else
  H_sum = squeeze(sum(sum(abs(H))));
end

% Select bandwidth for 'zoom' analysis if desired and reset parameters (add _z)
```

```
fig1 = figure;
plot(frequency, H_sum);

iz = input('Enter 0 for baseband and 1 for zoom analysis ');

if iz == 0                  % base band

    fnyq_z = fnyq;
    nfreq_z = nfreq;
    df_z = df;
    dt_z = dt;
    np21_z = np21;
    np22_z = np22;
    np2_z = np2;
    npts_z = npts;
    freq_z = frequency;
    H_z = H;

    if e == 1
      H_sum_z = squeeze(sum(abs(H_z)));
        else
      H_sum_z = squeeze(sum(sum(abs(H_z))));
    end

    else if iz == 1  % 'zoom'

    fig1 = figure;
        plot(frequency, H_sum);

    f1 = input('Enter lower frequency bound for fitting?  ');
    f2 = input('Enter upper frequency bound for fitting?  ');
    fp1 = round(f1/df) + 1;
    fp2 = round(f2/df) + 1;

    fnyq_z = frequency(fp2) - frequency(fp1);     % new Nyquist for band limited FRF
    nfreq_z = fp2 - fp1 + 1;    % new no of frequencies for band limited FRF
    df_z = df;        % df unchanged
    dt_z = 1 / (2*fnyq_z); % new dt for band limited FRF
    np21_z = nfreq_z;
    np22_z = np21_z + 1;
    np2_z = nfreq_z - 1;
    npts_z = 2 * np2_z;

    freq_z = zeros(nfreq_z,1);
    freq_z(1:nfreq_z) = frequency(fp1:fp2);
```

```
    H_z = zeros(r,e,nfreq_z);
    H_z(:,:,1:nfreq_z) = H(:,:,fp1:fp2);          % Set up band limited FRFs

    % Calculate sum blocks for H_z for use in stabilisation diagram and plot to check

    if e == 1
      H_sum_z = squeeze(sum(abs(H_z)));
    else
      H_sum_z = squeeze(sum(sum(abs(H_z))));
    end

    fig2 = figure;
    plot(freq_z, H_sum_z);
    pause
  end
end

% Calculate inverse FFT stored in h to yield impulse response function IRF - to achieve
this
% the FRF must be extended to include negative frequency values as conjugates
% in reverse order

h = zeros(r,e,npts_z);

for ie = 1:e;
  for ir = 1:r;
    Hstore = squeeze(H_z(ir,ie,:));              % store current FRF in 1D array
    Hstore_ext = [Hstore(1:np21_z);conj(Hstore(np2_z:-1:2))]; % extend for ifft
    hstore = ifft(Hstore_ext);                   % inverse FFT for stored array
    h(ir,ie,:) = real(hstore);                   % restore to 3D array of IRFs
  end
end

% Choose a number of points from the decay to encompass the bulk of the active region
fig2 = figure;
plot(real(hstore(1:np2_z)))                      % plot sample IRF (last one generated)
N = input('Enter no of points in decay to be fitted?  ');

% Loop around for smax - ie all orders of s (no of submatrices) needed for modes_max
% and store frequency and damping values for stabilisation diagram - looping on s
% is to avoid the duplication of models that occurs when looping around modes is used
% s is effectively the model order of the matrix difference equation - with e>1 it is
% not possible to identify every single no of modes from 1:modes_max!

modes_max = 4 * nmodes;                          % max no of modes in fit (arbitrary)
smax = ceil(modes_max*2/e);                      % max size of s (depends on e)
```

```
freq_est_all = zeros(modes_max,smax);
zeta_est_all = zeros(modes_max,smax);

% Alter 1 to 2 for loop to overcome e=1 problem JRW 30/1/02 - but problem of 'half
modes' remains

for s = 2:smax                                  % s is order of block polynomial
equation

  s
  mm = s*e;                                     % model order >= 2*no of modes
  smodes = floor(mm/2);                         % no of modes for this s loop
    s1 = s + 1;
    se = s*e;
    Ns = N-s;
    Y = zeros(Ns*r,e);
    PHI = zeros(Ns*r,se);
    THETA = zeros(se,e);

  % Fill up matrices with blocks consisting of
    % impulse response function matrices at different time values

  wait_handle = waitbar(0, 'Generating matrices');
    wcount = 1;

    rcount = 1;
    for ib = s1:N
        Y(rcount:rcount+r-1,:) = squeeze(h(:,:,ib));        % fill Y matrix
    ecount = 1;
    for jb = 1:s
        PHI(rcount:rcount+r-1,ecount:ecount+e-1) = h(:,:,ib-jb); % fill PHI matrix
        ecount = ecount + e;

    end
    rcount = rcount + r;
        wcount = wcount + 1;
    waitbar(wcount/Ns);
    end
    close(wait_handle)

    % Solve for THETA via Least Squares
    THETA = PHI\Y;

    % Set up sparse block Hessenburg matrix from submatrices in THETA
    A = zeros(se,se);
    A(:,1:e) = THETA;
```

```
    A(1:(s-1)*e,e+1:se) = eye((s-1)*e);

    % Solve for estimated frequency and damping values via eigenvalues of A

    [Vec,Val] = eig(A);
    L = diag(Val);
    el = log(L)/dt_z;
  omegan_z = abs(el);

  % Add lower frequency limit to frequencies determined prior to calculating damping

  omegan = omegan_z + 2 * pi * freq_z(1);

    zeta_est = -real(el)./omegan;
    freq_est = omegan /(2*pi);
    [freq_est,index] = sort(freq_est);
  zeta_est = zeta_est(index);

  % Store every other value to allow for complex conjugate roots
    ialt = (1:2:se-1);
    freq_est = freq_est(ialt);
  zeta_est = zeta_est(ialt);
  [freq_est zeta_est]

  % Store results
    [no_freq,dummy] = size(freq_est);
    freq_est_all(1:no_freq,s) = freq_est;
    zeta_est_all(1:no_freq,s) = zeta_est;

end

% Call stabplot function
torus_stab(freq_z',H_sum_z,freq_est_all,zeta_est_all,modes_max,smax,e,1,5);
pause
```

The next program plots the stability diagram from the polyreference program. This program was written in part by Dr. Jan Wright and Eric Ruggiero.

```
function jan_torus(f,FRF,freq,damp,max_modes,nmodels,e,fm,dm);

% Plot a stability plot from LSCE data over a range of fitted models
% Check for convergence to within given bounds
% f is frequency vector, FRF is SISO FRF vector (eg sum FRFs), purely for plotting
% freq and damp are matrices of freq and damping results, where
% the first m rows of column n hold the values relating to the nth model fitted.
% max_modes is the max no of modes in the curve fit
% nmodels is the number of different models fitted by LSCE
% e is number of exciters
% fm and dm are the (percentage) freq and damping bounds (eg 1 and 5)
% Plot FRF and initial freq estimates

axis([f(1) max(f) 0 max_modes])
FRF = FRF*max_modes/max(FRF);
fig2 = figure;
plot(f,FRF,'--',freq,1:max_modes,'w.')
xlabel('Frequency (Hz)')
ylabel('No of modes estimated')
hold on
zoom on

% Stabilization matrix - codes for whether freq or freq + damp are stabilized
stab = zeros(size(freq));


% Initial estimates
s = 1;
m1 = floor(s*e/2);              % no of modes for s=1 (first model order fitted)
f1 = freq(1:m1,1);
d1 = damp(1:m1,1);
for k = 1:m1
  plot(f1(k),m1,'g.')
  axis([f(1) max(f) 0 max_modes])
end

% Loop for all remaining estimated models
for s = 2:nmodels
    mm = s * e;                     % model order
    m = floor(mm/2);                % no of modes fitted
    f2 = freq(1:m,s);
    d2 = damp(1:m,s);
```

```
    for k = 1:m
    count(k) = 0;                          % counter to indicate whether f2 stabilized
  end

% Loop for each result in current vector f1
    for j = 1:m1
% Define confidence bands for current frequencies
    fbl = f1(j)*(1-fm/100);
    fbu = f1(j)*(1+fm/100);
% Loop for each frequency in new vector f2 and compare to f1(j)
        for k = 1:m
% Compare frequencies
            if f2(k)>fbl & f2(k)<fbu        % ie lies in the given freq band
        count(k) = 1;                      % flag to show f2 value stabilised and plotted
% Compare dampings
                dbl = d1(j)*(1-dm/100);
            dbu = d1(j)*(1+dm/100);
        if d2(k)>dbl & d2(k)<dbu
          plot(f2(k),m,'r*')
          axis([f(1) max(f) 0 max_modes])
                stab(k,s)=2;               % ie stabilized in frequency & damping
              else
                plot(f2(k),m,'b+')
          axis([f(1) max(f) 0 max_modes])
            stab(k,s)=1;               % ie stabilized in frequency but not damping
            end
      end
    end
    end

  % Plot remaining f2 points as not stabilized
  for k = 1:m
    if count(k) == 0
      plot(f2(k),m,'go')                   % frequency not stabilized so plot
      axis([f(1) max(f) 0 max_modes])
    end
  end

% Move to next estimated model and update current vector and
% remember current no of modes
    f1 = f2;
    d1 = d2;
    m1 = m;
end
figure(fig2)
hold off
```

The following program was used to calculate the coefficients of the PPF filter for both the plate and torus experiments. Simply modify zp and wp depending on the application.

```
clc;
clear;

% You need to give inputs in the below.

%zp=input('Give the value of Damping Ratio of the beam (in percent):  ');
%wp=input('Give the value of Natural Frequency of the beam in Hz :  ');
%gg=input('Give the value of Gain (0.01):    ');
% 0.2 and 7.8

zp=0.15
wp=37.3*1.05

%zp= 0.10 wp=12.9 work best
% controller gain
%gg=0.03; %old value
%gg=.1  % working value

wp=wp*2*pi;

% computing PPF filter parameters through the tuning equation
zf=sqrt((1.02*zp^2)^2/((1.02*zp^2)^2+0.16));
wf=wp/(1.02*sqrt(1-zf*zf));

% building a filter transfer function
numc=[wf*wf];
denc=[1 2*zf*wf wf*wf];
sysc=tf(numc,denc);

% converting to discrete domain from continuous domain
sysd=c2d(sysc,0.001);

% obtain transfer function in discrete time
[numd,dend,Tss]=tfdata(sysd,'v')
```

APPENDIX B: 3M Damping Foil (2552) Data Sheets

Source: http://products.3m.com/us/electronics_mfg/products/electronics_mfg.jhtml

3M

Damping Foil

2552

Technical Data

Product Description

This product consists of a room temperature pressure sensitive viscoelastic polymer on a dead soft aluminum foil. **Designed for application to vibrating panels and support members**. The combination of viscoelastic polymer and an aluminum foil backing (a constrained layer damper, or CLD) has proved to be a unique construction with exceptional ability to control resonant vibrations in the temperature range of 32° to 140°F (0° to 60°C), with survivability from -25° to 175°F (-32° to 80°C).

Typical Damping Properties

The high-energy dissipative polymer used in 3M™ Damping Foil 2552 can afford excellent control of resonance-induced vibrations. When applied to a vibrating structure, the polymer used in 2552 converts vibration to negligible heat. Vibration amplitudes and structure-borne noise can be consequentially reduced.The performance of most damping devices is highly dependent on the interaction between the device and the system to which it is applied. A constrained layer control system is no different than a typical damping device and its ability to provide the desired performance is affected by parameters other than temperature and frequency. Namely the geometry, stiffness and the structure to which the control system is applied will affect the performance.

The loss factor of a material is a dynamic property that can define damping performance:

The following data are the results of Damping Foil 2552 being tested per ASTM E756-83. A sample of 2552 was applied to a 8.0 inch by 0.5 inch by 0.06 inch steel beam. The beam was tested over a temperature range of -40° to 140°F, in increments of 10°F. Beam modes 2 through 7 were monitored for system damping measurements.

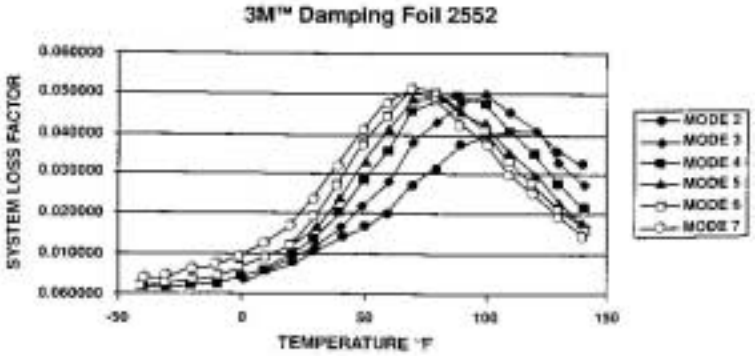

Typical Damping Properties cont.

Test Method: The following data were obtained by doing a frequency sweep from 1 to 100 radians/sec (0.16 to 16 Hz) at 5 different temperatures: -20°, 10°, 0°, 10°, and 22°C. A 3 point bend geometry was used on the Rheometrics RSA II. Time – temperature superposition was used to create the master curve for a reference temperature of 22°C.

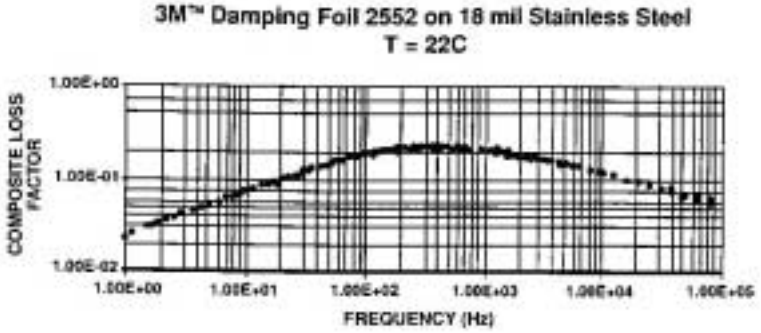

Data Interpolation:

To determine the damping properties at ambient temperature (72°F, 22°C), proceed as follows:

1) Locate the desired frequency on the bottom HORIZONTAL scale.
2) Follow the chosen frequency up to the point of intersection with the plotted data.
3) From this intersect, go left to the vertical scale.
4) Read the COMPOSITE LOSS FACTOR for the chosen frequency.

NOTE: Please note that these data have been determined by combining 2552 with a panel of 0.018" thick stainless steel with a hardness of T-22. These data are presented as a reference as to the damping that can be achieved from 2252 when combined with a material of this description and tested at ambient temperature (72°F, 22°C).

Solvent and Fuel Resistance

When properly laminated between two impervious materials, the polymer will resist intermittent exposure to mild acids and alkalies, most oils, grease, gasoline, kerosene, JP-4 fuel, hydraulic fluids, and other typical aromatic and aliphatic hydrocarbon and ketone solvents.

NOTE: Continuous submersion in chemical solutions like solvents or fuels is not recommended.

Damping Foil

2552

Product Construction and Typical Physical Properties

Note: The following technical information and data should be considered representative or typical only and should not be used for specification purposes.

		ASTM Test Method
Aluminum Backing:	10.0 mils (0.25 mm)	
Acrylic Viscoelastic Polymer:	5.0 mils (0.13 mm)	
Easy-release Liner:	58# poly-coated paper	
Total Product Thickness:	15.0 mils (0.38 mm)	
Total Product Weight:	0.17 lbs./sq. ft.	
Adhesion to Steel:	65 oz./in. (72 N/100 mm)	D-3330
Tensile Strength:	126 lbs./in. (2205 N/100 mm)	D-3759
Elongation at Break:	12%	D-3759
Temperature Use Range:	-25° to 175°F (-32° to 80°C) Peak damping from 32° to 140°F (0° to 60°C)	
Minimum and Maximum Widths:	2 in. minimum, 23.5 in. maximum	
Available Formats:	**Roll Lengths:** Standard length 36 yds. • 2" to 4": up to 108 yds. • Wider widths available to 180 yds. • Dispensers available for purchase through 3M. **Sheets and Die-Cut parts:** 3M can introduce you to fabricators with a background of handling this product and the capability to provide sheet goods and die cut dampers to their customer's specifications. **Custom Dispenser:** Designed for manual or automatic operation, this custom dispenser removes protective liner from 3M™ Damping Foil 2552 before cutting to a predetermined length. Built to hold and dispense 3M Damping Foil 2552's 6" core with a roll size up to 2" wide by 108 yds. Engineered for table top usage, this custom dispenser measures 31"L x 22"H x 10"W and weighs only 45 pounds.	

Characteristics

- Excellent aging qualities of the polymer.
- Wide temperature range for damping. Usable from -25° to 175°F (-32° to 80°C), with peak damping from 32° to 140°F (0° to 60°C).
- Liner on product offers the user die-cut capability.
- PSA for ease of application.

Application Ideas

- Industrial applications.
- Electronic equipment and appliances.
- Reduce resonant noise, vibration and fatigue in metal, plastic panels and support structures.
- Almost anywhere plastic or metal contact with materials that can result in potentially damaging vibration.

Custom Application Support

- 3M provides technical support, from optimizing the design of your custom noise/vibration solution, through fabrication and timely delivery. Follow-up support is worldwide.

APPENDIX C: MFC® Device Properties

Source: Wilkie, W. K., Bryant, R. G., High, J. W., Fox, R. L., Hellbaum, R. F., Jalink A., Little B. D., and Mirick P. H., 2000, "Low-Cost Piezocomposite Actuator for Structural Control Applications," Proceedings of the 7th SPIE International Symposium on Smart Structures and Materials, Newport Beach, CA, March 5-9.

Representative LaRC-MFC™ baseline actuator properties:

property	symbol	value	units
thickness (average)	t	0.092	in
width (excluding electrode power rails)	w	2.25	in
length (excluding terminal pads)	l	3.375	in
mass per unit area (active region)	m	1.25	g/in^2
poled capacitance per unit area (active region)	C/A	0.96	nF/in^2
longitudinal Young's modulus (fiber axis)	E_1	5.0E+06	psi
lateral Young's modulus (electrode axis)	E_2	1.1E+06	psi
effective longitudinal induced strain coefficient	d_{11}	530	με/kV/mm
effective lateral induced strain coefficient	d_{12}	-210	με/kV/mm
maximum operational piezoelectric induced free strain	$\varepsilon_{1\,max}$	990	με (peak)
maximum operational piezoelectric induced free stress	$\sigma_{1\,max}$	4800	psi (peak)
strain-electric field hysteresis	*hyst.*	~15	%

REFERENCES

1. Agnes, G., and Rogers, J. W., 2000, "Piezoelectric Excitation of Inflatable Space Structures for Modal Testing," *Proceedings of the 7th Annual Smart Materials and Structures Conference, International Society for Optical Engineering*, SPIE 3985-88, Newport Beach, CA, pp. 806-816.

2. Allemang, R. J., D. L. Brown, and W. Fladung, 2000, "Modal Parameter Estimation: Unified Matrix Polynomial Approach," *Proceedings of the 12th International Modal Analysis Conference*, pp. 501-514.

3. Briand, G., Wicks, A. L., and Inman, D. J., 2000, "Vibration Testing for Control of Inflated Objects," in *Proceedings of 18th Annual International Modal Analysis Conference*, pp. 501-514.

4. Chmielewski, A. B., 2000, "Overview of Gossamer Technology," *Gossamer Spacecraft: Membrane and Inflatable Structures Technology for Space Applications*, Christopher H. M. Jenkins, ed., AIAA, Vol. 191, pp. 1-33.

5. Chmielewski, A. B., Moore, C., and Howard, R., 1999, "The Gossamer Initiative," *IEEE*, Paper No. 0-7803-5846-5/00.

6. Clark, S. K., Dodge, R. N., and Nybakken G. H., 1974, "Dynamic Properties of Aircraft Tires," *Journal of Aircraft*, Vol. 11, No. 3, pp. 166-172.

7. Cole, Daniel G., 1992, *Design of, and Initial Experiments with, a MIMO Plate Control Testbed*, MS Thesis, Virginia Polytechnic Institute and State University, Blacksburg, VA.

8. Dornheim, Michael A., 2000, "Inflatable Structures Take to Flight," http://www.lgarde.com/programs/iaearticle/awarticle.html.

9. Dosch, J. J., Inman, D. J., and Garcia, E., 1992, “A Self-Sensing Piezoelectric Actuator for Collocated Control,” *Journal of Intelligent Material Systems and Structures*, Vol. 3, p. 166.

10. Fanson, J.L. and Caughey, T.K., 1987, "Positive Position Feedback Control for Large Space Structures", *Proceedings of 28th AIAA Structures, Structural Dynamics and Materials Conference*, Monterey, CA, pp. 588-598.

11. Freeland, R. F., 2000, “History of Relevant Inflatable High-Precision Space Structures Technology Developments,” *Gossamer Spacecraft: Membrane and Inflatable structures Technology for Space Applications*, Christopher H. M. Jenkins, ed., AIAA, Vol. 191, pp. 33-48.

12. Goh, C. J. and T. K. Caughey, 1985, “One the Stability Problem Caused by Finite Actuator Dynamics in the Collocated Control of Large Space Structures,” *International Journal of Control*, Vol. 41, pp. 787-802.

13. Griffith, D. T., and Main, J. A., 2000, “Modal Testing of an Inflated Thin Film Polyimide Torus Structure,” *Proceedings of IMAC XVIII*, February, pp. 1035-1041.

14. Guan, D. H., Yam, L. H., Mignolet, M. P., and Li, Y. Y., 2000, “Experimental Modal Analysis of Tires,” *Experimental Techniques*, November/December, pp. 39-45.

15. Hegewald, Thomas, 2000, *Vibration Suppression Using Smart Materials in the Presence of Temperature Changes*, MS Thesis, Virginia Polytechnic Institute and State University, Blacksburg, VA.

16. Leigh, L., Hamidzadeh, H., Tinker, M. L., and Slade, K. N., 2001, "Dynamic Characterization on an Inflatable Concentrator for Solra Thermal Propulsion," *42nd AIAA/ASME/ASCE/AHS/ASC Structures, Structural Dynamics, and Materials Conference and Exhibit*, Seattle, WA, 15-19 March, pp.1-7.

17. Lewis, J. A., 2000, *Finite Element Modeling and Active Control of an Inflated Torus Using Piezoelectric Devices*, MS Thesis, Virginia Polytechnic Institute and State University, Blacksburg, VA.

18. McEver, M. A., 1999, *Optimal Vibration Suppression Using On-line Pole/Zero Identification*, MS Thesis, Virginia Polytechnic Institute and State University, Blacksburg, VA.

19. Noor, A., and Tanner, J., 1985, "Advances and Trends in the Development of Computational Models for Tires," *Computers & Structures*, Vol. 20, No. 1-3, pp. 517-533.

20. Park, G., Kim, M.-H., and Inman, D. J., 2001, "Integration of Smart Materials into Dynamics and Control of Inflatable Space Structures," *Journal of Intelligent Material Systems and Structures*, in press.

21. Poh, S. and A. Baz, 1990, "Active Control of a Flexible Structure Using a Modal Positive Position Feedback Controller," *Journal of Intelligent Material Systems and Structures*, Vol. 1, July, pp. 273-288.

22. Rubenstein, S. P., Saunders, W. R., Ellis, Graham K., Robertshaw, H. H., and Baumann, W. T., 1991, "Demonstration of a LQR Vibration Controller for a Simply-Supported Plate," *Recent Advances in Active Control of Sound and Vibration*, Rogers, C. A. and C. R. Fuller, eds., Virginia Polytechnic Institute and State University, Blacksburg, VA, April 15-17.

23. Ruggiero, Eric, Gyuhae Park, Daniel J. Inman, and John A. Main, 2002, "Smart Materials in Inflatable Structure Applications," *Proceedings of 43rd AIAA/ASME/ASCE/AHS/ASC Structures, Structural Dynamics, and Materials Conference, AIAA Gossamer Spacecraft Forum*, April 22-25, Denver, CO.

24. Salama, M., Kuo, C. P., Garba, J., Wada, B., and Thomas, M., 1994, "On-Orbit Shape Correction of Inflatable Structures," AIAA Paper No. 94-1771, pp. 348-355.

25. Sirohi, J., and Chopra, I., 2000a, "Fundamental Behavior of Piezoceramic Sheet Actuators," *Journal of Smart Material Systems and Structures*, Vol. 11, January, pp. 47-61.

26. Sirohi, J., and Chopra, I., 2000b, "Fundamental Understanding of Piezoelectric Strain Sensors," *Journal of Smart Material Systems and Structures*, Vol. 11, April, pp. 246-257.

27. Slade, K. N., Tinker, M. L., Lassiter, J. O., and Engberg, R., 2001, "Dynamics of an Inflatable Structure in Vacuum and Ambient Conditions," *AIAA Journal*, Vol. 39, No. 5, May, pp. 894-901.

28. Sun, F. P., Liang, C., and Rogers, C. A., 1994, "Structural Modal Analysis Using Collocated Piezoelectric Actuator/Sensors – an Electromechanical Approach," *SPIE*, Vol. 2190, February, pp. 238-249.

29. Sun, F., Rogers, C. A., and Liang, C., 1995, "Structural Frequency Response Function Acquisition via Electric Impedance Measurement of Surface Bonded Piezoelectric Sensor/Actuator," *Proceedings of the 36th AIAA/ASME/ASCE/ASC Structures, Structural Dynamics, and Materials Conference and AIAA/ASME Adaptive Structures Forum*, Part 5, New Orleans, LA, April, pp. 3450-3458.

30. Tinker, M. L., 1998, "Passively Adaptive Inflatable Structure for the Shooting Star Experiment," AIAA Paper No. 98-1986, pp. 2320-2326.

31. Tzou, H.-S., 1998, "Multifield Transducers, Devices, Mechatronic Systems, and Structronic Systems with Smart Materials," *The Shock and Vibration Digest*, Vol. 30, No. 4, July, pp. 282-294.

32. Wang, B. T., 1998, "Structural Modal Testing with Various Actuators and Sensors," *Mechanical Systems and Signal Processing*, Vol. 12, No. 5, pp. 627-639.

33. Wang, B.-T., and Chen, R.-L., 2000, "The Use of Piezoceramic Transducers for Smart Structural Testing," *Journal of Smart Material Systems and Structures*, Vol. 11, September, pp. 1-12.

34. Wilkie, W. K., Bryant, R. G., High, J. W., Fox, R. L., Hellbaum, R. F., Jalink A., Little B. D., and Mirick P. H., 2000, "Low-Cost Piezocomposite Actuator for Structural Control Applications," *Proceedings of the 7th SPIE International Symposium on Smart Structures and Materials*, Newport Beach, CA, March 5-9.

35. Williams, R. B., E. M. Austin, and D. J. Inman, 2001, "Limitation of Using Membrane Theory for Modeling PVDF Patches on Inflatable Structures," *Journal of Intelligent Material Systems and Structures*, at press.

36. Yam, L. H., Guan, D. H., and Zhang, A. Q., 2000, "Three-dimensional Mode Shapes of a Tire Using Experimental Modal Analysis," *Experimental Mechanics*, Vol. 40, No. 4, December, pp. 369-375.

VITA

Eric John Ruggiero

Eric John Ruggiero was born on August 10, 1979 to John and Nancy Ruggiero in Lawrence, Massachusetts. He graduated valedictorian of the Class of 1997 from Sanborn Regional High School in Kingston, New Hampshire. In the Fall of 1997, Eric began his studies in Mechanical Engineering at Virginia Polytechnic Institute and State University in Blacksburg, Virginia. Throughout his undergraduate career at Virginia Tech, Eric joined numerous organizations, including Pi Tau Sigma, Tau Beta Pi, the National Society of Collegiate Scholars, the American Society of Mechanical Engineers, and the National Society of Professional Engineers. He was also very involved in campus ministry through the Newman Community Catholic Campus Ministry organization. From 1999-2000, Eric served as a student campus minister for the Newman Community. During his tenure as student campus minister, Eric helped organize the community's 75th anniversary celebration and traveled to Oaxaca, Mexico to live and work with the poor.

As an undergraduate, Eric used his summers to intern with different companies and to learn more about the working world. In 1999, he worked at Osram Sylvania in Hillsborough, New Hampshire as a product development engineer. In 2000 and 2001, Eric worked at Raytheon Systems Company in Andover, Massachusetts as a manufacturing engineer. In particular, Eric worked in the circuit card assembly division responsible for such defense contracts as the Patriot missile, Tomahawk missile, Javelin weapons system, and many others.

Eric was the recipient of many scholarships and awards during his undergraduate career at Virginia Tech. Some of the awards he received included the Marshall Hahn Engineering Scholarship, Seay Scholarship, Faculty honors Scholarship, Litton Industries Scholarship, Hal L. Moses Scholarship, and the Shorb Award, awarded to a Mechanical Engineering senior for outstanding leadership and contribution to the field of engineering.

Further, Eric was also the recipient of Virginia Tech's most prestigious undergraduate award, the Virginia Tech Man of the Year in 2001. In competition with the entire University community, Eric received the award based on his demonstration of the ideals upon which the University is founded upon—*ut prosim*.

Eric was accepted into the 5 year MS / BS program in Mechanical Engineering at Virginia Tech in 2000, and began preliminary research for his advisor, Dr. Daniel J. Inman, in the Spring of 2001. He performed research on identifying the dynamic characteristics of an inflated torus, and used this research as the premise for the remainder of his thesis work.

In August of 2001, Eric married Jennifer L. Vercoe of Colchester, Vermont. The couple moved to Blacksburg, Virginia so Eric could continue his Masters research and for Jennifer to teach 1st grade at Falling Branch Elementary in Christiansburg, Virginia. Eric concluded his Masters research in two semesters after numerous conference paper and journal paper publications and presentations. Eric capped off his Masters research by receiving the prestigious Paul E. Torgersen Research Excellence Award, an award given to the top Masters student who demonstrates both excellence in research as well as significant contributions to the field of engineering.

Eric and Jennifer currently reside in Blacksburg, Virginia. Eric and his wife will be traveling to Phoenix, Arizona this summer to see the countryside and to work for Honeywell Space Systems. Eric will be returning to Virginia Tech in the Fall to continue his graduate education and earn his Ph.D. in Mechanical Engineering.